SIMULATION OF URANIUM(VI) SPECIATION, SORPTION, AND DIFFUSION IN MONTMORILLONITE CLAY IN THE PRESENCE OF CALCITE IMPURITIES

_____

A University Thesis Presented to the Faculty

of

California State University, East Bay

_____

In Partial Fulfillment

of the Requirements for the Degree

Masters of Science in Chemistry

By

Jonathan Pistorino

May 2019

Abstract

Uranium mobility in subsurface environments is a core area of study concerning the long-term storage of nuclear waste in deep geological repositories. Montmorillonite, the dominant component of the abundant geological material bentonite has highly desirable properties for a potential engineered barrier material, such as providing a strong sorbent for many radioactive contaminants, and a low porosity and permeability, which limits U(VI) transport to diffusion-based transport mechanisms. The goal of this study was to simulate uranium(VI) solution speciation, sorption and diffusion behavior in montmorillonite for various repository-relevant chemical conditions. Uranium(VI) solution speciation is characterized across a wide pH range (3-9) and over various total U(VI) concentrations (0.1, 1.0, 2.4, and 10 uM), partial pressures of CO_2 (closed, atmospheric, 1 % and 2 % CO_2 systems), and in the presence or absence of calcite, a mineral which is a known impurity in bentonite. In addition, U(VI) sorption onto montmorillonite surfaces is simulated as a function of system conditions based on two published surface complexation models; one of which does not include corrections of the adsorption energy from the presence of an electrostatic potential at the surface but allows for the sorption of U(VI)-carbonate solution species and another which accounts for the effectof the electrostatic potential and does not allows for the adsorption of carbonate Uranium complexes at the surface. Finally, the diffusion of U(VI) through a clay plug is evaluated in a parametric modeling study based on the analytical solution for Fick’s law of

diffusion. Diffusion models account for U(VI) sorption based on surface complexation reactions, as well as an accumulation of uranium within diffuse layers close to clay surfaces . The results of this study and the toolbox developed, will allow the reader to further understand U(VI) solution speciation, sorption, and diffusion behavior, and hence the relevant processes driving U(VI) mobility in these systems.

SIMULATION OF URANIUM(VI) SPECIATION, SORPTION, AND DIFFUSION IN MONTMORILLONITE CLAY IN THE PRESENCE OF CALCITE IMPURITIES

By

Jonathan Pistorino

Approved:	Date:
Dr. Ruth Tinnacher	5-14-2019
Dr. Patrick Huang	5/14/2019
Dr. Christophe Tournassat	5/14/2019

Acknowledgements

Without a doubt this experience would not have been possible without the leadership, insight, cheer, and motivation of my advisor Dr. Ruth Tinnacher. With her support, we were able to outline and execute a project that will be meaningful to the geochemical community and hopefully to future students in her laboratory who will spearhead further efforts of this exceptional project.

I also could not imagine completing this project without the guidance of Dr. Christophe Tournassat. Christophe gave me encouragement in my modeling capabilities and provided some of the deepest insight into these very complex interactions. I am very pleased that we were able to meet multiple times but also work well at a distance.

I further more appreciate Dr. Huang for his instruction, mentorship and participation in reviewing this work. Dr. Huang also prepared me for the further study of inorganic materials through two sections of inorganic chemistry where he simplified group theory so that even I could understand it.

I would also like to thank the CSUEB Center for Student Research which supported the presentation of my work. In preparing for this prestigious event, I was forced to articulate my research at a level that I may not have achieved otherwise and for this I am grateful.

The most important support and backing came from my wife, Phyllis Pistorino. I was working full time during my attendance of this graduate program

and during the production of this research, which meant a lot of sacrifice on both our parts and for this teamwork I am infinitely grateful.

Table of Contents

List of Figures

List of Tables

1.0 Introduction

1.1 Purpose

The purpose of this thesis is to advance our collective understanding of the complex interactions between uranium(VI), the major component in spent nuclear fuel, and bentonite, a proposed barrier material for long-term storage in underground nuclear waste repositories. Similar systems and concepts have been studied by many other groups previously and hence, this study will build on this existing knowledge. In addition, this study will specifically focus on a mineral impurity (calcite) that may have strong effects on the system dynamics, which were previously neglected.

1.2 Uranium Waste

1.2.1 Sources of Uranium Waste

Nuclear waste is generated by a variety of activities such as nuclear power generation, nuclear propulsion (submarines), nuclear weapons manufacturing, and the medicinal industry. Although there are other components of nuclear waste that arise from nuclear fission, on average nuclear waste predominantly consists of uranium with an average compositional content of 94 % by weight.[1] National and international governing bodies have agreed upon a set of hazard classifications specified as High Level Waste (HLW, added hazard from thermal component), Intermediate Level Waste (ILW, needs shielding but no provision for dissipation), Low Level Waste (LLW, low radionuclide content therefore does not require shielding), and Very Low Level Waste (VLLW, measurable contamination but no regulation). At the end of 2013, the total

nuclear inventory of the member countries in the European Union was determined to be a mixture of 74 % LLW, 15 % VLLW, 10 % ILW, and 0.2 % HLW).[2,3]

1.2.2 Current Storage Practices

Radioactive waste from energy production is often temporarily stored in cooling pools near the nuclear reactor in which it was produced. Storing waste in non-corrosive drums within pools of water serves two purposes, to dissipate residual heat produced by the continuous radioactive decay, and to shield employees and other individuals from α radiation. Once the waste has cooled sufficiently, the fuel rods are then often stored in dry caskets on the production site.

However, this strategy is planned to be adjusted once a long-term storage solution is agreed upon and implemented.[4,5] Research regarding the long-term storage of HLW produced by nuclear weapons research is underway at The Waste Isolation Pilot Plant (WIPP) in Carlsbad, New Mexico. This facility was opened in 1999 for this specific purpose, and is managed by the United States Department of Energy.[6]

1.2.3 Environmental and Health Threats

A multitude of incidents have occurred which have demonstrated the risks associated with nuclear power production, and in the U.S. temporary nuclear waste storage. From the Three Mile Island partial core meltdown and the famous Chernobyl meltdown incident in the Ukraine to the more recent flooding and

meltdowns at nuclear power plants in Fukushima, Japan after an earthquake and tsunami, past incidents have shown the impacts of the release of radioactive contaminants due to a natural disaster or technical issues.[7] Although these indecencies occurred during production, any of these disasters could also apply to temporary storage sites of nuclear waste with similarly disastrous outcomes.

For this thesis, the toxicity and mobility of uranium is the focus, as it is the dominant element in the majority of the world's currently-stored nuclear waste. Uranium poses a significant health threat no matter what its physical state. Because it is constantly undergoing radioactive decay, any human contact, whether particulate or dissolved, may have detrimental effects. There is no safe lower limit for α radiation.[8]

It has been shown in previous publications, that uranium in high level nuclear waste streams is predominantly present in the +6 oxidation state.[9,10] Hence, in this work we will not focus on uranium in the +4 oxidation state, as U(IV) is only sparingly soluble in aqueous solutions.

Uranium is understood to have no biological function and is therefore considered non-essential to life. Although historically people have used sources of radiation to produce a variety of health benefits, the majority of these efforts have been unscientific and misguided. In modern medicine, radiation therapy is used to treat certain types of cancer in a controlled, methodical fashion. Uncontrolled uranium exposure presents two different forms of toxicity to living organisms: radiological and chemical.

Regarding radiological toxicity, radioisotopes with shorter half-lives are generally considered to be more toxic, as well as radionuclides generating beta and gamma radiation. Alpha radiation can be blocked by something as simple as a plastic container, a sheet of paper or the air gap between a human and the source of emission. Beta and gamma radiation have higher penetrating power and require more specialized shielding such as aluminum or lead.

The U.S. Environmental Protection Agency (EPA) has explicit guidelines for acceptable levels of radionuclides in drinking water.[11] Their quick reference guide (Table 1-1) shows the maximum contaminant level (MCL) alongside a maximum contaminant level goal (MCLG), which is an enforceable goal of the agency regarding contaminant concentrations. The unit “mrem” is short for milli roentgen equivalent man (rem), which is a measure of the health effect of ionizing radiation on the human body. A picoCurie or “pCi” is a non-SI unit of radioactivity, and is equivalent to “the radium emanation in equilibrium with one gram of elemental radium.”

Table 1-1. Maximum Contaminant Level and Maximum Contaminant Level goals for drinking was as determined by the EPA[12]

Regulated Contaminants		
Regulated Radionuclide	**MCL**	**MCLG**
Beta/photon emitters*	4 mrem/yr	0
Gross alpha particle	15 pCi/L	0
Combined radium-226/228	5 pCi/L	0
Uranium	30 µg/L	0
*A total of 168 individual beta particle and photon emitters may be used to calculate compliance with the MCL.		

Although uranium has no known biological function, chemical and radiation effects can negatively affect biological systems. The route of exposure and the chemical species of uranium during exposure can have an impact on the degree of toxicity experienced. Currently it is assumed that any level of exposure to radioactivity has an incremental impact; this assumption is called the linear-no threshold (LNT). However, based on lower limit detection values and the difficulty to correlate to health and exposure data, it is questionable whether background levels of radiation contribute to the development of cancer.

The primary hazard of uranium for living organisms is its chemical toxicity. Chemical toxicity of uranium is heavily dependent on the speciation of uranium, which is also a major focus of this work. For instance, uranium equilibrated in hard water (with high concentrations of calcium or magnesium carbonate), forming the associated carbonate species, is much less bioavailable than uranium in softer water where hydroxyl species are dominant.[13] As for many other contaminants, the route of exposure for uranium greatly affects its toxicity, e.g. as inhalation has more severe effects than ingestion. Absorption during ingestion can be affected by uranium solubility. Hence, for this route the chemical form of uranium matters, as different uranium species have different solubilities.

1.3 Deep Geological Repositories

The most favored idea for long term storage of radioactive waste is its burial within a deep geological repository. Many of the sites under investigation have characteristics that can create a favorable environment for these harmful

radioactive materials. One important requirement is that the site should be situated below the water table, so that once nuclear waste canisters corrode, radioactive contaminants do not have a direct path into the biosphere. Another important site characteristic is the type of rock formation that will contain the waste itself. There are three top choices for geological media. First, high-strength rocks provide low porosity and permeability. These types of rocks include igneous, metamorphic and some sedimentary rocks. Second, mud rock or clay provide self-annealing properties. This means that if this material fractures, the gap will not be sustained over a meaningful time scale. Third, the last possible media could be rock-salt as it has similar characteristics to clays, specifically a low porosity.[14]

The proposed disposal site most popularized in the U.S. news and best known to the average individual is Yucca Mountain, Nevada. This site was in favor until it was deemed to be insufficient due to two inherent features: high facture transmissivity and high ground-water temperature.[15]

1.4 Engineered Barrier Systems

1.4.1 Main Idea

It is assumed that even within a well-designed repository, embedded canisters will eventually be compromised, and nuclear waste will be exposed. The three mechanisms driving this exposure are corrosion of the steel or copper canister, shear loads from incidences such as an earthquake, and impacts of isostatic loads possibly caused by future changes in the environment such as the formation of glaciers in the north. Located in the placement rooms (3) depicted in the image below (Figure 1-1), bentonite clay is the major component of the engineered barrier system surrounding the canisters embedded in the repository. The unique chemical properties of this material have shown great promise in retarding the mobility of uranium and other radionuclides.[16]

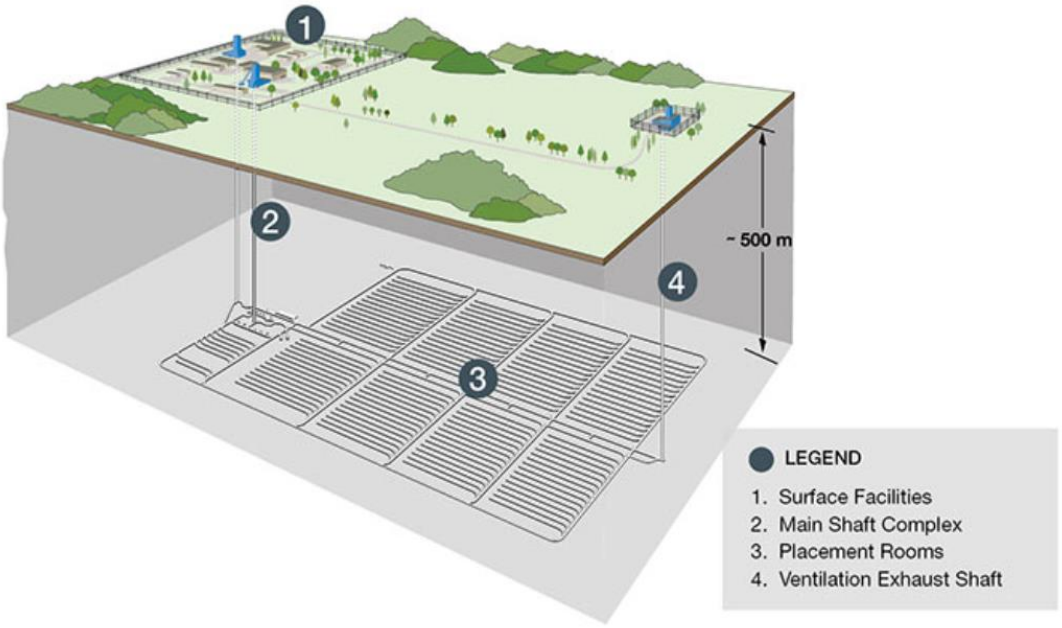

Figure 1-1. Repository design which will utilize a clay barrier system to retain nuclear waste.[16]

1.4.2 Bentonite

Bentonite is a geological, clay-rich material that has been proposed as a major component of engineered barrier systems in nuclear waste repositories. Bentonite's major component is montmorillonite clay, which will be discussed independently in the following section. However, it also contains a variety of mineral impurities such as quartz, feldspar, zeolites, and calcite.[17] Although this application would apply the use of a montmorillonite clay-rich bentonite, there are also other type of clayey rocks where the main clay species is illite or kaolinite. Bentonite is currently used in a variety of industrial applications based on its

properties; one example is its current use as a ground water barrier in landfills due to its low permeability and great sorbent properties.

1.4.3 Montmorillonite Clay

Montmorillonite is a smectite clay, which means that its internal layers consist of 2:1 tetrahedral octahedral sheets of alumina.[18] This clay has been studied for is potential sorption properties with respect to radionuclide mobility and nuclear waste storage. For instance, montmorillonite is able to adsorb uranium quite well compared to other materials. Montmorillonite is ideal for the application as a barrier material, as it swells in the presence of water and the large pores are closed off. Flow is then limited by the nanometer sizes pores in the interlayer spaces. As a result, radionuclide transport in bentonite is expected to be limited to diffusion processes, while advective transport can be excluded.

Montmorillonite's negative surface sites are associated with cations, such as sodium, calcium or potassium. The sodium variety is of particular interest for this application, as it expands heavily when it becomes wet. This characteristic will drastically reduce the possibility of fast advective transport of radioactive contaminants through a potential barrier. The negatively charged sites on montmorillonite surfaces are also responsible for the sorption of cations (e.g., Na^{+}, K^{+}, Ca^{2+}) and radioactive contaminants.

Based on its structure, montmorillonite provides two types of surface sites for contaminant sorption. First, sites on basal montmorillonite surfaces are relevant for cation exchange reactions at low pH and ionic strength conditions.

Second, surface sites on montmorillonite edge surfaces are involved in surface complexation reactions, which can occur over a wide range of pH and ionic strength conditions. In this study, only uranium systems with fairly high ionic strength conditions (0.1 M NaCl background electrolyte) are evaluated; hence cation exchange reactions can be neglected in these systems.

Radionuclide transport within the packed clay is heavily dependent on solution conditions, as we will see in detail later in this study. In addition, transport is also known to occur through interlayer pores (macropores) within clay particles if other conditions are met.[19] The interior to these pores is represented by a diffuse layer with an associated negative charge which can have an effect on ionic transport within the particles themselves.

1.4.4 Surface Complexation onto Montmorillonite

Uranium has been understood to chemically complex with montmorillonite edge sites, which can possess negative charge due to their chemical functionality. An example of a proposed structure of U(VI) sorbed to the smectite structure of montmorillonite is given below (Figure 1-2).[20]

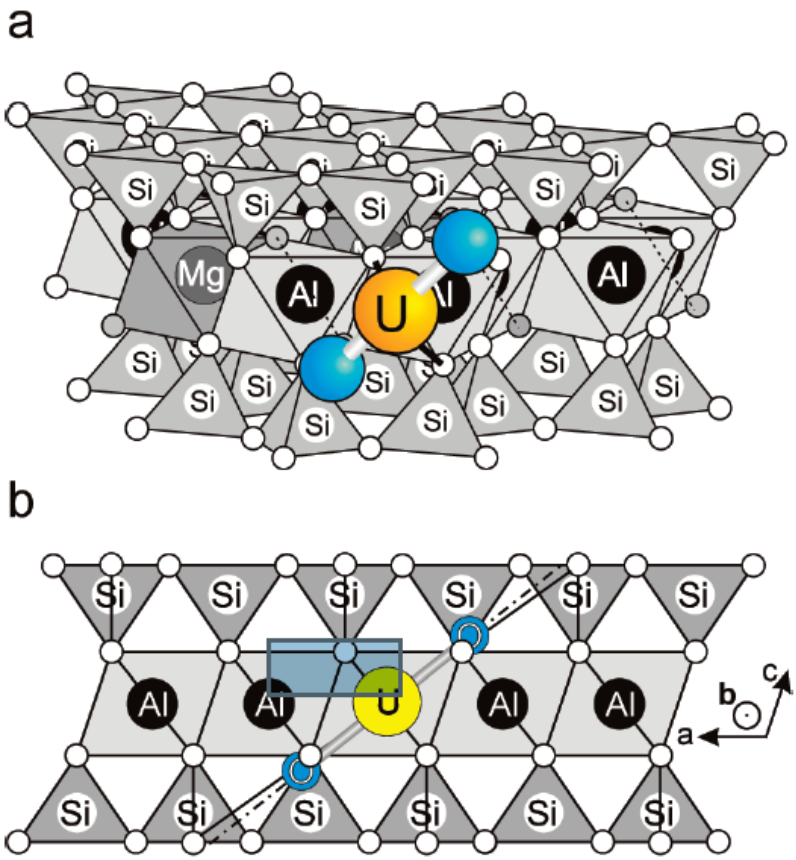

Figure 1-2. Proposed structures for U(VI) sorption on montmorillonite based on EXAFS data. A) front view. B) side view.[20]

Different types of surface complexation models have been developed, with increasing complexities with regards to their description of electrostatic surface potentials (Figure 1-3). The first image shows a non-electrostatic model (no correction due to electrostatic potential). The second image represents a very simple model, referred to as the constant capacitance model, where the electrostatic potential decreases linearly with distance from the surface. Third, the electrostatic double layer model is depicted with an asymptotic dependence of the electrostatic potential on the distance from the clay surface. Last, the triple

layer model is shown, which considers further complexities of the electrical structure at the surface.

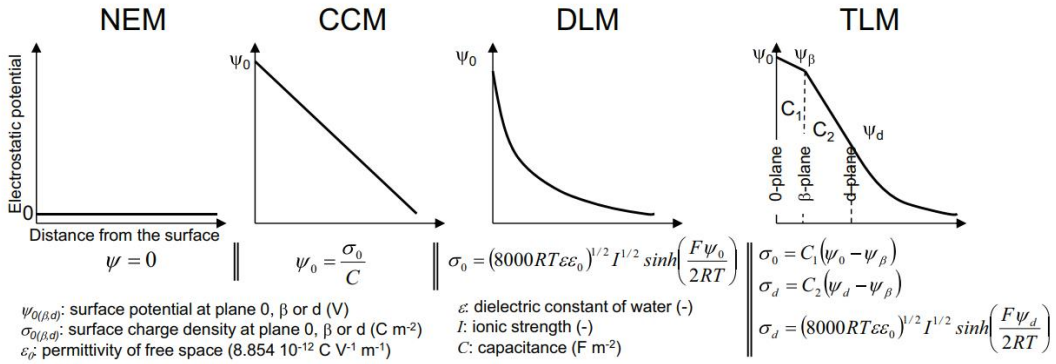

Figure 1-3. Electrostatic surface potential for different surface complexation models; from left to right: A) non-electrostatic model (NEM), B) constant capacitance model (CCM), C) double-layer model (DLM), D) triple-layer model (TLM)[21]

These types of surface complexation models were originally developed for mineral oxide surfaces, which are far less complex than montmorillonite surfaces. In montmorillonite, edge surface sites are further affected by their electrochemical interactions with basal surface sites. Hence, in a recent publication, an additional phenomenon has been taken into account, which is called the spill-over effect.[22] This effect results from the fact that the electrostatic surface potential that exists on basal planes of the clay can affect the electrostatic potential of clay edge sites, where surface complexation reactions occur. A diagram of this effect is shared below and reproduced from a presentation with the authorization of Dr. Christophe Tournassat (Figure 1-4). This latest finding has led to a new concept for montmorillonite surface

complexation models, which can robustly simulate the majority of experimental data collected to date.[23]

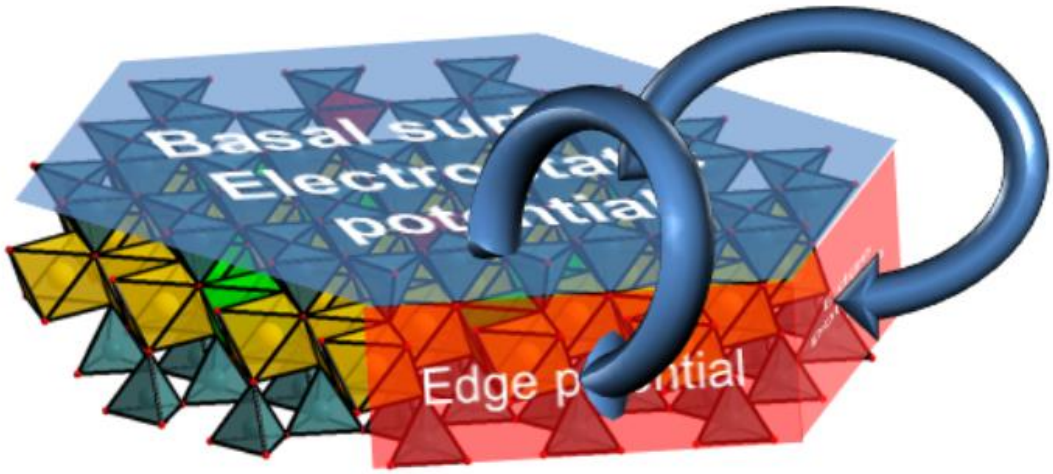

Figure 1-4. Diagram showing the electrostatic potential of basal montmorillonite surfaces sites spilling over to contribute to the edge sites' electrostatic potential[22]

With the surface complexation modeling task in this study, we will compare predictions of U(VI) sorption onto montmorillonite between two types of models: (1) a model solely based on surface chemical structure without consideration of the electrostatic potential, and (2) a model which also considers the surface electrostatic potential as well as the spillover effect.

1.4.5 Transport Pathways in Bentonite

Bentonite in the form of clay liners has long been utilized as a barrier material for waste disposal sites such as waste landfills. Bentonite has two main

pathways by which solubilized uranium can be transported through a particle or barrier. The first is diffusion through the macro-porosity between clay particles. This route of transport quickly becomes irrelevant under the expected repository conditions due to the swelling of the clay. Clay swelling decreases the contributions of macro-pores to the overall clay porosity, hence allowing virtually no diffusion through interstitial spaces.[24]

Hence, the key identified pathway by which molecules can be transported through swollen bentonite/montmorillonite are the pores that exist within the clay particles themselves, namely clay interlayers spaces. The interlayer pores are 1-2 nm in diameter (Figure 1-5)[25], and filled with cations to counter balance negative basal surface charges. Given these highly negatively charged basal interlayer environments, anionic solution species may become partially or fully excluded from interlayer water, which can, as will be shown later, impede the diffusion of anionic solution species.

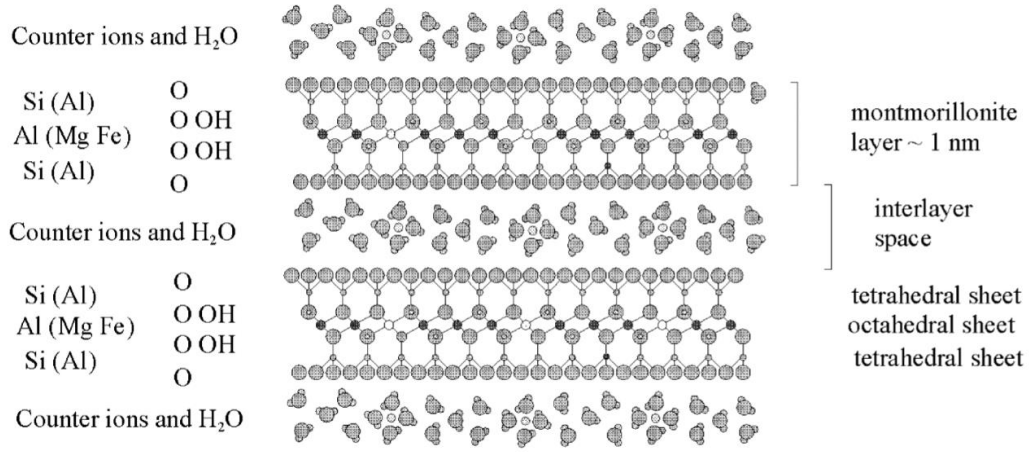

Figure 1-5. Structural diagram of two layers in a smectite mineral with the interlayer pore space depicted.[25]

1.5 Uranium(VI) Solution Chemistry

When elemental uranium(VI) is dissolved in an aqueous solution open to the atmosphere, it forms a variety of species with hydroxides and carbonates. The total U(VI) concentration in solution remains constant, while U(VI) can form a variety of solution species depending on chemical solution conditions. For instance, pH, dissolved inorganic carbon and other solutes can have a strong effect on the distribution of U(VI) between various species. Some of these species can be measured spectroscopically, but this approach is often costly and time consuming[26,27]. There are also low U(VI) concentration thresholds, under which analytical measurements are not possible.

It is therefore very helpful to describe U(VI) solution speciation in these systems based on computer-based calculations using existing thermodynamic data on U(VI) complexation reactions. Once an input file is built, it is quite simple to adjust modeling parameters to observe changes in speciation output, allowing the user to simulate many different conditions quickly and efficiently.

Other researchers have studied U(VI) speciation for a variety of reasons, for instance focusing on waste water from mining operations, radionuclide release events, as well as the development of storage solutions.[28,29] In this work, we will use U(VI) solution speciation simulations in order to better understand later U(VI) sorption and diffusion modeling results. For this purpose, we will present U(VI) speciation diagrams first, and then revisit them in later chapters. Hence, the computational results of these U(VI) solution speciation simulations

under various system conditions will provide the first major portion of this thesis. Last, these U(VI) speciation results are also relevant for subsequent laboratory sorption and diffusion experiments, which are part of a companion study.

1.6 Uranium(VI) Sorption onto Montmorillonite

Uranium(VI) sorption onto montmorillonite clay has been studied by a variety of researchers[30,31,32,33,34,35,36] The experimental set-up and procedures are often quite similar. A solution which has been tailored to the conditions to be investigated is then put into contact with a known quantity of clay, and equilibrated over time to allow for sorption reactions to occur. The solution phase is then separated from the clay, and the uranium concentrations remaining after sorption equilibration are quantified.

Uranium(VI) sorption is usually studied as a function of pH and other variables such as total U(VI) concentration and inorganic carbon aqueous concentration.[37,38] Fewer studies have evaluated U(VI) sorption in the presence of bentonite impurities like calcite.[39] However, this detail is important as calcite is always present in the bentonite material intended for future engineered barrier systems. Ionic strength is often fixed at a relatively high concentration through a background electrolyte, so that experimental changes in uranium(VI) solution concentrations have no substantial effects on the total ionic strength conditions in the system. Sorption is allowed to proceed for a time approximating steady state, roughly 48 hours or more. Calcium can be added in the more soluble form of

calcium chloride or can be evaluated by allowing for the dissolution of calcite minerals over time.

This modeling work utilizes some non-adjustable modeling parameters for site types and protolysis reactions from two previous publications, Marques et al. (2012) (which were drawn from an earlier publication by Bradbury and Baeyens, 1997) and Tournassat et al. (2018). These two models are distinct from each other in that the Marques model only takes into account chemical equilibrium constants to describe surface complexation reactions. The Tournassat model, however, also includes electrostatic contributions from the surface as well as the previously discussed spillover effect. The Marques model includes numerous surface site types, and is again different in that it includes the direct sorption of uranium-carbonate species. In contrast, the Tournassat model only includes one surface site type with three chemical surface reactions, but no direct surface reactions including uranium-carbonate solution species. The later U(VI) sorption chapter will cover the differences in simulated U(VI) sorption between these two models, and include a discussion on how the U(VI) solution speciation for a given set of conditions relates to its sorption behavior.

1.7 Uranium(VI) Diffusion Studies

For a future nuclear waste repository, it will be integral to know when uranium will first breech a barrier material, as well as the uranium flux across the barrier at the given conditions. This phenomena and behavior has been studied both by uranium diffusion experiments and modeling studies which have led to

an improved understanding in this area.[40,41] In this work, we will utilize a surface complexation model as well as a modern understanding of diffuse double layers on clay surfaces. This will allow us to determine not only the retardation of U(VI) transport based on its sorption, but also the effects of chemical solution conditions on U(VI) flux through the barrier material.

1.8 Summary

In order to fully understand uranium mobility in engineered barrier systems of future nuclear waste repositories, it is first imperative to know what U(VI) solution species are present at the given chemical conditions. Knowing the size and more importantly the charge of U(VI) solution species allows us to predict U(VI) sorption and diffusion behavior. Furthermore, simulations of U(VI) sorption behavior will provide insights into expected trends for U(VI) retardation, and hence one of the two important parameters describing U(VI) transport. Overall, this study will help us to gain a more holistic understanding of uranium(VI) mobility in these clay materials in the presence of a calcite impurity.

2.0 Modeling Methods – General Introduction

2.1 PHREEQC

PHREEQC is a software package developed by the United State Geological Survey[42], which allows for the computation of chemical speciation in solutions and on surfaces with components defined by the user. The software works by referencing a periodically updated geochemical database of accepted equilibrium constants and their chemical reactions to simulate all interactions between of the chemical components in the system of interest. As a first step, an input file is created, which is then executed by the software. The resulting output files then contain the results of the chemical speciation calculation, which can be plotted with Excel or other graphing programs. Many more advanced calculations can be accomplished within PHREEQC which allow for the summation of charged species and the eventual creation of charge speciation diagrams.

2.2. Beginner's All-purpose Symbolic Instruction Code (BASIC)

Basic is a general-purpose programming language and was originally invented in 1964. It is included as an embedded interpreter by the original creators of PHREEQC. It generally consists of instructions on numbered lines along with formulas that may include variables and operators for the expressed purpose of simplifying instructions that would have to be explicitly typed out in PHREEQC. For the purpose of this work, BASIC was extensively used in order to truncate instructions within PHREEQC and accomplish such feats as looping

EQUILIBRIUM_PHASES simulations across pH ranges while incrementally increasing values. It can also be harnessed to express PHREEQC's internal graphing functionality but due to the ability to export data sets and the wide range of available graphic software this capability was not utilized. A detailed description of BASIC functionality used in this work can be found in the subsequent appendices.

2.3 Graphic Layout Engine (GLE, http://www.gle-graphics.org/)

GLE is a text-based graphing software which allows for the creation of high-quality images of data sets using very specific formatting instructions. The images can be exported in Enhanced Metafile (EMF) format and contain the image as a vector graphic to allow for high quality reproduction and the ability to scale the image cleanly. GLE employs LaTex, a plain text word processing software that then applies formatting instructions in the output (the opposite of "what you see is what you get" word processors like Microsoft Word). GLE is similar in that updated instructions to the graphical output will not become apparent until the working programming file is saved. All graphs within this publication were produced through the GLE software.

GLE was also utilized to perform the diffusion calculations within this work. To reproduce these results the user must have GLE installed and execute an appropriate diffusion file located in the same folder as the associated Diff_eq.gle file located in the Diffusion folder within the modeling code appendix.

2.4 Source Code Repository

In order to reproduce any modeling accomplished in this work, the appropriate source code has been compiled within a zipfile that will be hosted by the CSUEB library in conjuncture with this thesis. The zipfile contains different folders for speciation, sorption, and diffusion and the user will have to navigate to each and familiarize themselves with PHREEQC or GLE including the correct installation methodology in order to reproduce these specific results.

3.0 Chemical Speciation

3.1 Introduction

Chemical speciation is defined as the distribution of a given element amongst different chemical forms, called chemical species, in a system. When an element is present in aqueous solution, it can react with a variety of other elements to form specific species, with each having its own characteristics. This species character can further determine other important contaminant properties, such as its sorption to mineral surfaces, mobility and toxicity in the environment.

The results from speciation calculations are useful for two main reasons: First, they support the selection of specific chemical conditions and the interpretation of results for a companion experimental study evaluating the effects of calcite impurities on U(VI) sorption and diffusion behavior. Second, these results will also allow us to choose the chemical conditions in later U(VI) sorption (Chapter 5) and diffusion (Chapter 6) models that might be most useful in testing specific hypotheses. In this context, the aspects of U(VI) speciation that are of specific interest the U(VI) solution complexes, and more importantly their overall charge. Both parameters will become important later on in this work in order to understand U(VI) sorption and transport characteristics.

For these simulations carried out in the geochemical modeling software PHREEQC we will vary system conditions, such as pH, partial pressures of atmospheric CO_2 and calcium or calcite concentrations in order to characterize their effects on U(VI) equilibrium solution speciation. Four different total U(VI) concentrations are used during the simulations of U(VI) speciation: 0.1, 1.0, 2.4

and 10 µM. These concentration levels are chosen primarily based on experimental considerations, since they are relatively low, which reduces risks of accidental radiation doses, but are still within the detection limits of liquid scintillation counters. In addition, they are above and below U.S. EPA drinking water limits of 30 µg/L.[12]

Initially, uranium(VI) speciation results will be presented as chemical speciation diagrams on log-log scales (pC-pH diagrams) with similar y-axis scales for all diagrams so that all important species may be viewed, even if their concentrations are relatively low. This similar axis scaling will allow for a direct comparison between species under each condition across the pH range probed. In addition to traditional chemical speciation diagrams, we also introduce a new form of so-called charge speciation diagrams.

In the following subsections, a wide variety of speciation diagrams with increasing levels of complexity will be discussed. The aim is to slowly build an understanding of how each component (pH, uranium, carbonate and calcite concentrations) affect U(VI) solution speciation, which must be understood before progressing to sorption and diffusion modeling in later chapters. In addition, U(VI) solution speciation will be the first major component to be evaluated when tailoring repository conditions or when determining the effects of changing conditions on the mobility of U(VI) in the environment.

3.2 Chemical Speciation of Uranium in PHREEQC

3.2.1 PHREEQC Database of Reactions and Equilibrium Constants

In order for PHREEQC to calculate U(VI) solution speciation for a given system, equilibrium constants for U(VI) complexation reactions in solution must be referenced from a database as discussed in the Methods Section (Chapter2). The table below (Table 3-1) summarizes all of the hydrolysis and carbonate complexation reactions and their equilibrium constants for the uranyl ion (UO_2^{2+}) that are used within the PHREEQC calculations. The reactions and values listed in Tables 3-1 and 3-2 are extracted from the ThermoChimie thermodynamic database (https://www.thermochimie-tdb.com/), and are current at the publication date of this thesis.

Table 3-1. Uranium(VI) hydrolysis reactions (ThermoChimie_PHREEQC_eDH_v9b0.dat)

Hydrolysis Reactions	**log K**
$UO_2^{2+} + H_2O \rightleftharpoons UO_2(OH)^+ + H^+$	-5.25
$UO_2^{2+} + 2H_2O \rightleftharpoons UO_2(OH)_2 + 2H^+$	-12.15
$UO_2^{2+} + 3H_2O \rightleftharpoons UO_2(OH)_3^- + 3H^+$	-20.25
$UO_2^{2+} + 4H_2O \rightleftharpoons UO_2(OH)_4^{2-} + 4H^+$	-32.40
$2UO_2^{2+} + H_2O \rightleftharpoons (UO_2)_2(OH)^+ + H^+$	-2.7
$2UO_2^{2+} + 2H_2O \rightleftharpoons (UO_2)_2(OH)_2^{2+} + 2H^+$	-5.62
$3UO_2^{2+} + 4H_2O \rightleftharpoons (UO_2)_3(OH)_4^{2+} + 4H^+$	-11.9
$3UO_2^{2+} + 5H_2O \rightleftharpoons (UO_2)_3(OH)_5^+ + 5H^+$	-15.55
$3UO_2^{2+} + 7\ H_2O \rightleftharpoons (UO_2)_3(OH)_7^- + 7H^+$	-32.20
$4UO_2^{2+} + 7\ H_2O \rightleftharpoons (UO_2)_4(OH)_7^+ + 7H^+$	-21.90

In Table 3-1, every reaction involves one or more uranyl ions and water, often to form various polyuranic and/or polyhydroxyl species. The other product on the right hand-side of the equations is one or more protons, indicating that all of these chemical equilibria are governed by the pH conditions in the system. Due to this relationship, pH plays an integral role in the outcome of U(VI) solution speciation.

Table 3-2. Carbon dioxoide reactions in aqueous solution (ThermoChimie_PHREEQC_eDH_v9b0.dat)

CO_2 Aqueous Dissolution Reactions	**log K**
$2H^+ + CO_3^{2-} \rightleftharpoons CO_2(g) + H_2O$	16.680
$H^+ + CO_3^{2-} \rightleftharpoons HCO_3^-$	10.330
$2Na^+ + CO_3^{2-} \rightleftharpoons Na_2(CO_3)$	1.120
$Na^+ + H^+ + CO_3^{2-} \rightleftharpoons Na(HCO_3)$	10.080

Table 3-3. Uranium(VI) complexation reaction with dissolved carbon dioxide (ThermoChimie_PHREEQC_eDH_v9b0.dat)

Uranium(VI) Carbonate Reactions	**log K**
$UO_2^{2+} + CO_3^{2-} \rightleftharpoons UO_2(CO_3)^0$	9.94
$UO_2^{2+} + 2CO_3^{2-} \rightleftharpoons UO_2(CO_3)_2^{2-}$	16.61
$UO_2^{2+} + 3CO_3^{2-} \rightleftharpoons UO_2(CO_3)_3^{4-}$	21.84
$2UO_2^{2+} + CO_3^{2-} + 3H_2O \rightleftharpoons (UO_2)_2CO_3(OH)_3^- + 3H^+$	-0.860
$3UO_2^{2+} + CO_3^{2-} + 3H_2O \rightleftharpoons (UO_2)_3CO_3(OH)_3^+ + 3H^+$	0.66

For solutions in contact with atmospheric CO_2, U(VI) complexation reactions with dissolved carbonate species (Table 3-2) now also have to be included. In Table 3-3, each of the reactions involve carbonate, and some also involve water as reactants. In open systems, the concentrations and speciation of dissolved carbonate are also pH dependent (Table 3-2). This means that all U(VI)-carbonate complexation reactions will be affected by the available amount of CO_2 in solution, which is again dependent on pH and the partial pressure of CO_2 in the system. Last, in the presence of a calcite ($CaCO_3$(s)) impurity, we also have to include calcite dissolution/precipitation reactions and the formation of ternary Ca-uranium(VI)-carbonate species in solution (Table 3-4).

Table 3-4. Calcite reactions with reactants found in U(VI) solutions (ThermoChimie_PHREEQC_eDH_v9b0.dat)

Calcite Reactions	**log K**
$Ca^{2+} + CO_3^{2-} \rightleftharpoons CaCO_3$	3.4
$Ca^{2+} + H_2O \rightleftharpoons Ca(OH)^+ + H^+$	-12.780
$Ca^{2+} + H^+ + CO_3^{2-} \rightleftharpoons Ca(HCO3)^+$	11.43
$Ca^{2+} + UO_2^{2+} + 3CO_3^{2-} \rightleftharpoons CaUO_2(CO_3)_3^{2-}$	27.18
$2Ca^{2+} + UO_2^{2+} + 3CO_3^{2-} \rightleftharpoons Ca_2UO_2(CO_3)_3$	30.70

3.2.2 Example of a Speciation Diagram: U(VI) Speciation in the Absence of CO_2 (Closed System)

In the following example, we will introduce how a chemical speciation diagram is evaluated for the speciation of 1.0 µM U(VI) in a background electrolyte (0.1M NaCl) typically used in sorption experiments of a companion study, and in the absence of atmospheric CO_2. A fairly simple diagram is depicted (Figure 3-1) showing a variety of complexes that are formed as pH increases along the x-axis from acidic to basic conditions. At any given pH, the fractions of individual species, can be added up to the total U(VI) concentration present in the system, in this case 1.0 µM. The complex speciation diagram can be evaluated from low to high pH in order to recognize which species become dominant as pH rises. A minor species, UO_2Cl^+ is formed at acidic conditions when uranium complexes with free chloride ions in solution, which were added with the background electrolyte (0.1 M NaCl). Otherwise, U(VI) speciation in this closed system is controlled by the formation of U(VI)-hydroxide complexes.

These speciation diagrams allow us to make observations, such as that UO_2^{+2} and $UO_2(OH)^+$ are both present at the same concentration at a pH around 5.5. Below this pH value, UO_2^{+2} is clearly the dominant species, and above $UO_2(OH)^+$ dominates until $(UO_2)_2(OH)_5^+$ takes over briefly between pH 7.0 and 7.5. After this a neutral species, $UO_2(OH)_2$ prevails until roughly pH 8, where a negative species arises ($UO_2(OH)_3^-$). Charge is an important characteristic of any chemical system. Even in this simple solution, a variety of charged U(VI) species appear with overall charges ranging from +2 to -1. This change in overall charges

for U(VI) solution species from cationic species at acidic pH toward anionic species at basic pH will become very important in later sections focusing on U(VI) sorption (Chapter 5) and diffusion (Chapter 6).

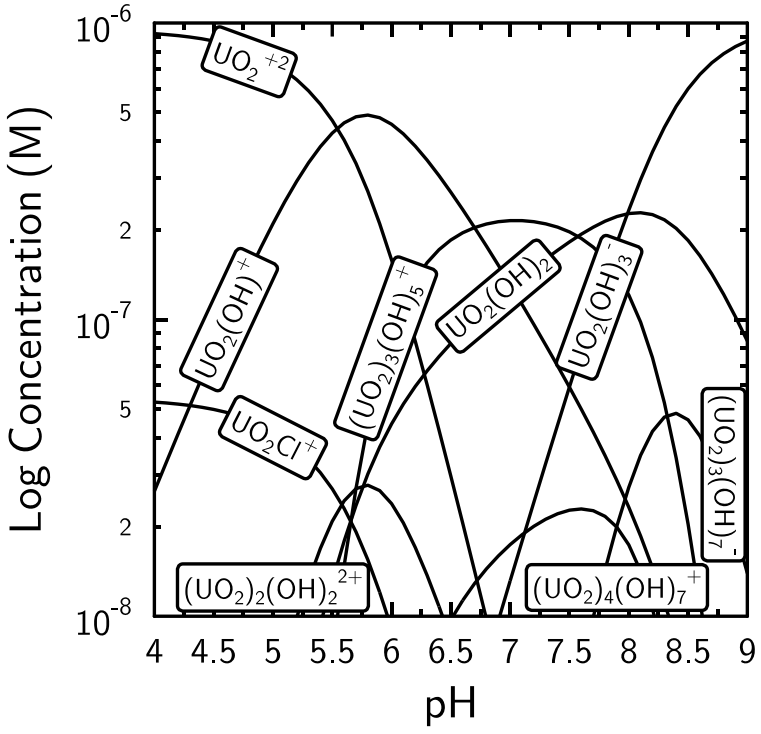

Figure 3-1. Uranium(VI) speciation for U(VI) = 1.0 µM, pCO_2 = 0, I = 0.1 M NaCl, no calcite.

3.3 Modeling Results

3.3.1 Uranium Speciation as a Range of Total U(VI) Concentrations in a Closed System

In this section, simulations were accomplished across 0.1, 1.0, 2.4 and 10 µM U(VI) only in the presence of the standard 0.1 M NaCl background electrolyte. As described earlier, uranium(VI) speciation in a closed system is primarily controlled by its complexation with hydroxide anions. The diagrams become observably more complex as the concentration of uranium in the system increases (Figure 3-2), forming greater quantities of polynuclear species that are absent at lower U(VI) concentrations. For example, if a species such as $(UO_2)_3(OH)_5^+$ is tracked, at a total U(VI) concentration of 0.1 µM it is one of the most minor species in the system only appearing between pH 5.5 and 8. As the total uranium concentration increases from 0.1 µM to 10 µM, not only does the pH range where this species is relevant broaden from ~pH 5-9; it also becomes the dominant species in the system over most of these conditions. This initial example shows the increasing complexity that can arise when studying U(VI) speciation as a function of chemical system conditions, and highlights the need for computer-based modeling when studying such multifaceted systems.

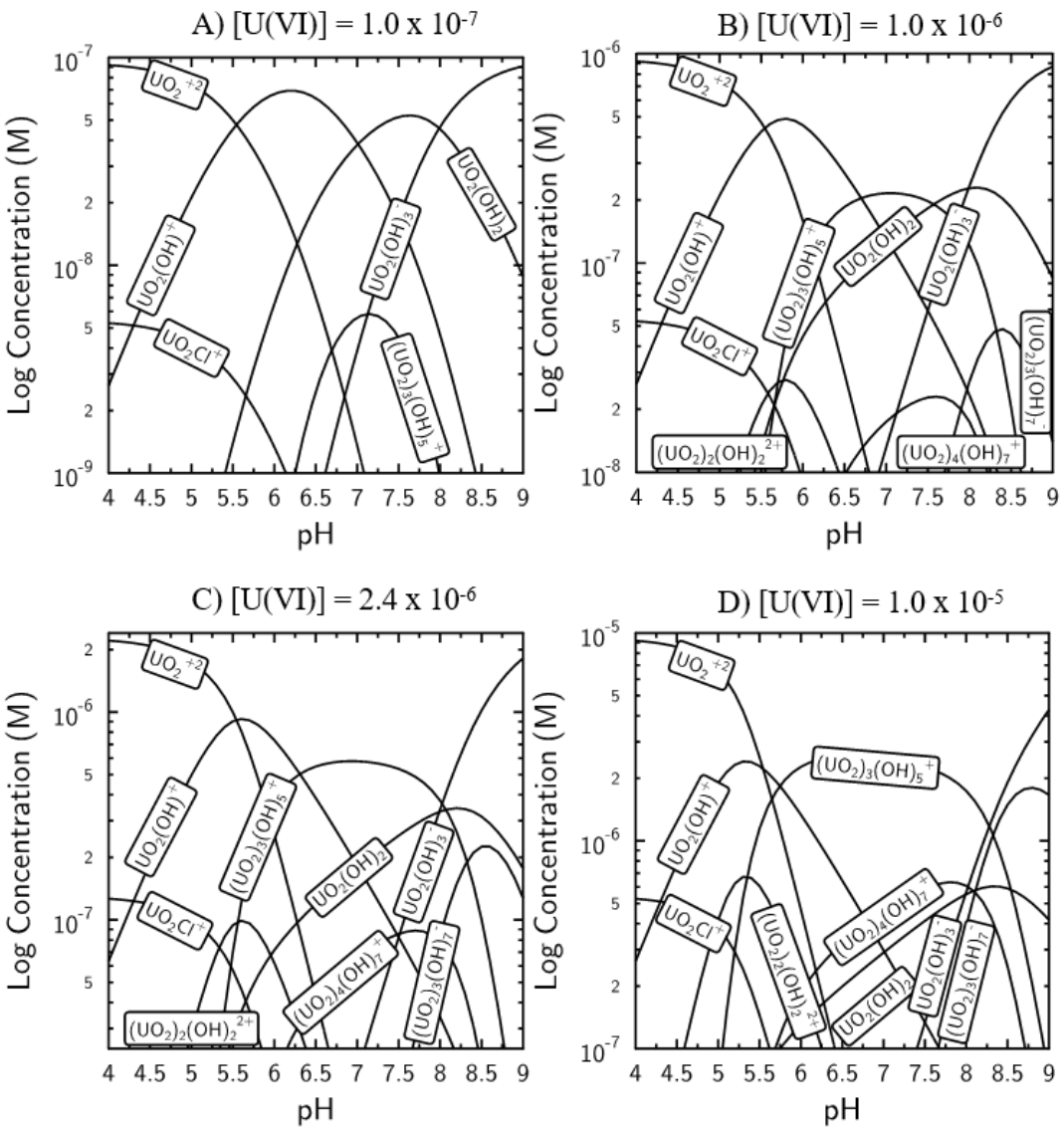

Figure 3-2. Uranium(VI) speciation in a closed system as a function of total U(VI) solution concentration. [U(VI)] = A) 0.1, B) 1.0, C) 2.4 and D) 10 μM. I = 0.1 M NaCl.

In order to more easily evaluate speciation diagrams, the output files were manipulated with an instruction to sum all similarly charged species. The resulting charge species concentrations were plotted in a similar fashion to the more classic diagrams (Figure 3-3). These figures will be referred to as charge speciation diagrams for the rest of this work. Viewing these diagrams allows for a quick determination of the dominant charge of the species present in a given pH range, and also to determine at which pH the system shifts from cationic to neutral and anionic species. As the concentration of U(VI) increases in the closed systems simulated, the +2 charge pH window and dominance remains relatively constant. The same can be observed for the -1 charged species in the most basic pH range. The biggest change comes with respect to the neutral and +1 charged species, where the amount of neutral species continues to diminish with increased U(VI) concentration while +1 charged species appear in higher concentrations across a greater pH window. This is mainly due to the high concentrations of $(UO_2)_2(OH)_5^+$ that form with increasing concentrations of uranium(VI).

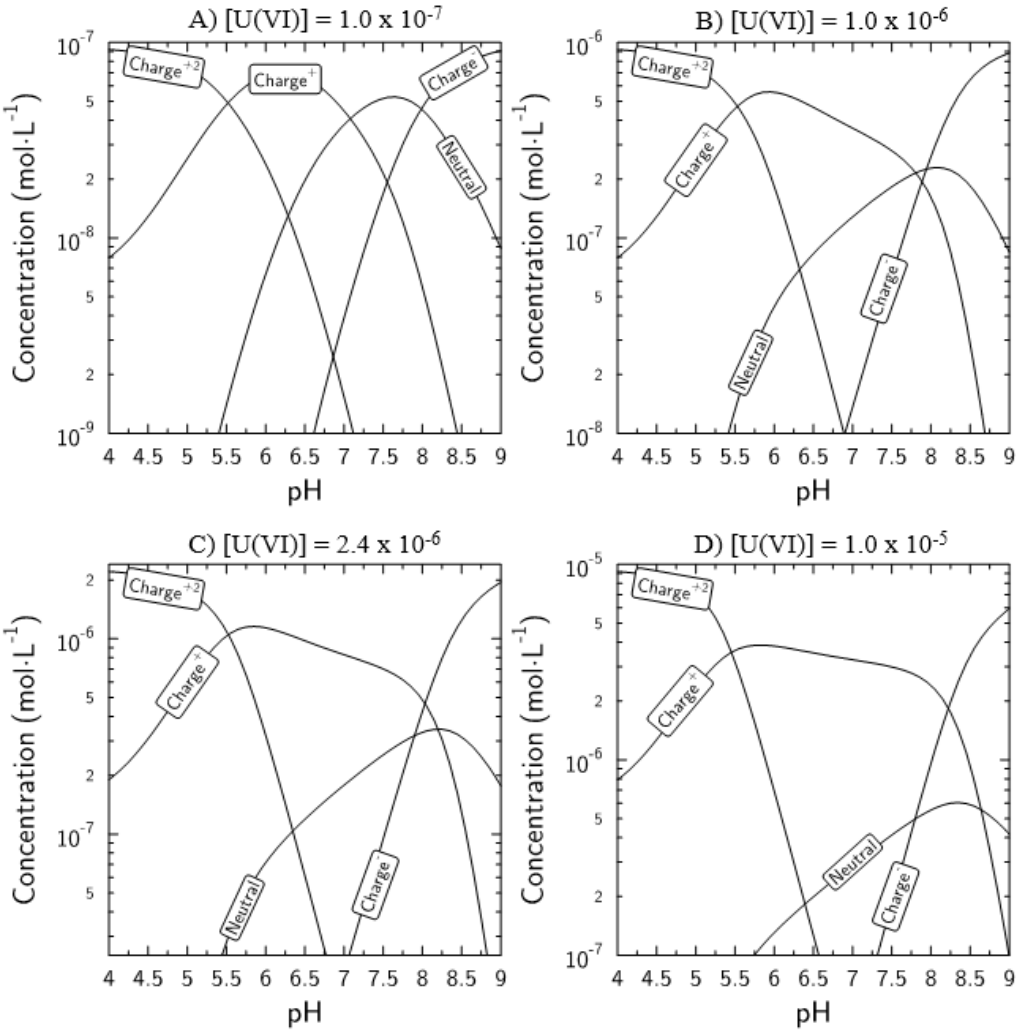

Figure 3-3. Charge speciation of uranium(VI) solutions closed to the atmosphere at [U(VI)] = A) 0.1, B) 1.0, C) 2.4 and D) 10 uM. I = 0.1 M NaCl.

3.3.2 Carbonate Speciation in the Presence of a Background Electrolyte Solution

Before discussing the effects of carbonate on uranium(VI) solution speciation, it is important to understand the trends of inorganic carbon species in solution across the pH scale evaluated (Table 3-2). From Figure 3-4, it can be seen that inorganic carbon concentrations in solution increase substantially with increasing pH. When CO_2(g) dissolves in water, it ultimately forms aqueous CO_2 and carbonic acid (H_2CO_3) with hydrogen ions present in water. As pH increases, H_2CO_3 can then subsequently deprotonate to create bicarbonate (HCO_3^-), and later carbonate (CO_3^{2-}). Due to the presence of the NaCl background electrolyte, these anions combine with Na^+ ions present in solution to form dissolved sodium (bi)carbonate species ($NaHCO_3$ and $NaCO_3^-$). This observed increase in total inorganic carbon concentrations in solution will help to understand the formation of uranium-carbonate species in simulations with increasing partial pressures of CO_2 (pCO_2 = -3.45, -2, and -1.697).

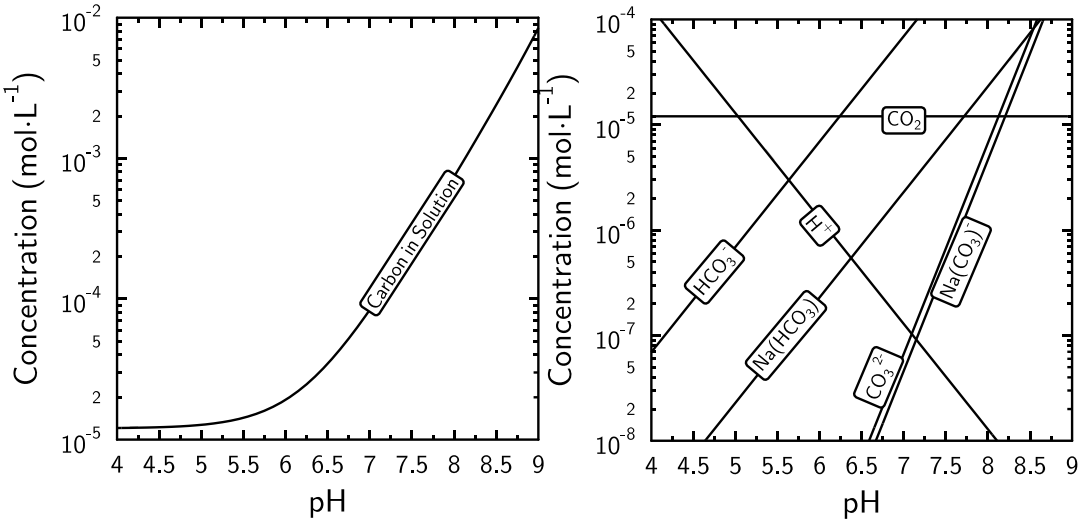

Figure 3-4. Inorganic carbon concentrations in solution at atmospheric partial pressure shown as total inorganic carbon (TIC, left) and broken down by species (right). The CO_2(aq) species defined in PHREEQC represents the sum of CO_2(aq) and H_2CO_3(aq).

3.3.3 Effects of CO_2 (g) on U(VI) Solution Speciation: Fixed U(VI), Variable pCO_2

With the following sets of simulations, we investigated the effects of varying partial pressures of CO_2 (g) on U(VI) solution speciation over a range of pH conditions. A range of partial pressures of CO_2 was simulated to include values that are relevant for experimental, as well as repository conditions, and to fully understand the resulting changes in U(VI) speciation. First, the atmospheric pressure of carbon dioxide (pCO_2 = -3.45) was chosen as it is the most common condition in experiments repository conditions exhibit commonly higher partial pressures of CO_2. Hence, 1 and 2 % CO_2 conditions (pCO_2 = -2 and -1.697) were also investigated. Uranium(VI) speciation can be calculated in the presence of CO_2 as described in detail in the input files shown in the Appendix D. These simulations can be accomplished in a variety of ways, but in this study the keyword EQUILIBRIUM_PHASES was chosen to simulate U(VI) solution speciation in equilibrium with CO_2 in the atmosphere.

To be more specific, simulations were based on the use of the SOLUTION, EQUILIBRIUM_PHASES, and SELECTED_OUTPUT keywords (Figure 3-5). First a solution containing uranium(VI) and the background electrolyte (NaCl) is created in the model. Then, the output species are defined so that each relevant solution complex will have a column in the output table. Lastly, the solution is subjected to a BASIC loop which allows us to fix the pH and to equilibrate the chosen partial pressure of CO_2 with the previously created solution. The resulting species concentrations are then plotted against pH to create the speciation diagram.

```
DATABASE ThermoChimie_PHREEQC_eDH_v9b0.dat

PHASES #must have this phase relationship to control
Fix_pH #pH in EQUALIBRIUM_PHASES
H+ = H+
log_k 0

SELECTED_OUTPUT
 -reset false
 -file JCP.loop1
USER_PUNCH  #utilized to punch all to file named above (JCP.loop1)
 -start
1150   punch eol$ + 'SOLUTION 1' #Initial Solution
1155   punch eol$ + ' pH 7 '
1157   punch eol$ + ' pe 10 '
1160   punch eol$ + ' Na 100'  #electrolyte to control
1170   punch eol$ + ' Cl 100 charge' #ionic strength
1180   punch eol$ + ' U(6) 0.001' #uranium concentration in mM
1181   punch eol$ + 'END'

1185   punch eol$ + 'SELECTED_OUTPUT'
1186   punch eol$ + '-file 1e-6 U(VI) Closed.prn'
1187   punch eol$ + '-molalities UO2+2 UO2(OH)+ UO2(OH)2 UO2(OH)3-
UO2(OH)4-2  (UO2)2(OH)+3  (UO2)3(OH)4+2  (UO2)3(OH)5+  (UO2)3(OH)7-
(UO2)4(OH)7+   (UO2)2(OH)2+2  UO2Cl+ UO2Cl2 UO2(CO3)  (UO2)3(CO3)(OH)3+
(UO2)3(CO3)6-6  (UO2)2(CO3)(OH)3-  (UO2)11(CO3)6(OH)12-2  UO2(CO3)2-2
UO2(CO3)3-4    Ca2UO2(CO3)3  CaUO2(CO3)3-2'
1190 for j = 3 to 10 step 0.05 #pH range evaluated every 0.05 incraments
1195   punch eol$ + ' USE SOLUTION 1'
1200   punch eol$ + ' EQUILIBRIUM_PHASES 1'
1201   punch eol$ + ' Fix_pH ' + str$(-j) + 'NaOH 10' #references j above
1202   punch eol$ + ' CO2(g) -3.45 10' #partial pressure, moles
1203   punch eol$ + 'END'
1204 next j

 -end
SOLUTION 0
END
```

Figure 3-5. Input file used to simulate the speciation of 1 µM U(VI) equilibrated with atmospheric CO_2 across the pH range from 3 to 10 using pH increments of 0.05.

Across the range of CO_2 concentrations evaluated in models with a total U(VI) concentration of 1 µM, U(VI) solution speciation changes drastically (Figure 3-6). At atmospheric pressures of CO_2, two species, $UO_2(OH)_2$ and $UO_2(OH)_3^-$,

become insignificant due to domination of carbonate species in this pH range. However, other hydroxide species appear, $(UO_2)_2(OH)_2^{+2}$ and $(UO_2)_3(OH)_5^{+}$, as well as four new uranium carbonate species (UO_2CO_3, $(UO_2)_2(CO_3)(OH)_3^{-}$, - $UO_2(CO_3)_3^{-4}$, and $UO_2(CO_3)_2^{-4}$).

As CO_2 partial pressure continues to increase, more CO_2 is forced into the system causing additional complexation reactions between uranyl and carbonate species. As a result, many of the minor species seen previously disappear leading to the dominance of a few carbonate species UO_2CO_3, $UO_2(CO_3)_2^{-2}$, $(UO_2)_2(CO_3)(OH)_3^{-}$ at high pH. For instance, the first figure on the top left (Fig. 3-6A) shows the insignificant concentrations of carbonate species present in a closed uranium(VI)-electrolyte system. At atmospheric CO_2 (Fig. 3-6B), a few U(VI)-carbonate complexes appear toward neutral pH, as CO_2 dissolves more readily in neutral and basic solutions. The first carbonate species becomes dominant at pH ~6.4 ($(UO_2)_2(CO_3)(OH)_3$). This species is a large carbonate containing molecule, but it is still neutrally charged. However, at ~pH 8, a strongly negative charged species ($UO_2(CO_3)_3^{-4}$) becomes dominant. At 1 % CO_2 (Fig. 3-6C), many of the polyhydroxyl species disappear and the diagram simplifies from ten to just seven dominant species. Due to the increased availability of inorganic carbon, UO_2CO_3 dominates this system beginning just below pH 5.5. A negative species peaks at a lower pH than in the previous conditions, starting at around pH 7.25, which then gives way to the highly negative $UO_2(CO_3)_3^{-4}$. Finally, at 2 % CO_2 (Fig. 3-6D), there is even more CO_2 available. While the type of U(VI)

solution species that are present do not change compared to the 1 % CO_2 system, they appear at high concentrations earlier in the pH scale.

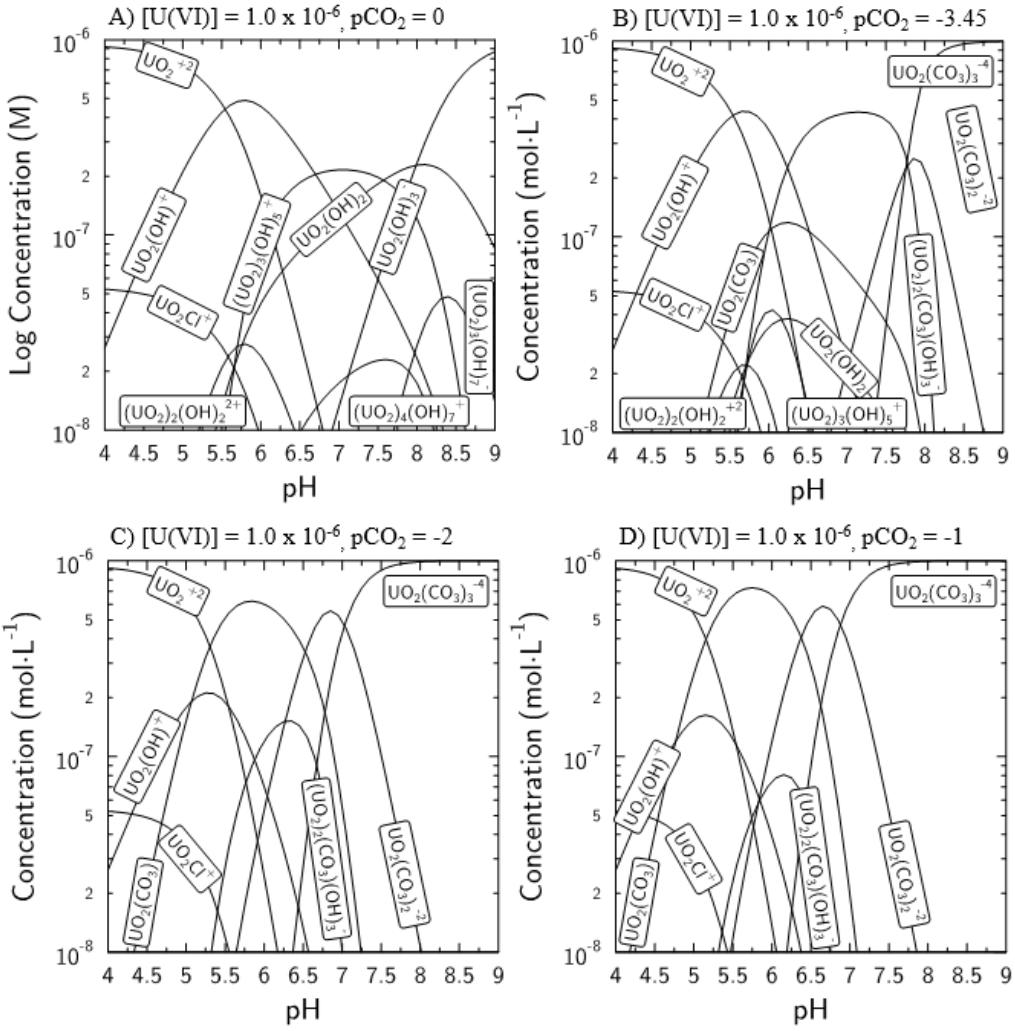

Figure 3-6. Uranium speciation for [U(VI)] = 1 μM, I = 0.1 M NaCl. A) closed system, pCO_2 = 0; B) atmospheric CO_2, pCO_2 = -3.45; C) 1% CO_2, pCO_2 = -2; D) 2% CO_2, pCO_2 = -1.

3.3.4 Effects of CO_2 on U(VI) Solution Speciation: Variable U(VI) Concentrations, Variable pCO_2

In this section we will further compare differences in U(VI) solution speciation and charge speciation between systems of variable total U(VI) solution concentrations and partial pressures of CO_2. In matrix diagrams, we will first compare systems at zero and atmospheric CO_2 with four, different total U(VI) solution concentrations (0.1, 1.0, 2.4 and 10.0 μM U(VI)). This is followed by a similar comparison for systems at atmospheric and elevated (2 %) CO_2 conditions over the same range of total U(VI) solution concentrations.

As seen in Figure 3-7, in the presence of CO_2 new U(VI)-carbonate species arise (bottom row), while some of the more complex polyhydroxyl species, which are relevant in CO_2-free systems, disappear (top row). In all atmospheric CO_2 systems simulated, the highly negatively charged $UO_2(CO_3)_3^{-4}$ species is found.

At neutral pH, the dominance of $(UO_2)_2(OH)_5^-$ grows with increasing total U(VI) concentrations in closed systems (Figure 3-7, top row). A similar phenomenon is observed at neutral pH for UO_2CO_3 species in systems exposed to atmospheric CO_2 (Figure 3-7, bottom row). Hence, overall at neutral pH the presence or absence of CO_2 does not only affect the chemical speciation of U(VI), but also the overall charge of dominant species, changing from positive in CO_2-free systems to neutral and negative charges in atmospheric CO_2 systems.

While observing changes in U(VI) solution speciation is important, it is also noteworthy to identify pH ranges where changes in CO_2 conditions have

very little effect. In these systems (Figure 3-7), in acidic pH regions UO_2^{+2} dominates to a similar degree under all conditions evaluated. This behavior can be explained by the very low inorganic carbon concentrations in solution at low pH (Figure 3-4).

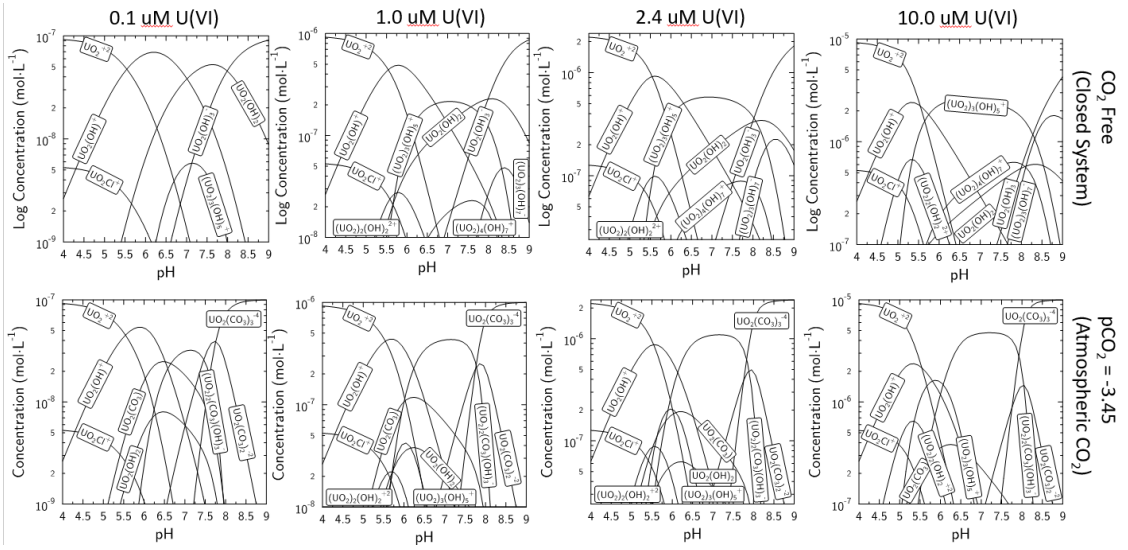

Figure 3-7. Matrix comparison of U(VI) solution speciation between systems closed to CO_2 (top row) and open to atmospheric CO_2 (pCO_2 = -3.45, bottom row). Total U(VI) concentrations are varied between 0.1, 1.0, 2.4 and 10.0 µM U(VI) from left to right.

Changes in dominant U(VI) species charges in the absence and presence of atmospheric CO_2 can be better observed if a similar matrix style diagram is applied to overall U(VI) species charges (Figure 3-8). In CO_2-free systems, at low total U(VI) concentrations each charge category dominates nearly the same size window of pH conditions (Figure 3-8, top row). As concentrations of U(VI)

increase, concentrations of neutral U(VI) species begin to decrease and +1 charged and -1 charged species become more dominant. At atmospheric CO_2, increasing total U(VI) concentrations lead to a slightly lower influence of +1 charged species (Figure 3-8, bottom row), while -1 charged and -4 charged U(VI) species dominate most of the circumneutral and basic pH ranges.

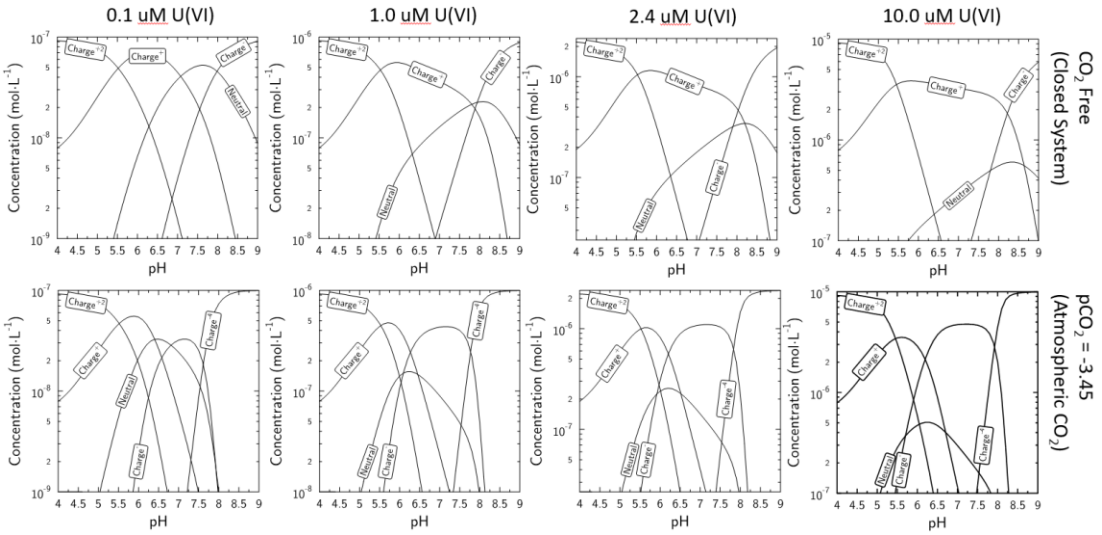

Figure 3-8. Matrix comparison of U(VI) charge speciation between systems closed to CO_2 (top row) and open to atmospheric CO_2 (pCO_2 = -3.45, bottom row). Total U(VI) concentrations are varied between 0.1, 1.0, 2.4 and 10.0 µM U(VI) from left to right.

This evaluation of CO_2 effects on U(VI) solution speciation can be taken further by comparing atmospheric CO_2 systems (pCO_2 = -3.45) with systems exposed to 2 % CO_2 (pCO_2 = 1.697, Figures 3-9 and 3-10). Based on simulation results shown in Figure 3-9, the increase in CO_2 partial pressure results in a greater dominance of $UO_2(CO_3)_3^{4-}$ species. Their influence is now relevant over a larger pH window and starts at lower pH values, from initially pH 8 to now pH 7.

As a result, a strongly negative species is now present at lower pH conditions, beginning at neutral pH.

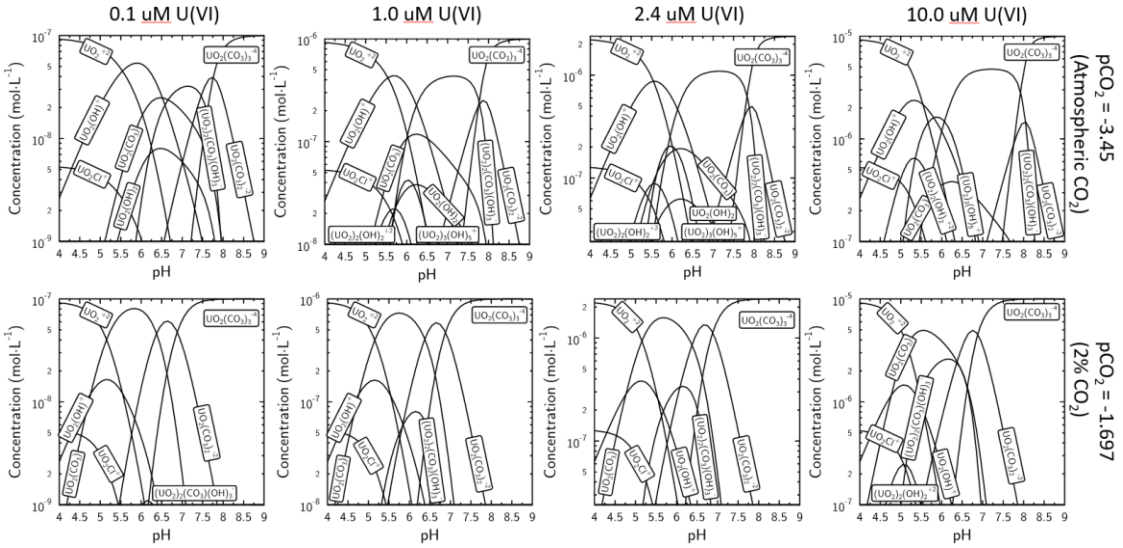

Figure 3-9. Matrix comparison of U(VI) solution speciation between systems at atmospheric (pCO_2 = -3.45, top row) and elevated CO_2 (2%, pCO_2 = -1.697, bottom row). Total U(VI) concentrations are varied between 0.1, 1.0, 2.4 and 10.0 µM U(VI) from left to right.

When charge speciation is evaluated for atmospheric and 2 % CO_2 systems (Figure 3-10), the dominance of the $UO_2(CO_3)_3^{-4}$ species, and hence of -4 charged species, at elevated CO_2 becomes even more apparent. This increase of -4 charged species at elevated CO_2 ultimately leads to a decrease in -1 charged U(VI) solution species relative to atmospheric CO_2 systems at the same total U(VI) concentrations. In comparison with the atmospheric CO_2 series, this broad influence of -4 charged U(VI) species over circumneutral and basic pH ranges occurs for all U(VI) concentrations simulated.

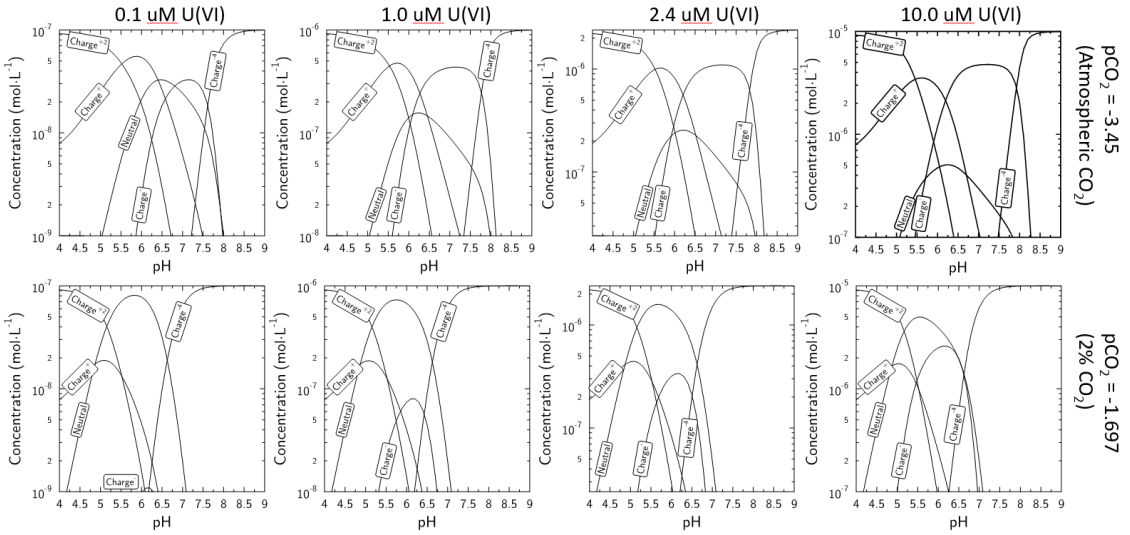

Figure 3-10. Matrix comparison of U(VI) charge speciation between systems at atmospheric (pCO_2 = -3.45, top row) and elevated CO_2 (2%, pCO_2 = -1.697, bottom row). Total U(VI) concentrations are varied between 0.1, 1.0, 2.4 and 10.0 μM U(VI) from left to right.

3.3.5 Chemical Speciation of Calcium in the Presence of Uranium(VI)

In the next series of U(VI) solution speciation simulations, we included a calcite impurity at a 1.5 mM concentration.[43] The concentration of calcite used in the simulations for this project has been established as a relevant value for bentonite systems with calcite impurities in the literature (ADD REF). It is understood that different sources of bentonite may have different concentrations of impurities. However, we will use only one singular value for the calcite concentration for the remainder of this study. This value is 1.5 mM calcite, which corresponds to a 23 % calcite impurity assuming 0.5 g of montmorillonite per 1 kg of water in later simulations of U(VI)-montmorillonite sorption experiments.

Before evaluating U(VI) solution speciation in the presence of this mineral, we will first characterize calcium solution speciation in the presence of the background electrolyte (0.1 M NaCl) and a fixed concentration of U(VI) (1.0 μM) in open and closed systems.

Figure 3-11 depicts the dramatic differences in calcium speciation when the system is either closed (left) or open (right) to atmospheric CO_2. The closed system has a limited supply of inorganic carbon, as its only source is the dissolution of calcite. As pH increases, HCO_3^- concentrations increase, while previously dominating species like CO_2/H_2CO_3 are depleted due to deprotonation. On the other hand, under atmospheric conditions there is an excess in inorganic carbon in the form of atmospheric CO_2. Hence, the concentrations of all carbon containing species are only limited by solution conditions (i.e., pH), and complexation or dissolution constants. In the closed system, shown on the left (Figure 3-11), ternary Ca-uranium(VI)-carbonate species begin to appear at a lower pH (pH~5.75) than in the system at atmospheric CO_2 conditions on the right (~pH 7). Lastly, there is a sharp decrease in the concentrations of calcium containing species at pH 8.2. This is due to the precipitation of calcite minerals under basic conditions, which reduces the concentrations of dissolved calcium available for complexation reactions.

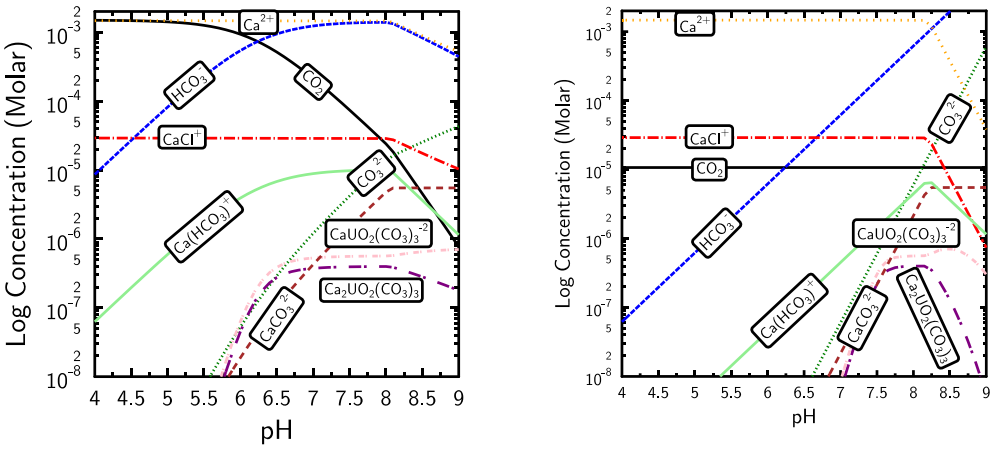

Figure 3-11. Chemical solution speciation of calcium in the presence of [U(VI)]=1.0x10^{-6} Mand I=0.1 M NaCl: [Calcite]=1.5mmol/L, left: closed and right atmospheric CO_2 (pCO_2=-3.45) conditions.

3.3.6 Effect of Calcite on Uranium(VI) Solution Speciation: Variable Uranium(VI) and pCO_2 Concentrations

Next, we will characterize the effects of a 1 mM calcite impurity on U(VI) solution speciation over a range of CO_2 conditions and total U(VI) solution concentrations. In the following discussion, we will use the same series of matrix diagrams as shown in section 3.3.4 for U(VI)-carbonate systems, while now also including the calcite impurity. Again, we will present classic U(VI) solution speciation diagrams first, followed by simplified charge speciation diagrams.

In a first matrix diagram (Figure 3-12), we compare U(VI) solution speciation for zero and atmospheric CO_2 conditions in the presence of calcite across four total U(VI) concentrations. In comparison to calcite-free systems, U(VI) solution speciation in all calcite systems is dominated by ternary calcium-U(VI)-carbonate solution species at circumneutral and alkaline pH conditions. Furthermore, in closed systems these ternary U(VI) species become dominant at lower pH values compared to systems in equilibrium with atmospheric CO_2. This can be explained by looking at the calcium speciation diagram (Fig. 3-11) and noticing that in the closed system calcium and carbonate concentrations are directly proportional to each other, as there is no external carbonate source in the form of atmospheric CO_2. In closed systems, ternary species are able to form at lower pH values because any carbonate has already been consumed into other U(VI) species. In the atmospheric CO_2 system, both uranium and calcium favor species formation with the excess carbonate present and only at more basic pH do the ternary species form.

In addition, in all of these speciation diagrams a “kink” in the concentration of calcium-containing species is observed at pH 8.2 due to calcite precipitation. Calcite precipitation decreases the total concentrations of dissolved Ca^{2+} in these systems (e.g. Figure 3-11, left), which creates a competition for calcium between various forms of Ca-U(VI)-carbonate solution complexes.

In the closed system, U(VI) solution speciation does not change very drastically as total concentrations of U(VI) increase. However, when systems are equilibrated with atmospheric CO_2 some significant changes are noticed immediately in comparison to CO_2-free systems. In the low to neutral pH regions between ~5 and ~6, the previously dominant $UO_2(CO_3)$ species is greatly reduced and $UO_2(OH)^+$ becomes dominant in the absence of atmospheric CO_2. There is also initially, at low U(VI) concentration, a brief window where $(UO_2)_2(CO_3)(OH)_3^-$ is dominant and becomes more so as U(VI) concentration increases. In the basic region there is also a robust restriction on the pH window of the Ca-uranium ternary species which closes from pH 5.75 to 6.5. $UO_2(CO_3)_3^{-4}$ also has a constrained pH window as more of the carbonate is participating in the $(UO_2)_2(CO_3)(OH)_3^-$ species.

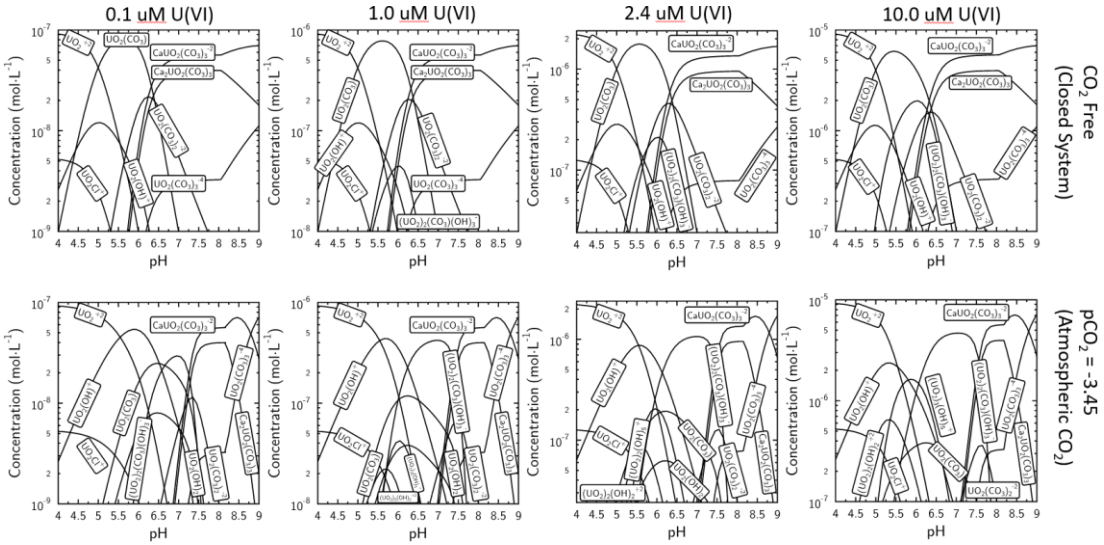

Figure 3-12. Matrix comparison of U(VI) solution speciation between systems closed to CO_2 (top row) and open to atmospheric CO_2 (pCO_2 = -3.45, bottom row) in the presence of 1.5 mM calcite. Total U(VI) concentrations are varied between 0.1, 1.0, 2.4 and 10.0 μM U(VI) from

Uranium(VI) charge speciation is drastically changed with the addition of calcite in absence and presence of atmospheric CO_2 (Figure 3-13). In CO_2 free systems, the only charges that dominate are +2, neutral and -2 corresponding to acidic, neutral and alkaline pH regions. At atmospheric CO_2, neutral U(VI) species become less relevant, and with increasing uranium(VI) concentrations the dominant charges are +2, +1, and -2. Last, in contrast to calcite-free systems, -4-charged U(VI) species only gain relevance at very alkaline pH conditions. This leads to a much greater diversity in the overall charges of U(VI) solution species at neutral to basic pH values in the presence of calcite impurities. This effect will become important for the discussion of U(VI) diffusion behavior in a later chapter.

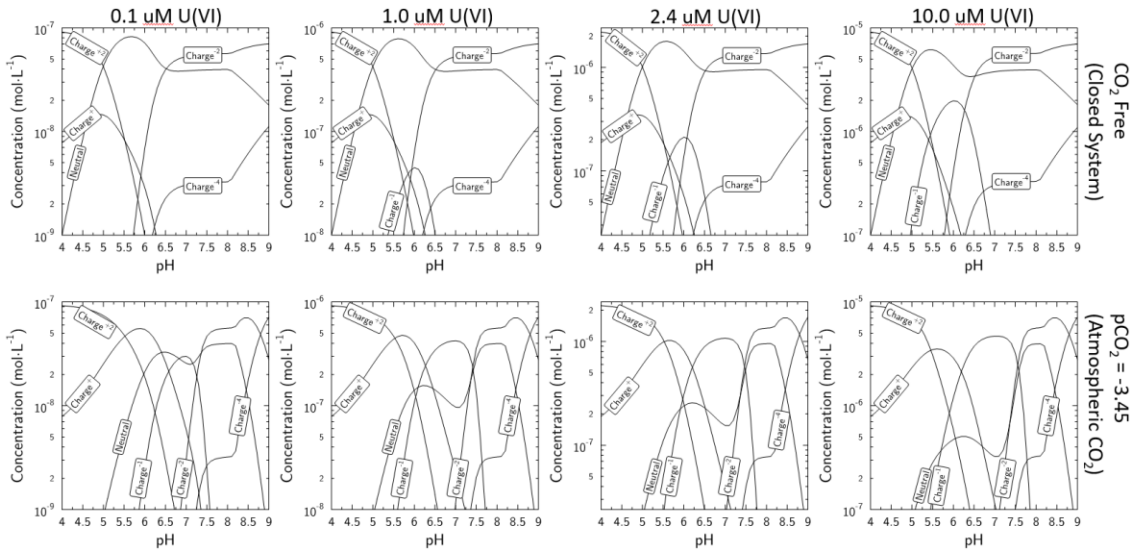

Figure 3-13. Matrix comparison of U(VI) charge speciation between systems closed to CO_2 (top row) and open to atmospheric CO_2 (pCO_2 = -3.45, bottom row) in the presence of 1.5 mM calcite. Total U(VI) concentrations are varied between 0.1, 1.0, 2.4 and 10.0 μM U(VI) from left to right.

To further examine the effects of calcite at higher CO_2 concentrations, we now compare systems in equilibrium with atmospheric and 2 % CO_2 (Figure 3-14). At higher CO_2 levels, ternary Ca-U(VI)-carbonate complexes show an expanded pH window of dominance, shifting the starting pH from 7.5 to 6.5. Furthermore, higher CO_2 concentrations lead to the dominance of UO_2CO_3 in the lower pH region, replacing previously-dominant hydroxide species, which has further effects on the U (VI) charge speciation.

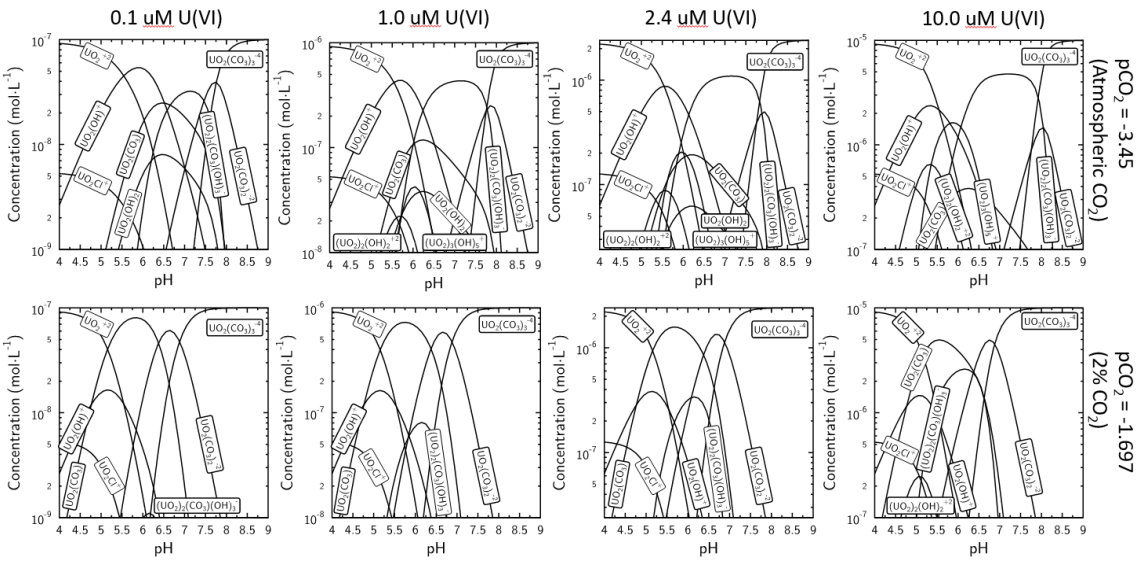

Figure 3-14. Matrix comparison of U(VI) solution speciation between systems at atmospheric (pCO_2 = -3.45, top row) and elevated CO_2 (2%, pCO_2 = -1.697, bottom row) in the presence of 1.5 mM calcite. Total U(VI) concentrations are varied between 0.1, 1.0, 2.4 and 10.0 µM U(VI) from left to right.

Uranium(VI) charge speciation changes drastically again when the partial pressure of CO_2 is increased from atmospheric to 2 % levels in the presence of 1.5 mM calcite (Figure 3-15). In contrast to atmospheric conditions, neutral U(VI) species remain dominant at slightly acidic to neutral pH conditions at 2 % CO_2 across the entire U(VI) concentration range evaluated. In fact, the only apparent difference across the range of U(VI) concentrations is the weak growth of the -1 charged species which does not become dominant under the conditions studied. It is just as important to know under what conditions speciation does not change, so this finding is inherently valuable.

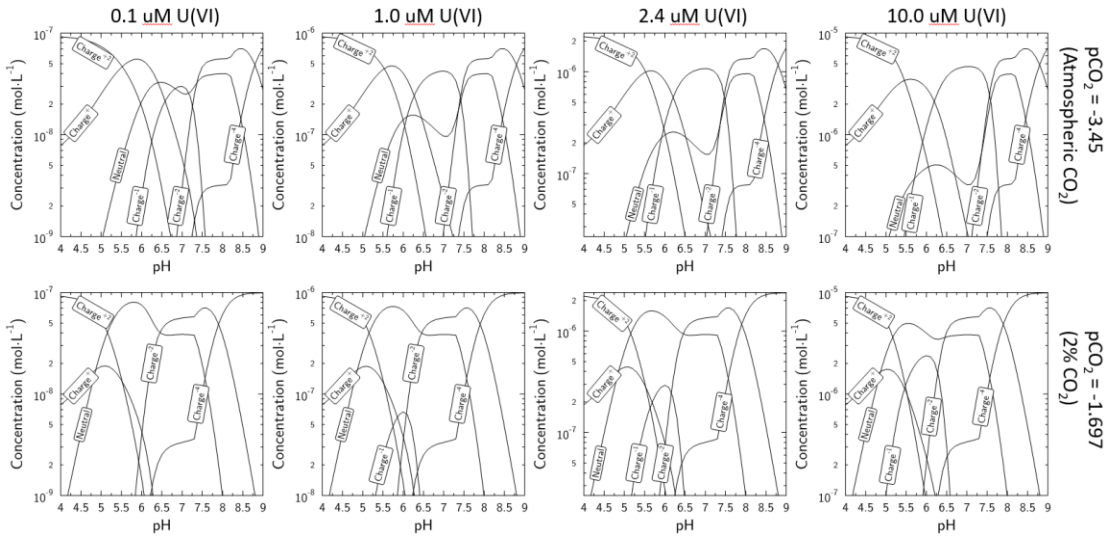

Figure 3-15. Matrix comparison of U(VI) charge speciation between systems at atmospheric (pCO_2 = -3.45, top row) and elevated CO_2 (2%, pCO_2 = -1.697, bottom row) in the presence of 1.5 mM calcite. Total U(VI) concentrations are varied between 0.1, 1.0, 2.4 and 10.0 µM U(VI) from left to right.)

3.3.7 Effect of Calcite on Uranium(VI) Solution Speciation: Absence and Presence of Calcite at Specific pCO_2 Conditions

Last, we will provide a direct comparison of U(VI) solution speciation between systems at specific partial pressures of CO_2, with or without calcite, and over the same range of U(VI) concentrations (Figure 3-16 to Figure 3-21). We will first evaluate the effect of calcite in CO_2-free systems over a range of four total concentrations of U(VI) in both chemical speciation and charge speciation matrix diagrams (Figures 3-16 and 3-17). This is then followed by the same type of comparison for atmospheric (Figures 3-18 and 3-19) and 2 % CO_2 (Figures 3-20 and 3-21) conditions.

In the absence of CO_2, at each condition a plethora of U(VI) species is available and many species are drastically different due to the presence of calcium and carbonate (Figure 3-16). In calcite-free systems, with the intial dominance of $UO_2(OH)^+$ and the rise of the $(UO_2)_3(OH)_5^+$ with increasing total U(VI) concentrations, a wide range of pH conditions is dominated by positive species (Figure 3-17). In contrast, in the presence of calcite, the system is generally dominated by neutral $UO_2(CO_3)$, and at more alkaline pH, negatively chargedl ternary Ca-U(VI)-carbonate species.

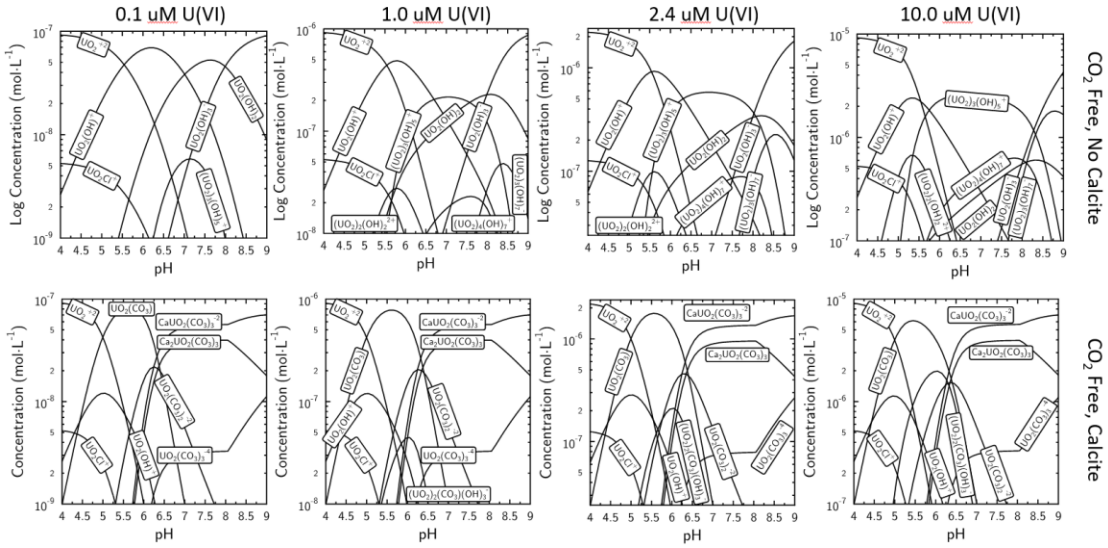

Figure 3-16. Matrix comparison of U(VI) solution speciation between CO_2-free systems (pCO_2 = 0) in the absence (top row) and presence (bottom row) of 1.5 mM calcite. Total U(VI) concentrations are varied between 0.1, 1.0, 2.4 and 10.0 µM U(VI) from left to right.

In charge speciation diagrams for closed systems (Figure 3-17), it can be clearly seen that positively charged species dominate over a pH range up to pH ~8 in calcite-free systems. In comparison, in the presence of calcite, neutral

species dominate at lower pH values, giving way to -2-charged species in the alkaline pH region.

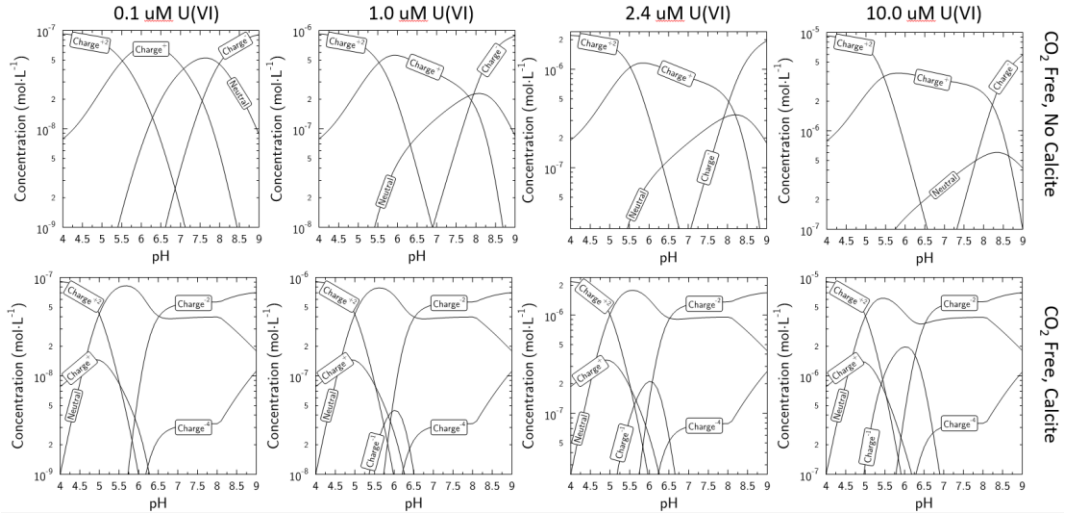

Figure 3-17. Matrix comparison of U(VI) charge speciation between CO_2-free systems (pCO_2 = 0) in the absence (top row) and presence (bottom row) of 1.5 mM calcite. Total U(VI) concentrations are varied between 0.1, 1.0, 2.4 and 10.0 µM U(VI) from left to right.

In the presence of atmospheric CO_2, the majority of changes in U(VI) solution speciation due to the presence of calcite are seen in the very basic pH region (Figure 3-18). Below pH 7.5, some minor changes in U(VI) solution speciation occur, but the major difference in the presence of calcite is the reduction of $UO_2(CO_3)_3^{-4}$ concentrations and the appearance of ternary U(VI) species, namely $CaUO_2(CO_3)^{-2}$ and $Ca_2UO_2(CO_3)_3$. This shift can be more clearly seen in the associated charge speciation diagrams (Figure 3-19). Neutral species are relevant both in the absence and presence of calcite, in the form of UO_2CO_3

or $Ca_2UO_2(CO_3)_3$. In the presence of calcite, U(VI) charge speciation at alkaline pH is more complex than in the absence of the mineral, given the brief dominance of a -2-charged species ($CaUO_2(CO_3)^{-2}$) and the staggered growth of the original -4-charged species ($UO_2(CO_3)^{-4}$).

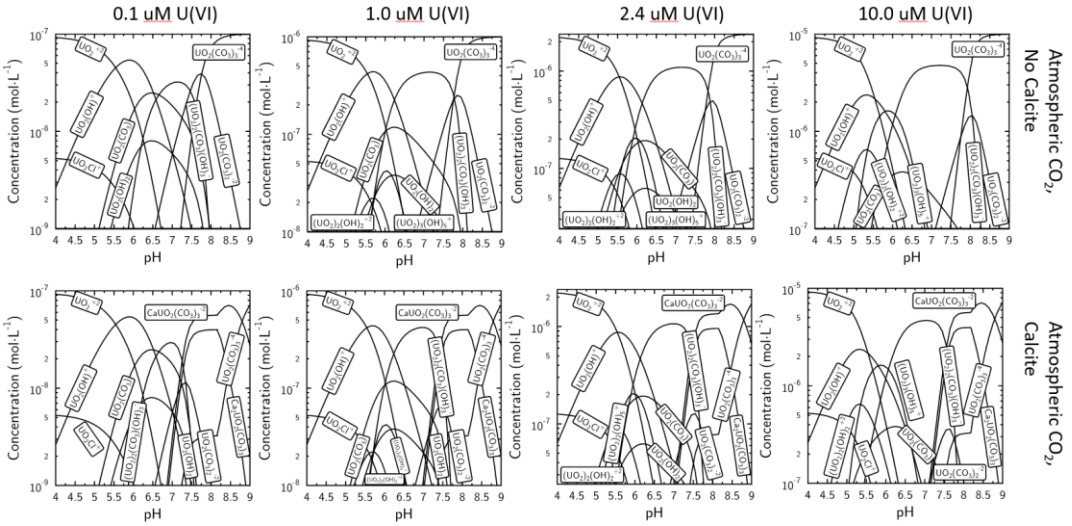

Figure 3-18. Matrix comparison of U(VI) solution speciation between atmospheric CO_2 systems (pCO_2 = -3.45) in the absence (top row) and presence (bottom row) of 1.5 mM calcite. Total U(VI) concentrations are varied between 0.1, 1.0, 2.4 and 10.0 μM U(VI) from left to right.

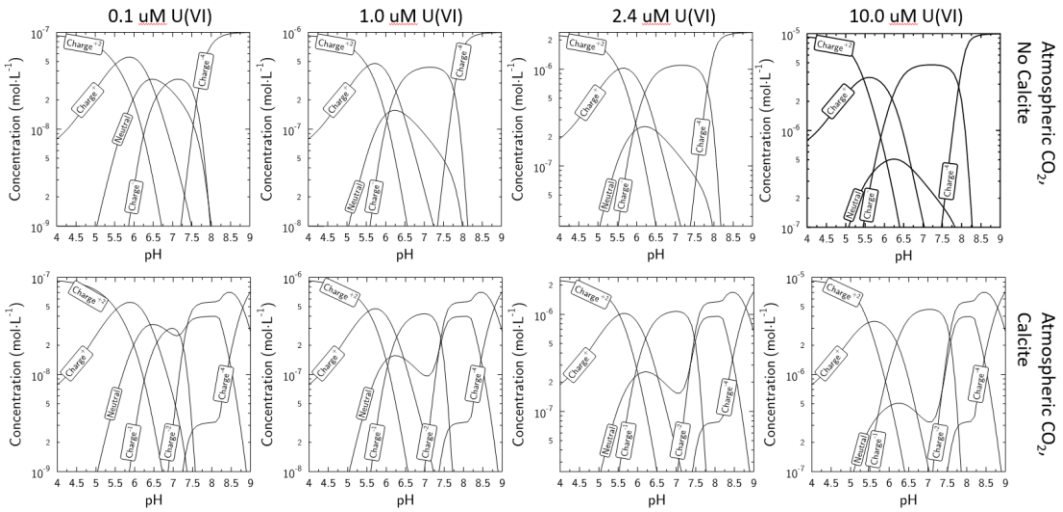

Figure 3-19. Matrix comparison of U(VI) charge speciation between atmospheric CO_2 systems (pCO_2 = -3.45)CO_2-free systems (pCO_2 = 0) in the absence (top row) and presence (bottom row) of 1.5 mM calcite. Total U(VI) concentrations are varied between 0.1, 1.0, 2.4 and 10.0 µM U(VI) from left to right.

Last, we will evaluate the effects of calcite on U(VI) solution and charge speciation at the highest, simulated CO_2 partial pressure at 2 % CO_2 (Figures 3-20 and 3-21). In these diagrams, we observe the same general trends as for atmospheric CO_2 systems in the presence and absence of calcite. However, the pH window of each of the previously discussed species is expanded, while the dominance relationships remain the same. In charge speciation diagrams at 2 % CO_2, the relationships remain again similar to atmospheric CO_2 systems but with the pH window neutral species is lengthened into the neutral pH region (Figure 3-21).

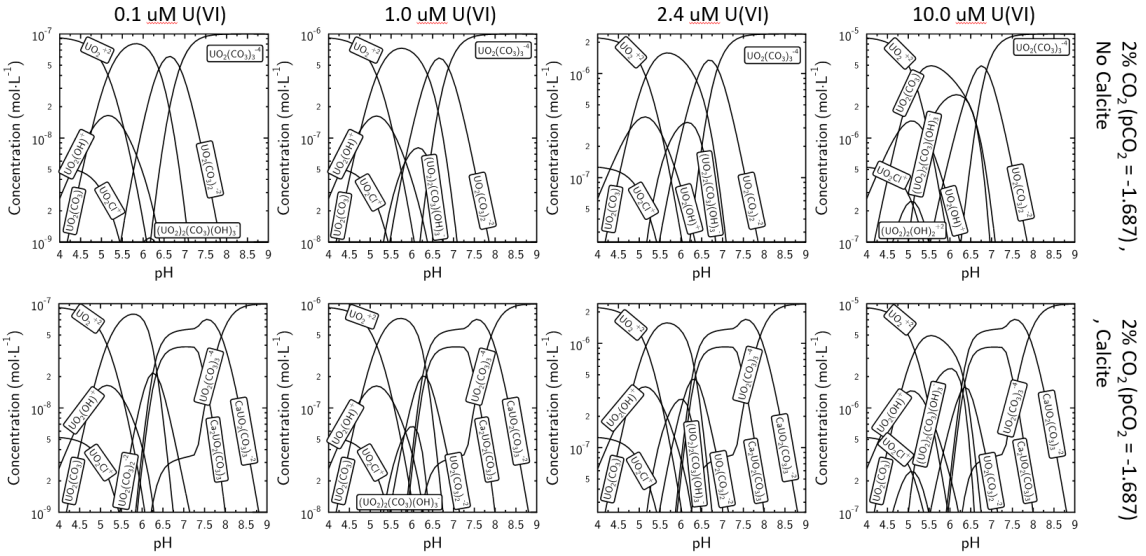

Figure 3-20. Matrix comparison of U(VI) solution speciation between 1% CO_2 systems (pCO_2 = -1.697) in the absence (top row) and presence (bottom row) of 1.5 mM calcite. Total U(VI) concentrations are varied between 0.1, 1.0, 2.4 and 10.0 μM U(VI) from left to right.

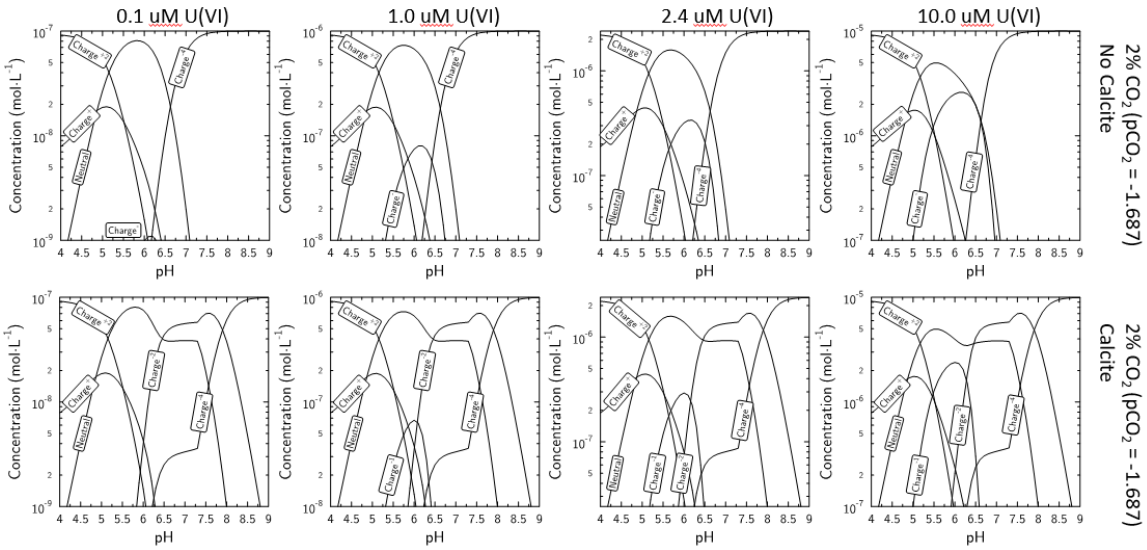

Figure 3-21. Matrix comparison of U(VI) charge speciation between 2% CO_2 systems (pCO_2 = -1.697) in the absence (top row) and presence (bottom row) of 1.5 mM calcite. Total U(VI) concentrations are varied between 0.1, 1.0, 2.4 and 10.0 μM U(VI) from left to right.

3.4 Summary and Conclusions for Uranium(VI) Solution Speciation Modeling

The major goal for this chapter was to gain a better understanding of how a variety of parameters (total U(VI) concentrations, CO_2 partial pressures, and the presence of calcite impurities) can affect the U(VI) solution and charge speciation over a range of pH conditions.

In the absence of CO_2, higher concentrations of uranium(VI) lead to a dominance of positively charged species into higher pH regions. For systems with fixed partial pressures of CO_2 (pCO_2 = -3.45, -2, -1.697), an increase in U(VI) concentrations favors the formation of polyuranic species, which results in a reduction in UO_2CO_3 (neutrally charged) and an increase in $(UO_2)_2(CO_3)(OH)_3^-$ (-1-charged).

As CO_2 concentrations increase, neutral UO_2CO_3 species become even more dominant in their respective pH window. This U(VI)-carbonate complex outcompetes other relevant species, such as negatively charged, polyuranic $(UO_2)_2(CO_3)(OH)_3^-$, which is more relevant when U(VI) is present at a higher concentration relative to carbonate.

The presence of calcite only affects U(VI) speciation beyond pH values of ~5 under the specific chemical conditions tested in this study. Once the -2-charged ternary Ca-U(VI)-carbonate complexes form, the concentrations of -2- and -4-charged binary U(VI)-carbonate complexes are reduced at pH >6.5. When Ca^{2+} from calcite is present in the system, a more negative character over all is apparent as the neutral species UO_2CO_3 suffers a pH window reduction. In the presence of calcite, all U(VI) speciation diagrams show sharp decreases or

increases in U(VI) species at pH 8.2, which are due to the precipitation of calcite and redistribution of the remaining dissolved Ca^{2+} amongst various U(VI) species at this pH.

4.0 Sorption of Uranium(VI) onto Montmorillonite

Montmorillonite has been studied as a sorbent for radionuclides for decades (ADD REFS!). There are two accepted surfaces sites at which contaminant sorption occurs on montmorillonite: cation exchange sites on basal surfaces and surface complexation sites at edge surfaces of the clay. These sorption mechanisms have been thoroughly described in previous works[20,43]

In order to simulate U(VI) sorption onto montmorillonite, this work uses a series of sorption reactions published by Marques et al. (2012), as described in further detail below. In addition, the so-called spillover effect first introduced into U(VI) surface complexation models by Tournassat et al. (2018) will also be taken into account. This is a physical effect caused by the electrostatic interactions between basal surface sites (cation exchange sites) and edge surface sites (surface complexation sites). It describes how the electrostatic surface potential of exchange sites affects the surface potential of surface complexation sites. When taken into account, this phenomenon allows for a more robust sorption model, which stipulates just one type of surface site and three surface reactions.

In this chapter, U(VI) sorption onto montmorillonite is simulated and evaluated over a range of total U(VI) concentrations from 1.0e-7M to 1.0e-5 M, which is the same concentration range previously evaluated in the speciation section. There are three main goals for this sorption chapter. First, we will characterize U(VI) sorption onto montmorillonite as a function of chemical solution conditions and in the presence and absence of calcite. Second, we will compare the predicted U(VI) sorption behavior between two different conceptual

models; one excluding (Marques et al., 2012) and one including (Tournassat et al., 2018) the spillover effect. Last, these simulations of U(VI) sorption characteristics will support the selection of chemical system conditions to be evaluated in later U(VI) diffusion models.

Each simulation of U(VI) sorption onto montmorillonite is set up at a constant ionic strength (0.1 M NaCl). It is important to note that not all U(VI) solution species are allowed to sorb to montmorillonite. However, when a given U(VI) species sorbs, the solution speciation will again re-equilibrate to represent the new effective molarity of U(VI) in solution.

The sorption behavior of contaminants is often described with sorption distribution constants (K_d values), which will also be used here for the presentation of simulated U(VI) sorption results. The sorption distribution coefficient (with units of L/kg) is defined as U(VI) concentrations sorbed over U(VI) concentrations remaining in solution after sorption equilibration. Therefore, when total U(VI) concentrations increase and sorption sites become saturated, U(VI) concentrations in solution can remain higher relatively, leading to a reduction in K_d values. In the following, we will first describe the modeling setup and results for the Marques et al. (2012) model, then the modeling setup for the Tournassat et al. (2018) model. This is followed by a comparison of simulation results between the two modeling concepts, and a summary of general conclusions.

4.1 Uranium(VI)-Montmorillonite Sorption Model by Marques

4.1.1 Modeling Setup

The sorption model for this section is built using sorption reactions and values published by Marques et al. (2012).[35] First, it is important to specify the number of sites available on montmorillonite at which sorption can occur (Table 4-1). Montmorillonite has two types of surface complexation sites in this model, strong and weak sites. Experimentally, often 0.5 grams of montmorillonite are used per 1 liter of solution. So this specific site concentration in terms of moles/L has been added to the last column of Table 4-1.

Table 4-1. Summary of non-adjustable parameters determined for Na-montmorillonite[35]

Site Type	Site Capacities (mol kg^{-1})	Sites for 0.5 g Mont (moles L^{-1})
$=Mont^{S}OH$	2×10^{-3}	1×10^{-6}
$=Mont^{W1,W2}OH$	4×10^{-2}	2×10^{-5}

*S, W1, W2 are strong (s) or weak (w) sites

Next, the protolysis reactions are stated (Table 4-2). These reactions only account for interactions between water and the clay itself.

Table 4-2. Protolysis reactions and constants for montmorillonite in water[35]

Protolysis Reactions	log $K_{Protolysis}$
$=Mont^{S,W1}OH + H^{+} \rightleftharpoons Mont^{S,W1}OH_2^{+}$	4.5
$=Mont^{S,W1}OH \rightleftharpoons =Mont^{S,W1}O^{-} + H^{+}$	-7.9
$=Mont^{W2}OH + H^{+} \rightleftharpoons =Mont^{W2}OH_2^{+}$	6.0
$=Mont^{W2}OH \rightleftharpoons =Mont^{W2}O^{-} + H^{+}$	-10.5

Then, the surface complexation reactions for uranium polyhydroxyl species need to be defined base on data from Marques et al. (2012). These

reactions and their associated reaction constants allow for the sorption of specific U(VI) species onto the simulated montmorillonite surface (Table 4-3).

Table 4-3. Summary of the surface complexation constants and selectivity coefficients characterizing the sorption of U(VI) on Na-montmorillonite in the absence of carbonate[35]

Surface Complexation Reactions	$Log^{S.W}$ K
$=Mont^{S}OH + UO_2^{2+} \rightleftharpoons =Mont^{S}OUO_2^{+} + H^{+}$	3.1
$=Mont^{S}OH + UO_2^{2+} + H_2O \rightleftharpoons =Mont^{S}OUO_2OH^{0} + 2H^{+}$	-4.6
$=Mont^{S}OH + UO_2^{2+} + 2H_2O \rightleftharpoons =Mont^{S}OUO_2(OH)_2^{-} + 3H^{2+}$	-12.6
$=Mont^{S}OH + UO_2^{2+} + 3H_2O \rightleftharpoons =Mont^{S}OUO_2(OH)_3^{2-} + 4H^{2+}$	-20.9
$=Mont^{W1}OH + UO_2^{2+} \rightleftharpoons =Mont^{W1}OUO_2^{+} + H^{+}$	0.5
$=Mont^{W1}OH + UO_2^{2+} + H_2O \rightleftharpoons =Mont^{W1}OUO_2OH^{0} + H^{+}$	-5.7
CE: $2Na^{+}$-clay + $UO_2^{2+} \rightleftharpoons UO_2^{2+}$-clay + $2Na^{+}$	0.45

Last, in the presence of atmospheric or elevated levels of CO_2 Marques et al. (2012) suggested to include surface complexation reactions for uranium(VI)-carbonate species and their constants (Table 4-4).

Table 4-4. Surface complexation constants on strong sites ($log^{S}K$) and weak sites ($log^{W1}K$) for U(VI)-carbonate complexes on Na-montmorillonite[35]

Surface Complexation Reactions	$Log^{S.W1}$ K
$=Mont^{S}OH + UO_2^{2+} + CO_3^{2-} \rightleftharpoons =Mont^{S}OUO_2CO_3^{-} + H^{+}$	9.8
$=Mont^{S}OH + UO_2^{2+} + 2CO_3^{2-} \rightleftharpoons =Mont^{S}OUO_2(CO_3)_2^{3-} + H^{+}$	15.5
$=Mont^{W1}OH + UO_2^{2+} + CO_3^{2-} \rightleftharpoons =Mont^{W1}OUO_2CO_3^{-} + H^{+}$	9.3

Based on these parameters compiled from Marques et al. (2012), PHREEQC can be used to generate these montmorillonite surfaces. These surfaces can subsequently be equilibrated with solutions containing uranium(VI) over a variety of chemical solution conditions, as previously outlined for U(VI) speciation modeling. Varying system conditions include a range of total U(VI)

concentrations, pH conditions, CO_2 partial pressures and systems with and without calcite.

4.1.2 Simulation Results: Uranium(VI) Sorption as a Function of Total U(VI) Concentrations

PHREEQC was used the equilibrate the surfaces developed within the Marques et al. (2012) model with U(VI) solutions at the conditions previously used for chemical and charge speciation simulations (total U(VI) concentrations from 0.1 to 10.0 M; pH from 4 to 9; partial pressures of zero, atmospheric, 1 % and 2 % CO_2; zero or 1.5 mM calcite). Results of these U(VI) sorption models were graphed in terms of K_d values (L kg^{-1}) versus pH, in order to understand how each of these solution parameters affects the U(VI) sorption behavior (Figures 4-1 and 4-2).

Overall, depending on chemical solution conditions (Figure 4-1), U(VI) K_d values span over two orders of magnitude ($1x10^5$ to $4x10^3$ L kg^{-1}) for a range of two orders of magnitude in total U(VI) concentrations ($1x10^7$ and $1x10^5$ M U(VI)). Increasing U(VI) concentrations have initially only a minor effect on K_d values, until substantially less U(VI) sorption occurs at the highest total U(VI) concentration (10^{-5} M). This behavior can be explained by the decreasing availability of a fixed number of montmorillonite surface sites. When U(VI) concentrations increase, uranium(VI) species are competing for a lower effective concentration of surface sites.

In addition, in each system U(VI) K_d values are reduced as partial pressures and effective concentrations of CO_2 in solution increase. This is caused by the formation of uranium carbonate aqueous complex, such as

$UO_2(CO_3)_3^{4-}$, which compete with the surface complexes. As CO_2 concentrations increase, the dominance of this U(VI)-carbonate solution complex further increases, which leads directly to a decrease in U(VI) sorption at elevated pH.

A third, major effect on U(VI) sorption can be identified in the presence of calcite, when calcite-free (solid lines) and calcite-containing (dotted lines) systems are compared (Fig. 4-1). In this case, the pH window where U(VI) sorption can occur is always truncated when calcite is present. This can be explained by the fact that in the presence of calcite U(VI) solution speciation always changes to now also include ternary Ca-U(VI)-carbonate species. Since there is no ternary species that bind to the surface according to this model, the overall sorption of U(VI) to montmorillonite is reduced.

The system that is most drastically affected by the addition of calcite is the closed (CO_2 free) system. According to results in Figure 4-1, U(VI) K_d values in closed systems are reduced by almost two orders of magnitude for the same pH values due to the presence of calcite. In addition, the pH window where U(VI) sorption can occur is much smaller due to the influence of this small amount of calcium carbonate. This strong effect of calcite on U(VI) sorption can be explained by the strong shift in U(VI) solution speciation in the absence and presence of calcite in closed systems (Chapter 3, Figure 3-16). Furthermore, the presence of calcite leads to broader influence of ternary Ca-U(VI)-carbonate solution complexes across the alkaline pH range in closed systems compared to atmospheric and elevated CO_2 systems (Chapter 3, Figures 3-12 and 3-14).

A final observation to be made from Figure 4-1 is the long “sorption tail” in closed, calcite-free systems (solid black lines) in comparison to open, calcite-free systems. This “tail” suggests a more constant U(VI) K_d value in closed than open systems in the absence of calcite. This trend can be explained by the fact that there are absolutely no U(VI) carbonate species formed in solution in CO_2- and calcite free systems, which leads to a more constant U(VI) sorption across the entire pH window.

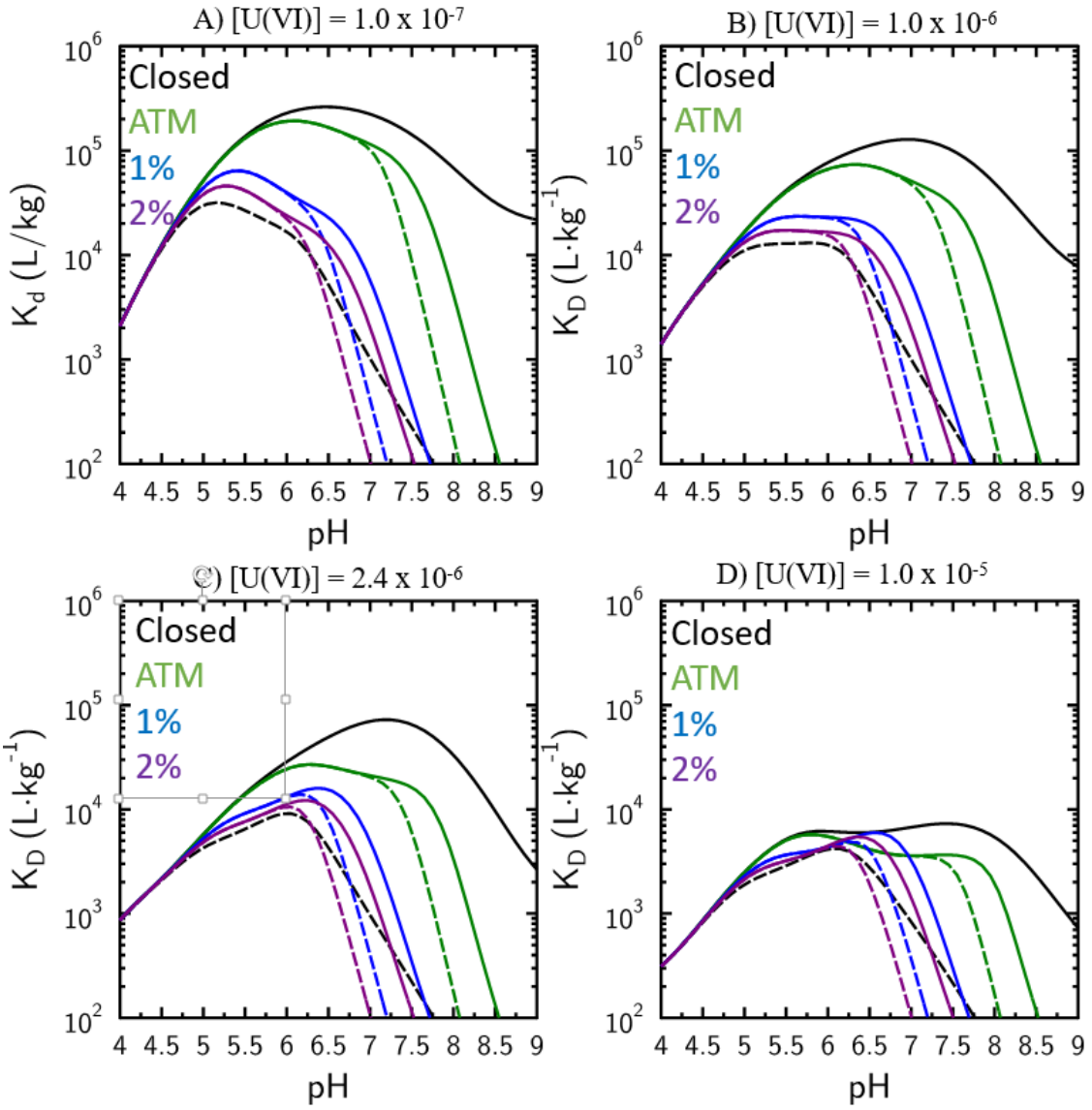

Figure 4-1. Simulated U(VI) sorption based on Marques et al. (2012) for 0.5 g/L of montmorillonite at four different U(VI) concentrations (A) 0.1 μM, (B) 1.0 μM, (C) 2.4 μM, (D) 10.0 μM U(VI), four different pCO_2 concentrations: CO_2-free (black), pCO_2 =-3.45 (green), pCO_2=-2 (blue), pCO_2=-1.697 (purple), and in the presence (dotted) or absence (solid) of 1.5 mM calcite.

4.1.3 Simulation Results as a Function of Partial Pressure of CO_2

An alternative way to visualize these modeling results is to plot each set of simulations for a specific partial pressure of CO_2, which allows for a series of additional observations. First, in the CO_2 free system (Figure 4-2A), a decrease in U(VI) sorption and K_d values can be seen with increasing U(VI) concentrations, both in the presence and absence of calcite. The addition of calcite to the system has a drastic effect on the pH range over which U(VI) sorption can occur, truncating the pH window from a pH value beyond 9 to a pH around 7.5.

The subsequent three images (Figures 4-2 B, C, and D) each demonstrate that with increasing CO_2 levels the upper pH limits for U(VI sorption are shifted to lower pH values. This behavior is due to the competition of U(VI)-carbonate species, which become more prevalent at higher CO_2 concentrations, with surface complexes.

Last, Figure 4-2 highlights again that when CO_2 is already present in the gas phase, the addition of calcite only causes a small further truncation in the pH windows for U(VI) sorption. In open systems, the addition of calcite leads to the formation of ternary Ca-U(VI)-carbonate solution species, but only in low quantities relative to the binary U(VI)-carbonate solution complexes.

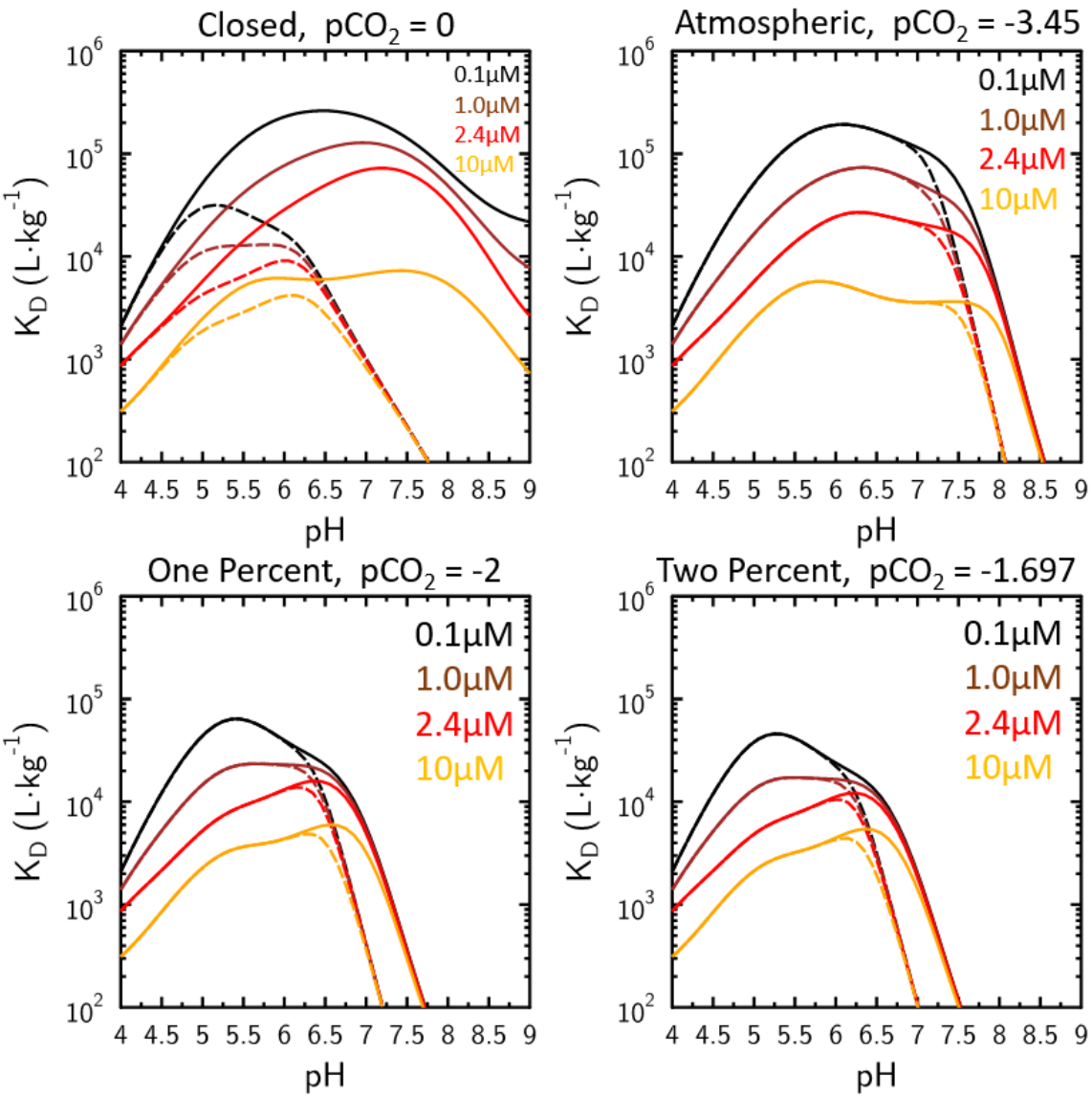

Figure 4-2. Simulated U(VI) sorption based on Marques et al. (2012) for 0.5 g/L of montmorillonite at four different partial pressures of CO_2: (A) $pCO_2 = 0$, (B) atmospheric CO_2 ($pCO_2 = -3.45$), (C) 1% CO_2 ($pCO_2 = -2$), (D) 2% CO_2 ($pCO_2 = -1.697$), at four different total U(VI) concentrations: 0.1 µM (black), 1.0 µM (orange), 2.4 µM (red), 10 µM (yellow), and in the presence (dotted) or absence (solid) of 1.5mM calcite.

4.1.4 Uranium(VI) Surface Speciation

In order to better understand the relevant sorption reactions occurring in these systems, it is also useful to plot speciation diagrams that specifically show U(VI) surface species adsorbed onto montmorillonite surfaces as a function of various system conditions. In other words, the following diagrams (Figure 4-3) show U(VI)surface species that appear on the product side of previously stated surface complexation reactions (Tables 4-3 and 4-4).

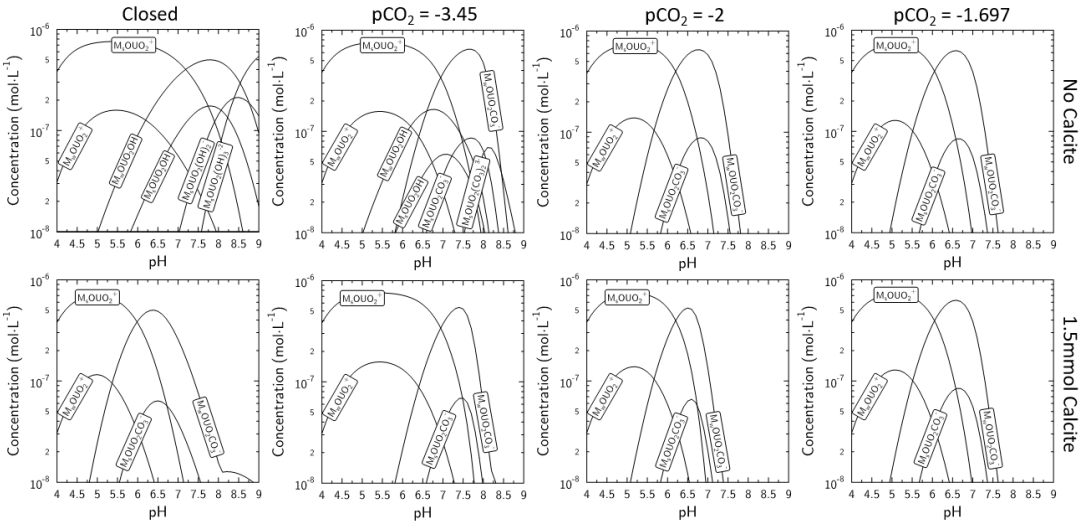

Figure 4-3. Uranium(VI) surface speciation for 1.0 μM U(VI) at all experimental conditions tested using the Marques et al. (2012) sorption model: pCO_2 = 0, -3.45, -2, and -1.697, in the absence (top) and presence (bottom) of 1.5 mM calcite.

In the absence of calcite (Figure 4-3, top), U(VI) surface speciation is quite complex at zero and atmospheric levels of CO_2, as the concentrations of cationic and neutral U(VI) solution species is high (Chapter 3, Figure 3-7). As CO_2 concentrations in calcite-free systems increase, the concentrations of hydroxyl

solution species is reduced, and U(VI)-carbonate complexes are increasingly important (Chapter 3, Figure 3-9). This trend in changing U(VI) solution speciation is also reflected in the U(VI) surface speciation for these systems, as the Marques model allows for an adsorption of U(VI)-carbonate complexes onto montmorillonite surfaces.

In systems which also contain calcite, U(VI) surface speciation is simplified in a similar fashion to the calcite-free systems in contact with elevated levels of CO_2. This is again due to the formation of U(VI)-carbonate species, both in solution and on the surface.

4.2 Uranium(VI)-Montmorillonite Sorption Model by Tournassat

4.2.1 Modeling Setup

Tournassat et al. (2018) proposed a different sorption model with a much smaller number of fitting parameters. This model specifically accounts for the spill-over effect described above, but does not include sorption reactions of U(VI)-carbonate solution complexes. In this model, U(VI) sorption is simulated with only three surface complexation reactions and one surface site type. As demonstrated in detail elsewhere (Tournassat et al., 2018), this conceptual model provides good fits of experimental U(VI) sorption data collected over a wide range of system conditions by various researchers, while limiting the number of model fitting parameters substantially.

Similar to the previous U(VI) sorption simulations based on the model developed by Marques et al. (2012), montmorillonite surface site concentrations,

surface protolysis reactions and U(VI) surface complexation reactions and constants had to be defined in PHREEQC. All of these modeling parameters have been summarized for the Tournassat et al. (2018) model below (Tables 5-5). Montmorillonite surfaces were subsequently equilibrated with the same set of U(VI) solution conditions as previously described in the U(VI) speciation chapter (Chapter 3) and for the U(VI) sorption modeling based on the Marques et al. (2012) concept. However, now they also include the influence of the electrostatic surface potential of basal exchange sites on the surface potential of complexation sites of the clay (Table 5-5).[22]

Table 4-5. Summary of the surface complexation constants characterizing U(VI) sorption on Na-montmorillonite[23] (reproduced with permission from authors).

Edge surface areas	Total	$14\ m^2 \cdot g^{-1}$
	Edge surface of B type	$7\ m^2 \cdot g^{-1}$
Protonation/deprotonation reactions	Log K	
	Si_T-Al_{Oc}-Si_T	Si_T-Fe^{III}_{Oc}-Si_T
$>SiteH_4^+ = >SiteH_3 + H^+$	−3.1	−1.2
$>SiteH_3 = >SiteH_2^- + H^+$	−7	−5.1
$>SiteH_2^- = >SiteH^{2-} + H^+$	−7	−8.6
$>SiteH^{2-} = >Site^{3-} + H^+$	−8.3	−8.6
	Si_T-Mg_{Oc}-Si_T	Si_T-Fe^{II}_{Oc}-Si_T
$>SiteH_4 = >SiteH_3^- + H^+$	−10.8	−6.6
$>SiteH_3^- = >SiteH_2^{-2} + H^+$	−10.8	−10.2
$>SiteH_2^{-2} = >SiteH^{-3} + H^+$	−13.2	−10.2
$>SiteH^{-3} = >Site^{-4} + H^+$	N.A.	−11.2
	Al_T-Al_{Oc}-Si_T	
$>SiteH_4 = >SiteH_3^- + H^+$	−4.9	
$>SiteH_3^- = >SiteH_2^{-2} + H^+$	−7	
$>SiteH_2^{-2} = >SiteH^{-3} + H^+$	−8.5	
$>SiteH^{-3} = >Site^{-4} + H^+$	−15.1	
U(VI) adsorption reactions on Si_T-Al_{Oc}-Si_T sites		Log K
$>SiteH_3 + UO_2^{2+} = >SiteH_3UO_2^{2+}$		4.8
$>SiteH_3 + UO_2^{2+} = >SiteHUO_2 + 2\ H^+$		−4.8
$>SiteH_3 + UO_2^{2+} + 2\ H_2O = >SiteUO_2(OH)_2^{-3} + 5\ H^+$		−25.3

4.2.2 Simulation Results as a Function of Total Uranium(VI) Concentrations

When comparing the modeling results between the models from Tournassat et al. (2018) and Marques et al. (2012), some similarities and a few strong differences can be observed (Figures 4-1 and 4-4). First, at the lowest total U(VI) concentration, U(VI) sorption profiles look very similar between the two models, with respect to the pH window for U(VI) sorption and magnitude of K_d values. However, as U(VI) concentrations increase, the predicted U(VI) sorption characteristics begin to differ, with the Tournassat et al. (2018) sorption model allowing for greater U(VI) sorption at higher pH values compared to the Marques et al. (2012) model.

Furthermore, increasing levels of CO_2 more drastically reduce U(VI) sorption in the model by Tournassat et al. (2012) than in the model from Marques et al. (2012). For the Tournassat model the shift in K_d values at peak sorption (~neutral) is from $2x10^5$ to $2x10^3$ L kg^{-1}, a full order of magnitude greater. With the Marques model, the peak sorption occurring around neutral pH for the lowest concentration tested of U(VI) (0.1 uM) is reduced from $K_d = 2x10^5$ to $3x10^4$ L kg^{-1}. This difference can be explained by the fact that neither binary nor ternary U(VI)-carbonate solution complexes can bind to the montmorillonite surface in the Tournassat model.

However, general U(VI) sorption trends in the presence of calcite are similar between the two conceptual models, with closed systems showing the strongest decrease in U(VI) sorption relative to calcite-free systems. Again, the addition of calcite and the formation of associated U(VI)-carbonate solution

complexes causes a much greater reduction in U(VI) K_d values in the Tournassat model than in the Marques model, by roughly one order of magnitude. This behavior occurs because in the Tournassat model, neither the Ca-U(VI)-carbonate nor the U(VI)-carbonate species are allowed to bind.

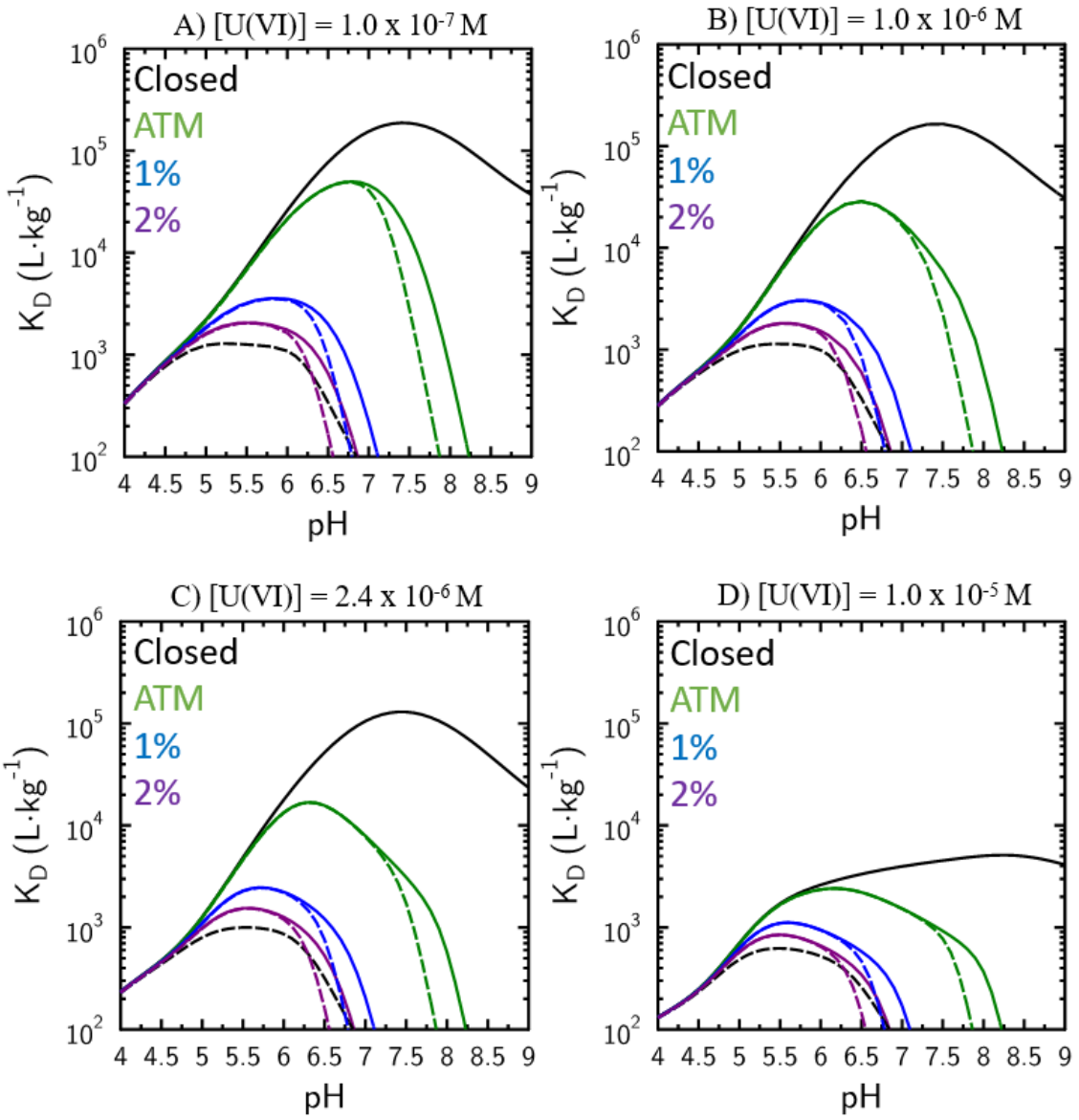

Figure 4-4. Simulated U(VI) sorption based on Tournassat et al. (2018) for 0.5 g/L of montmorillonite at four different U(VI) concentrations (A) 0.1 μM, (B) 1.0 μM, (C) 2.4 μM, (D) 10.0 μM U(VI), four different pCO_2 concentrations: CO_2-free (black), pCO_2 =-3.45 (green), pCO_2=-2 (blue), pCO_2=-1.697 (purple), and in the presence (dotted) or absence (solid) of 1.5 mM calcite.

4.2.3 Simulation Results as a Function of Partial Pressure of CO_2

When the simulation results based on the Tournassat et al. (2018) model are plotted in sets with varying partial pressures of CO_2 and across the range of evaluated U(VI) concentrations, the effects of varying total U(VI) concentrations can be observed more easily (Figure 4-5). As expected, when total U(VI) concentrations increases, U(VI) sorption decreases. In addition, U(VI) K_d values are also reduced as the partial pressures of CO_2 increase across the diagrams. For instance, in the presence of CO_2 U(VI) sorption does not nearly show the same magnitude even at very low total U(VI) concentrations , when compared to CO_2-free systems.

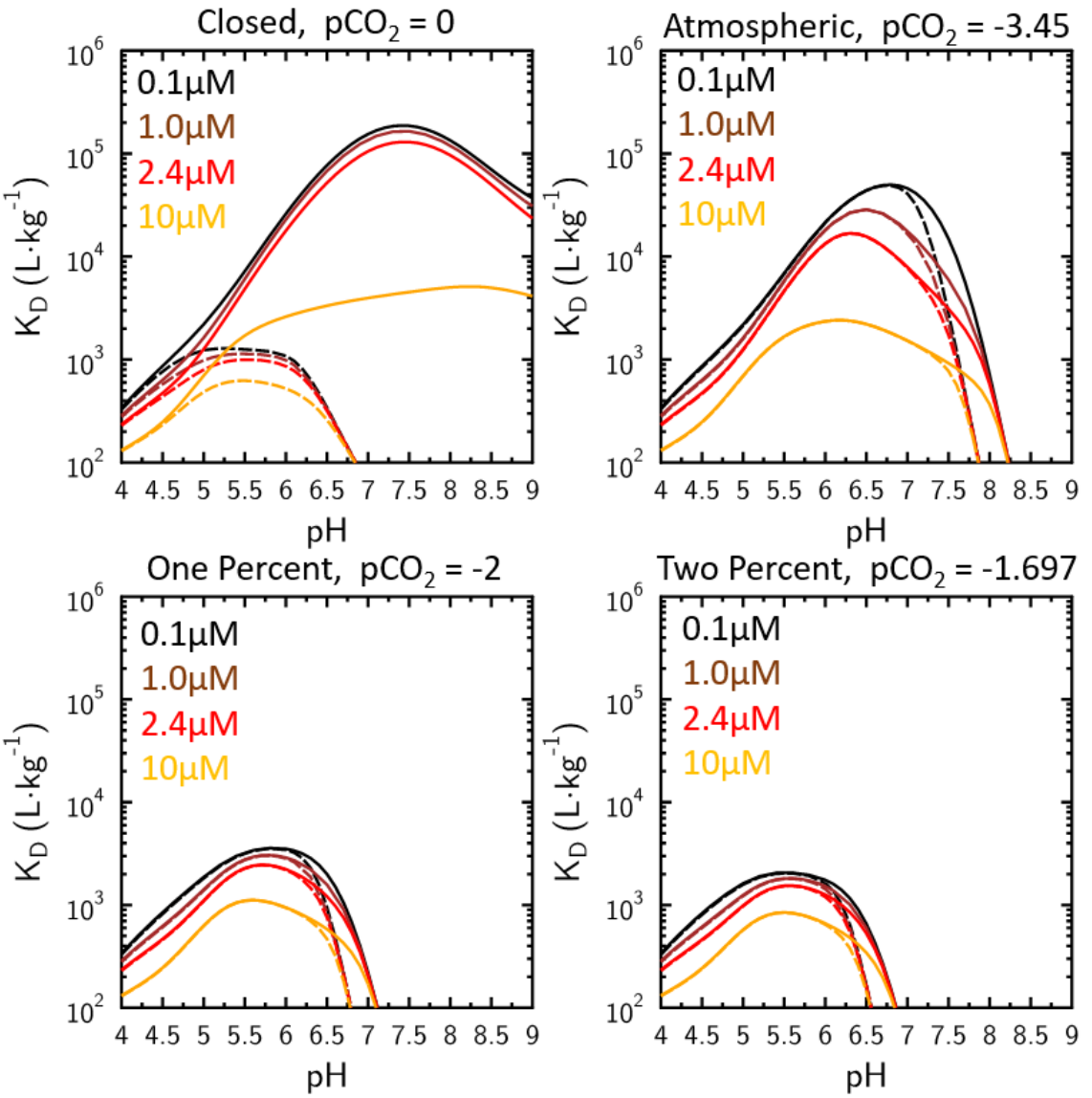

Figure 4-5. Simulated U(VI) sorption based on Tournassat et al. (2018) for 0.5 g/L of montmorillonite at four different partial pressures of CO_2: (A) pCO_2 = 0, (B) atmospheric CO_2 (pCO_2 = -3.45), (C) 1% CO_2 (pCO_2 = -2), (D) 2% CO_2 (pCO_2 = -1.697), at four different total U(VI) concentrations: 0.1 µM (black), 1.0 µM (orange), 2.4 µM (red), 10 µM (yellow), and in the presence (dotted) or absence (solid) of 1.5mM calcite.

4.2.4 Uranium(VI) Surface Speciation Based on Model from Tournassat et al. (2018)

For the Tournassat et al. (2018) model, surface speciation diagrams are expected to be drastically more simple, as there are only three surface species included in the modeling concept: Mont-$OHUO_2$, Mont-$OH_3UO_2^+$, and Mont-$OUO_2(OH)_2^{-3}$. In Figure 4-6, it can be seen that at low CO_2 concentrations or in the absence of calcite, which would also provide a source of inorganic carbon, anionic surface species, such as Mont-$OUO_2(OH)_2^{-3}$ exist at high pH conditions. Once CO_2 levels increase, this species disappears and the majority of the surface speciation diagrams look similar. However, it must be noted that with increasing CO_2 concentrations the pH window where U(VI) surfaces species are present at relevant concentrations continues to become smaller. This trend follows the same behavior as the corresponding U(VI) sorption data plotted in terms of U(VI) K_d values.

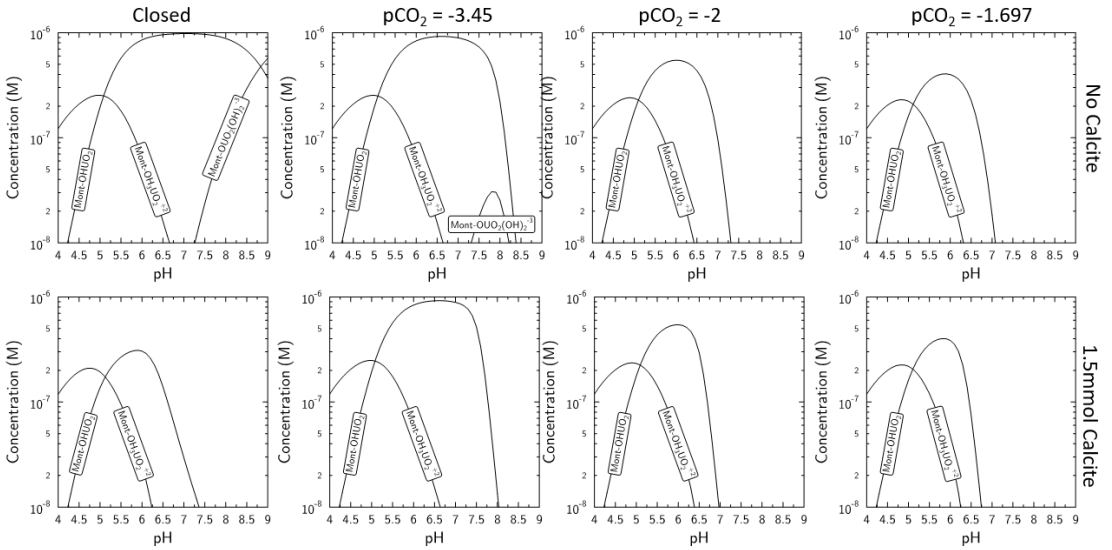

Figure 4-6. Uranium(VI) surface speciation for 1.0 μM U(VI) at all experimental conditions tested using the Tournassat et al. (2018) sorption model: pCO_2 = 0, -3.45, -2, and -1.697, in the absence (top) and presence (bottom) of 1.5 mM calcite.

4.3 Conclusions and Comparisons of Conceptual Sorption Models

In the following, we will summarize trends on specific chemical system conditions that were tested in both models. The closed systems showed the greatest window of pH sorption. Regardless of the allowed surface species, when CO_2 is excluded from the system, the cationic binding species exist in greater quantities (Chapter 3, Fig. 3-7). As more CO_2 is introduced to the system, the sorption between the two becomes more varied. It was expected that the Tournassat model would allow for less sorption due to its exclusion of uranium carbonate species but this is not the case (Figure 4-7). With respect to systems which have increasing carbonate concentration, the Tournassat model shows a lower degree of uranyl sorption, possibly due to the reduced constant for UO_2^{2+} binding (k=4.8 vs 3.1), allowing less of this present positive species to sorb.

(Table 4-3 and 4-5) This was determined by looking at the two provided sets of surface speciation (Fig. 4-3 and 4-6). Finally, calcite has an impact on the pH window of sorption for both models as neither allows for the surface complexation of Ca-U(VI)-ternary species meaning that the amount of calcite impurity in bentonite will certainly have a negative impact on retardation of uranium transport. Understanding the U(VI) K_d values for a variety of chemical system conditions provides the basis for one parameter of the parametric study in uranium(VI) diffusion models to follow (Chapter 5).

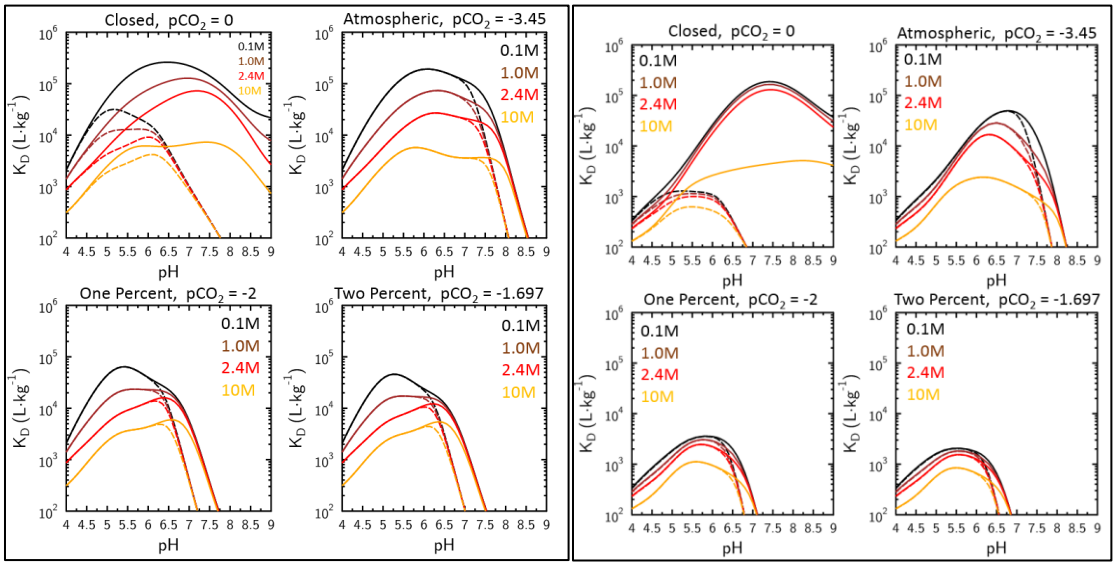

Figure 4-7. Side by side comparison of Marques and Tournassat models organized by pCO_2 and across U(VI) concentrations.

5.0 Uranium Diffusion in Montmorillonite

5.1 Background/Introduction

The ultimate goal of this work is to contribute to the body of understanding regarding uranium(VI) mobility in a future nuclear waste repositories. We have previously shown how the attenuation of U(VI) solution species can occur on the surface of montmorillonite through surface complexation modeling (Chapter 4). Although this parameter is a valuable in the understanding of uranium(VI) transport, uranium remaining in solution can still undergo diffusion in the porosity of the clay barrier. In this chapter we will couple the results of the surface complexation model by Tournsassat et al (2018) from the previous chapter with diffusive flux. Specifically, we will show how the different chemical conditions in the system (pH, pCO_2, presence of calcite) can affect U(VI) retardation and the subsequent diffusion of uranium(VI) through the clay barrier.

Numerous laboratories have developed experimental set-ups for increasingly accurate measurements of the diffusion of uranium(VI) tracers in montmorillonite clay. In the image found below (Figure 5-1), Tachi and Yotsuji developed this diagram to depict their laboratory set-up for a 1-D diffusion experiment. In the figure, container (a) contains the inlet reservoir with an initial concentration of uranium tracer. Indicator (b) is a peristaltic pump and the arrows indicate the direction of solution circulation. This aspect allows for continuous mixing of both reservoirs during experimental operation to ensure

homogenization. The clay material is packed within (c), the diffusion cell that is in this case, montmorillonite. Finally, reservoir (d) is the outlet and this is where samples of uranium are taken to measure diffusion through the cell over time. The outlet reservoir is constantly refreshed so as not to build a back-up gradient of uranium.

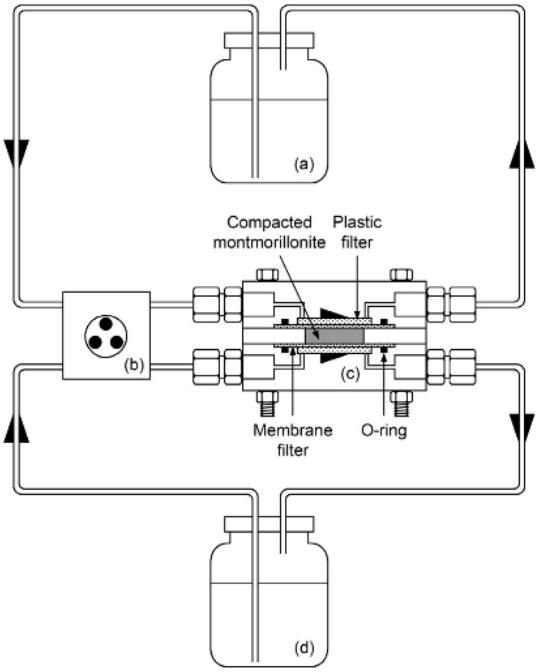

Figure 5-1. An example experimental set-up for diffusion experiments used to characterize U(VI) diffusion in clay systems (Tachi and Yotsuji 2014)

It is understood that in any potential future nuclear waste repository, the high degree of clay compaction will severely limit diffusive transport through the macropores and force diffusion to predominantly occur within clay interlayer

porosities. To better understand what this space looks like, an image is provided below (Figure 5-2).

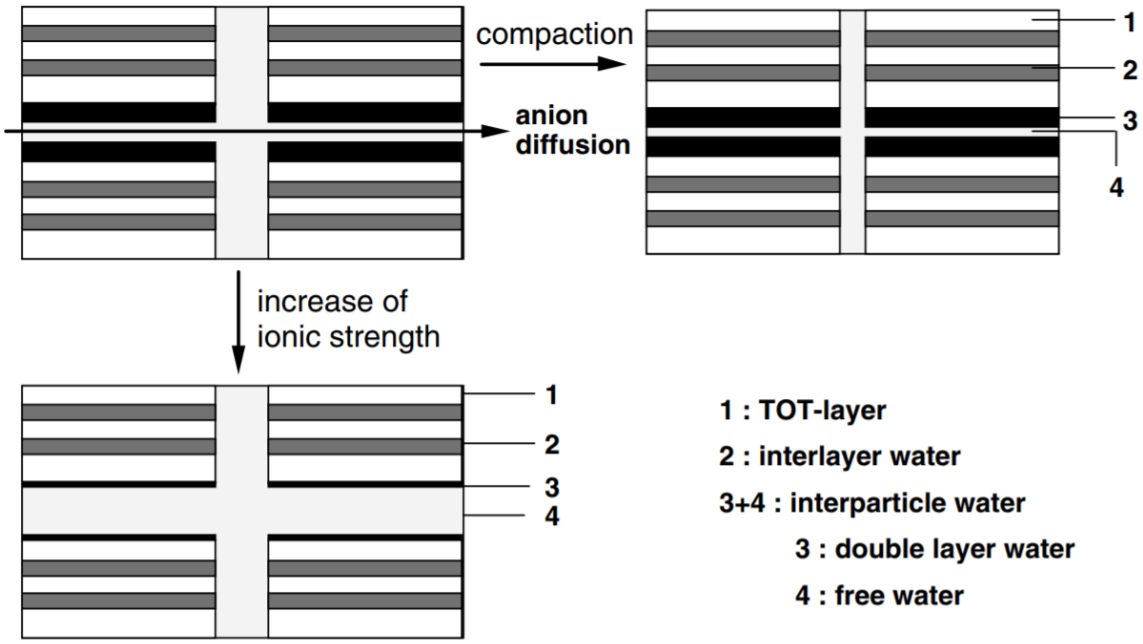

Figure 5-2. Effects of compaction and ionic strength on the macropores (interparticle pores) within clay material. Compaction leads to a reduction in pore size whereas ionic strength leads to a swelling and increase in size.

5.2 Uranium Diffusion Modeling Set-Up and Conceptual Understanding

5.2.1 Steady-State Concentration to Be Evaluated

The geochemical modeling program PHREEQC was not initially designed to simulate contaminant transport behavior, which can create some computational challenges. Hence, for this project it was decided to simulate U(VI) solution

speciation and sorption behavior in PHREEQC, and to couple these outputs with the analytical solution to Fick's law of diffusion in GLE. As a result, it was necessary to use a constant U(VI) K_d value, which was not affected by changes in U(VI) solution concentrations (C_{eq}), across the diffusion cell.

Hence, in order to construct a model to study uranium diffusion, some assumptions about the system conditions need to be made or evaluated. One of the first values that needs to be understood is at the concentration of U(VI) the system is equilibrated at steady-state across the clay plug. In order to determine which U(VI) concentration can be used for the conditions in this parametric study, it was first important to plot K_d vs. C_{eq} values. From (Fig. 5-3), it can be seen that at a concentration of U(VI) = 1E-8 M, U(VI) K_d values still show a concentration dependence in some of the lower CO_2 systems. Therefore, the concentration which was selected for this work was U(VI) = 1e-9 M, which was fully verified as a concentration providing constant K_d values by taking the derivative at that concentration. It is also relevant to notice that U(VI) K_d values from Marques model simulations are higher than those from the Tournassat for comparable partial pressures of CO_2, as seen in the previous section (Chapter 4).

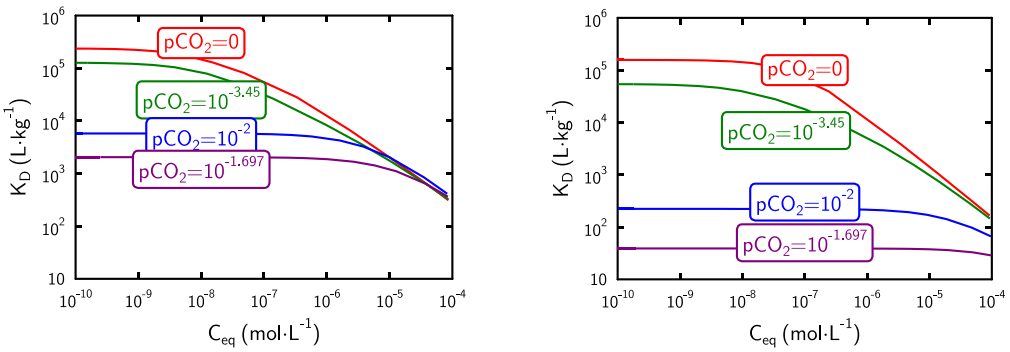

Figure 5-3. Graphical output of simulations of K_d vs C_{eq} for Marques (left) and Tournassat (right) surface complexation models.

5.2.2 Diffuse Double Layer Surface-Complexation Model

In diffusion cells packed with montmorillonite clay, U(VI) can be present in three main forms: (1) in the bulk water solution (mobile U(VI)), (2) in diffuse layer water close to montmorillonite surface (mobile U(VI)), or (3) sorbed onto clay surface complexation sites (immobile U(VI)). Under the assumed compaction with in a bentonite barrier, the mass of water in the diffuse layer is assumed to be 90% with the remainder comprising the bulk water (Appendix C).

Hence, if we are to accomplish a diffusion calculation it is important to define its underlying concepts and the assumptions that are made. We know from the previous section that the total U(VI) concentration must start at 1E-9M. This total U(VI) needs to be corrected to account for the accumulation of uranium species within diffuse layers relative to the bulk water. It is assumed that because of the negative charges in diffuse layers, the concentrations of cationic U(VI) species in

this volume will be higher than in the bulk water, e.g. U(VI) concentrations can be about 100-times more concentrated than in the bulk solution.

A detailed summary of the concepts behind these calculations is provided in Appendix B and C. Value are extracted from the U_distribution.phr.out file located in the Appendix D, and summarized in Table 5-1.

Table 5-1. U(VI) Diffusion parameters for different solution conditions

pH	pCO2	Ca [mM]	%cat	%neutral	%anions	Immobile Kd [L/kg]	Uranium in Diffuse Layer (moles)	U(VI) conc. in DL [M]	A
3	0	0	100	0	0	2.93E+01	6.12E-13	1.20E-07	120
5	0	0	100	0	0	2.31E+03	5.06E-13	9.95E-08	99
7	0	0	50	50	0	1.57E+05	4.08E-14	8.03E-09	8.0
9	0	0	0	10	90	3.78E+04	9.09E-16	1.79E-10	0.18
7	ATM	0	0	15	85	2.56E+02	4.01E-16	7.88E-11	0.08
7	1%	0	0	10	90	2.20E+02	3.69E-16	7.25E-11	0.07
7	1%	1.5	0	40	60	2.60E+01	5.66E-16	1.11E-10	0.11

An example output file is also shown in Figure 5-4 below. For instance, first the moles of U (5.063e-13 moles) are divided by the mass of water present in diffusive layers (5.089E-6 kg) to calculate the U(VI) molality in diffuse layer water (Eq. 5-1). Then this value is divided by the total U concentration (1.0e-9 M; Eq.5-2.) to calculate a corresponding accumulation factor (A) of ~100

$$\frac{5.063x10^{-13}}{5.089x10^{-6}} = 9.95x10 - 8 \quad (1)$$

$$\frac{9.95x10^{-8}}{1.0x10^{-9}} = 99.5 \quad (2)$$

```
Clay
        1.099e-10  Surface + diffuse layer charge, eq
       -5.655e-06  Surface charge, eq
       -1.158e-01  sigma, C/m²
       -9.582e-02  psi, V
        3.730e+00  -F*psi/RT
        4.166e+01  exp(-F*psi/RT)
        7.500e+02  specific area, m²/g
        4.712e+00  m² for   6.283e-03 g

        Water in diffuse layer: 5.089e-06 kg, 100.0% of total DDL-water.

        Total moles in diffuse layer (excluding water), Donnan calculation.
        Donnan Layer potential, psi_DL = -6.253e-02 V.
        Boltzmann factor, exp(-psi_DL * F / RT) = 1.140e+01 (= c_DL / c_free if z is +1).

        Element          Moles
        Cl           5.3130e-08
        H            7.4615e-10
        Na           5.7074e-06
        O            1.0256e-12
        U            5.0630e-13

Clay
        5.655e-06  moles
                                 Mole                 Log
        Species          Moles   Fraction  Molality   Molality

        Clay-        5.655e-06     1.000  1.000e+01      1.000
```

Figure 5-4. PHREEQC output file designed to show the significant values with which to calculate U(VI) accumulation inside the diffuse layer within the montmorillonite pores.

5.2.3 General Overview of Equations (Fick's law) and the Role of Sorption

If specific modeling conditions are chosen (constant K_d, constant pH, ionic strength, calcium and carbonate concentrations, and a total low U(VI) concentration of 1E-9 M $U(VI)_{Total}$) then the flux of uranium in this system can be

calculated with the following analytical solution (Eq. 5-1) for Fick's law of diffusion[44]:

$$Q_t = \frac{S \cdot C_0 \cdot D_e}{h} \cdot t - \frac{\alpha \cdot C_0 \cdot S \cdot h}{6} - \frac{2 \cdot \alpha \cdot S \cdot C_0 \cdot h}{\pi^2} \sum_{j=1}^{\infty} \frac{(-1)^j}{j^2} \exp\left(-\frac{D_e \cdot j^2 \cdot \pi^2 \cdot t}{L^2 \cdot \alpha}\right) \quad (1)$$

In this equation, Ft (in mol·m-2 ·s -1) is the instantaneous flux of U(VI) at the end of the clay packing, S (in m^2) is the surface of the sample in contact with each of the reservoirs, C0 (in $mol \cdot m^{-3}$) is the U(VI) concentration in the high concentration reservoir, De (in $m^2\ s^{-1}$) is the effective diffusion coefficient, h (in m) is the thickness of the sample, α is a rock capacity factor that relates the concentration in the porous media to the concentration in solution, L (in m) is the path length the solute would follow in water alone, and t (in s) is time. Water has a determined self-diffusion coefficient at a given experimental temperature (in this case all simulations are run at 25°C). This diffusion can subsequently be affected by other constituents added to a system so it is important to note that for this set of U(VI) diffusion simulations, the molecular diffusion coefficients were assumed to be the same for all U(VI) solution species, given the current uncertainty or lack of data for these values.

5.3 Results for Diffusion Modeling

Diffusions simulations were built with increasing levels in complexity, similar to conditions probed for speciation and sorption previously (Table 5-1). The first set

of conditions presented are for closed systems across a range of pH values without a calcite impurity (Figure 5-5). As pH increases, the simulations show very obvious trends with stronger U(VI) retardation and decreasing U(VI) fluxes. In the initial figure, it is very difficult to see U(VI) fluxes for all pH conditions tested; so two insets have also been provided to allow for more detailed observations.

The diffusion data presented below are mostly aligned with the expected U(VI) retardation due to U(VI) surface complexation reactions. In closed systems, as pH increases U(VI) K_d values also up to a point. However, the diffusion model does not appear to re-produce a reduction in U(VI) retardation for pH 9 in comparison to pH 7, which would be expected purely based on U(VI) K_d values and bulk diffusion.

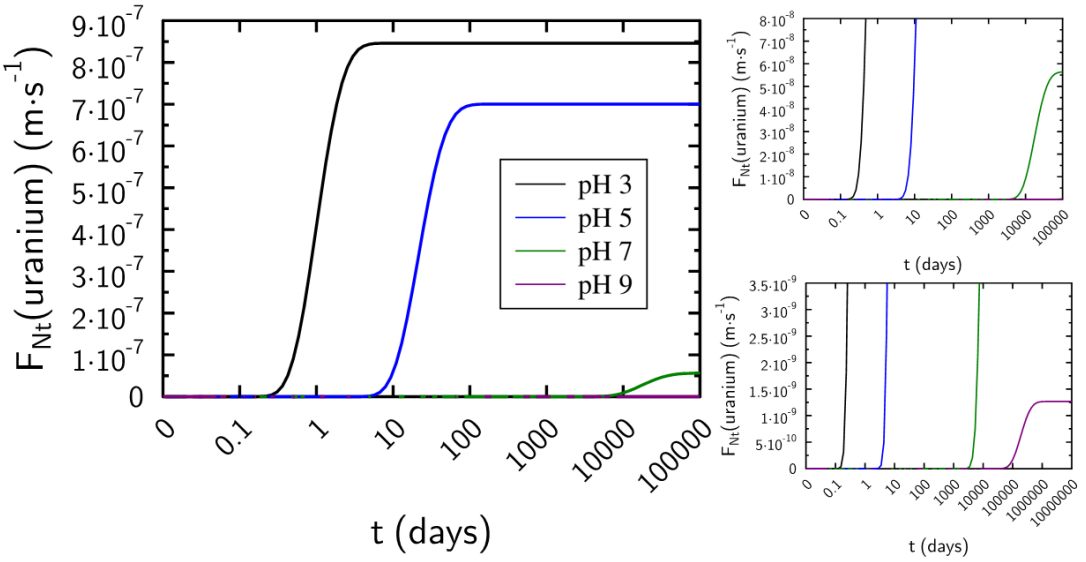

Figure 5-5. Diffusion simulations for a closed system across a range of pH (3,5,7,9). Insets have a reduced range of flux to hone in on retardation and flux of higher pH systems.

Hence, an additional phenomenon related to U(VI) solution speciation affects the overall U(VI) diffusion behavior. Tying U(VI) solution speciation in allows us to confirm the anion exclusion effect expected within the interlayer pores. At low pH (pH 3), the majority of U(VI) is UO_2^{2+} which would be expected to diffuse quickly in an anionic pathway. As pH is adjusted to 5, approximately one third of the species are now slightly less positively charged $UO_2(OH)^+$ which causes the observed reduction in U(VI) flux. When the conditions are neutral at pH 7, U(VI) species is about half neutral, causing over an order of magnitude reduction in diffusive flux. Lastly, at pH 9, the diffusive flux again drops by half an order of magnitude, as the dominant species is now the negatively charged $UO_2(OH)_3^-$ (Figure 5-6).

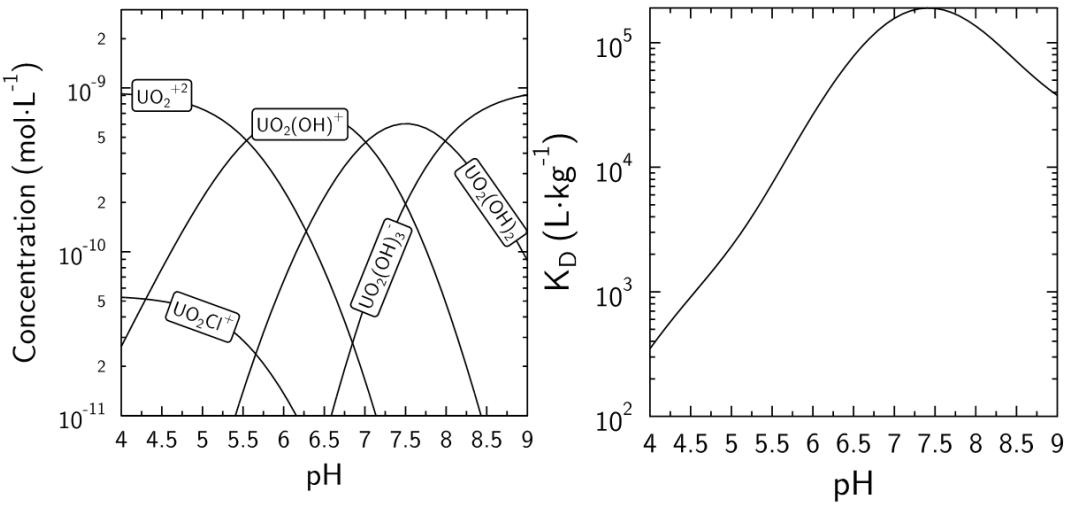

Figure 5-6. Speciation and Sorption for U(VI) concentration of 1E-9M in a closed system for comparison with diffusion results.

Other systems can also be evaluated by using the K_d and accumulation factors associated with their PHREEQC output files. Next we will compare a system with a fixed pH of 7, across the various partial pressures of CO_2 previously studied. Based on Figure 5-7, U(VI) retardation in closed and atmospheric systems is relatively similar as U(VI) accumulation in diffuse layers and U(VI) K_d values are found at similar orders of magnitudes. However, the 1% CO_2 system has an accumulation factor two orders of magnitude lower, which ends up reducing the steady state flux. The reduction in flux as CO_2 concentrations increase can be explained by looking at the corresponding speciation diagrams (Figure 5-8). As CO_2 is added to the system, cationic U(VI) solution species that previously dominated in the closed system, are replaced by $UO_2(CO_3)_2^{2-}$ and $UO_2(CO_3)_3^{4-}$ species, which will have limited diffusion through negatively-charged diffuse layer water.

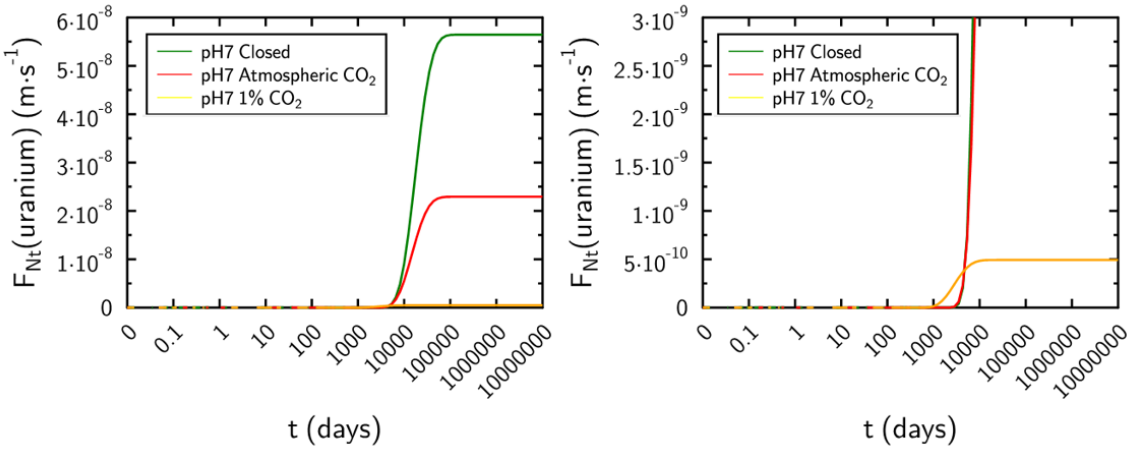

Figure 5-7. Diffusion simulations at pH7 for CO_2 conditions at closed (zero), atmospheric and 1% CO_2. Second image has a reduced flux range to focus in on retardation and flux for higher CO_2 systems.

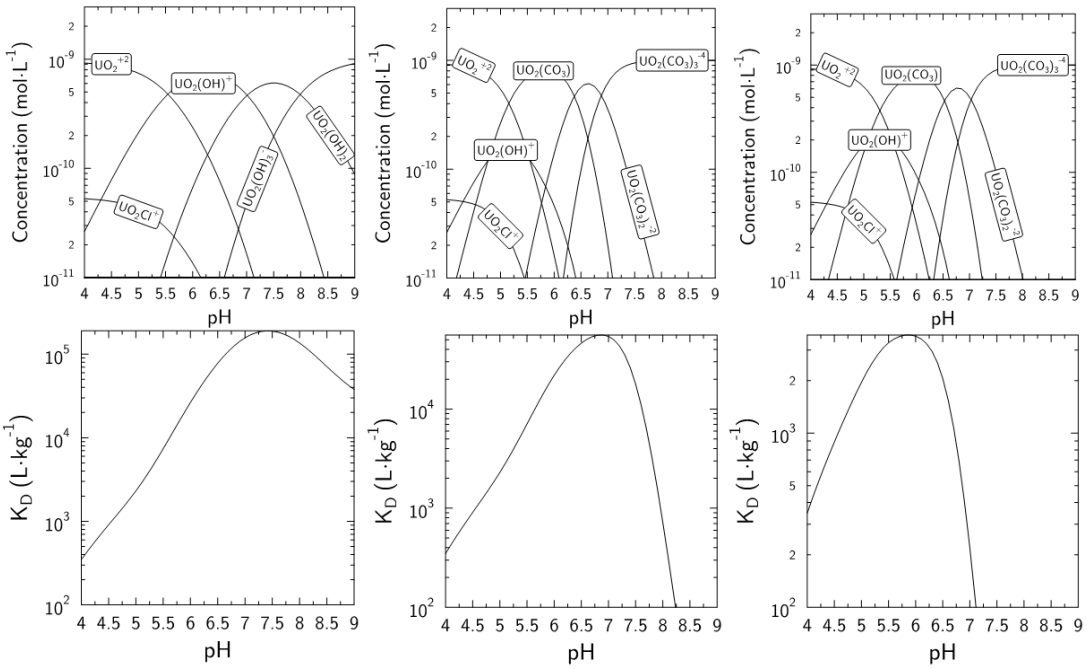

Figure 5-8. Speciation and sorption for U(VI) concentration of 1E-9M in a closed system for comparison with diffusion results. Top (left to right): Speciation for closed, atmospheric and 1% CO_2. Bottom (left to right): U(VI) sorption from Tournassat model for closed, atmospheric and 1% CO_2.

Lastly, we will compare three systems representing the spectrum of conditions throughout this work: a closed system at pH 7, to a system equilibrated with 1% CO_2 and also a system with 1% CO_2 and 1mmol calcite. The closed pH 7 system has been presented previously, and has a specific U(VI) retardation and flux as discussed above (Figure 5-9, black line). This system is equilibrated with CO_2, the flux is drastically reduced due to the exclusion of anionic U(VI) species from clay interlayer pores, but the retardation is also decreased based on the lower binding affinity for U(VI) species in this system. (Figure 5-9, orange line). When this 1% CO_2 system is subsequently equilibrated with 1mmol Ca^{2+}, the flux increases substantially due to the fact that less negatively charged U(VI) solution species exist in the presence of calcium. The transport is also enhanced due to the lack of sorption of newly-formed calcium-containing uranium species (Figure 5-9, brown line).

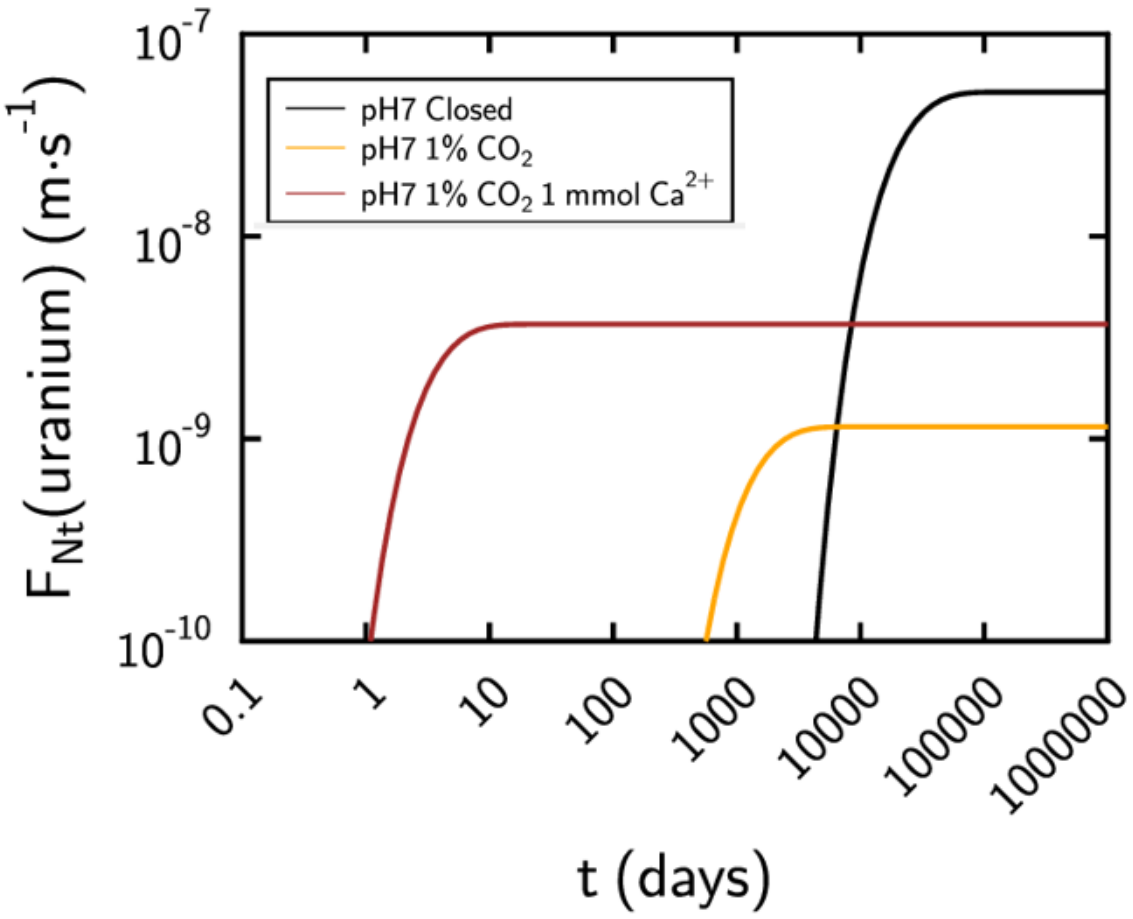

Figure 5-9. Diffusion simulations at pH7 for closed, 1% CO_2 and 1% CO_2 with 1mmol Ca^{2+}

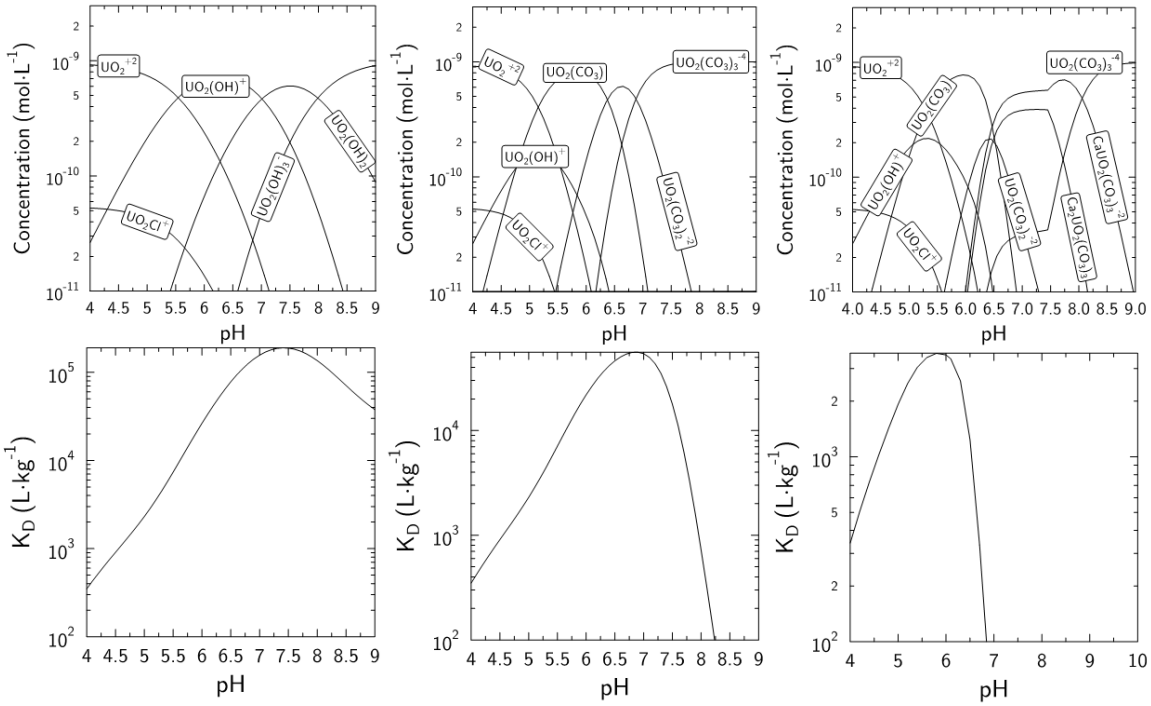

Figure 5-10. Speciation and Sorption for U(VI) concentration of 1E-9M for comparison with diffusion results. Top (left to right): Speciation for closed, 1% CO_2 and 1%CO_2 + 1mmol calcite. Bottom (left to right): Sorption from Tournassat model for closed, 1% CO_2 and 1%CO_2 + 1mmol calcite.

6.0 Conclusions and Future Directions

The three different components of this study, the simulation of U(VI) solution speciation, sorption and diffusion behavior, all have different implications for the overall understanding of the potential impacts of changing chemical conditions in nuclear waste repositories on uranium(VI) mobility. The results from speciation modeling show how drastically the concentrations of specific U(VI) solution species can change with shifts in solution conditions, such as pH, pCO_2, and calcite concentrations. The novel approach of depicting these various species in charge speciation diagrams allow for a better observation of relevant species

characteristics with respect to their sorption and transport behavior, e.g. the potential exclusion of anions from clay interlayer spaces. Our comparison of two types of surface complexation models provides further insights into U(VI) sorption distribution constants (K_d values) for a system at specific conditions. In a previous publication[23], it is has been shown that the conceptual model including the electronic spillover effect fits experimental U(VI) sorption data over a wider range of experimental conditions with fewer fitting parameters than a model containing uranium-carbonate surface complexes (Marques…ADD REF). This spillover sorption model was then integrated into subsequent diffusion calculations. This allowed us to demonstrate that U(VI) sorption drives U(VI) retardation, and determines the time when U(VI) breakthrough across a clay plug is observed. A final issue of major importance for U(VI) diffusion modeling is the accumulation of cationic U(VI) solution species in diffuse layers close to clay surfaces. Our diffusion model has been invaluable in tying the U(VI) K_d value extracted from surface complexation models to the accumulation factor describing the accumulation of U(VI) solution species in diffuse layers close to clay surfaces. Cationic U(VI) solution species accumulated in these in diffuse layers are mobile. They can enhance the overall steady-state fluxes of U(VI) across the clay plug, and potentially the engineered barrier in a future nuclear waste repository.

References

(1) Fieveson, H.; Mian, Z.; Ramana, M. V.; von Hippel, F. Spent Fuel from Nuclear Power Reactions - An Overview of a New Study by The International Panel on Fissile Materials. Internation Panel on Fissile Materials June 2011.

(2) *On the Implementation of the Obligations under the Joint Convention on the Safety of Spent Fuel Management and on the Safety of Radioactive Waste Management*; Review Meeting of Contracting Parties; European Atomic Energy Community: Vienna, Austria, 2018; p 97.

(3) *Classification of Radioactive Waste*; IAEA Safety Standards; General Safety Guide GSG-1; International Atomic Energy Agency: Vienna, Austria, 2009; p 68.

(4) Johnson, J. Radioactive Waste Safety. *Chem. Eng. News* **2013**, 2.

(5) Settle, F. A. Uranium to Electricity: The Chemistry of the Nuclear Fuel Cycle. *J. Chem. Educ.* **2009**, *86* (3), 316. https://doi.org/10.1021/ed086p316.

(6) Criteria for the Certification and Recertification of the Waste Isolation Pilot Plant's Compliance With the Disposal Regulations; Recertification Decision. Environmental Protection Agency July 19, 2017.

(7) *Radioactive Waste Management and Contaminated Site Clean-up: Processes, Technologies and International Experience*; Lee, W. E., Ed.; Woodhead Publishing series in energy; Woodhead Publishing: Oxford ; Philadelphia, 2013.

(8) Eckerman, K. F.; Ryman, J. C. External Exposure to Radionuclides in Air, Water, and Soil. **1993**, 238.

(9) Prazsky, M.; Adamek, A.; Binka, J. Determination of Oxidation States of Uranium and Plutonium in Cooling Solution of Spent Fuel Element Assemblies from NPP A-1. *J. Radioanal. Nucl. Chem. Artic.* **1989**, *129* (2), 289–294. https://doi.org/10.1007/BF02039826.

(10) Prazsky, M.; Adamek, A.; Binka, J. Determination of Oxidation States of Uranium and Plutonium in Cooling Solution of Spent Fuel Element Assemblies from NPP A-1. *J. Radioanal. Nucl. Chem. Artic.* **1989**, *129* (2), 289–294. https://doi.org/10.1007/BF02039826.

(11) Lowry, J. D.; Lowry, S. B. Radionuclides in Drinking Water. *J. - Am. Water Works Assoc.* **1988**, *80* (7), 50–64. https://doi.org/10.1002/j.1551-8833.1988.tb03068.x.

(12) Radionuclides Rule: A Quick Reference Guide. United States Environmental Protection Agency June 2001.

(13) Sofield, R. M.; Kantar, C. Uranium. In *Reference Module in Earth Systems and Environmental Sciences*; Elsevier, 2013. https://doi.org/10.1016/B978-0-12-409548-9.00804-6.

(14) Long, J. C. S.; Ewing, R. C. Yucca Mountain: Earth-Science Issues at a Geologic Repository for High-Level Nuclear Waste. *Annu. Rev. Earth*

Planet. Sci. **2004**, *32* (1), 363–401. https://doi.org/10.1146/annurev.earth.32.092203.122444.
(15) Stuckless, J. S.; Levich, R. A. The Road to Yucca Mountain—Evolution of Nuclear Waste Disposal in the United States. *Environ. Eng. Geosci.* **2016**, *22* (1), 1–25. https://doi.org/10.2113/gseegeosci.22.1.1.
(16) Sellin, P.; Leupin, O. X. The Use of Clay as an Engineered Barrier in Radioactive-Waste Management – A Review. *Clays Clay Miner.* **2013**, *61* (6), 477–498. https://doi.org/10.1346/CCMN.2013.0610601.
(17) Bennett, D. G.; Sällfors, G. Bentonite in Geological Disposal of Low and Intermediate Level Radioactive Waste. In: SSM's External Experts' Reviews of SKB's Safety Assessment SR-PSU – Engineered Barriers, Engineering Geology and Chemical Inventory: Initial Review Phase. *40882* **2016**. https://doi.org/10.13140/rg.2.2.17845.37605.
(18) Borchardt, G. *Montmorillonite and Other Smectite Minerals*, 1st ed.; Unpublished, 1977. https://doi.org/10.13140/RG.2.1.1292.2966.
(19) Teich-McGoldrick, S. L.; Greathouse, J. A.; Jové-Colón, C. F.; Cygan, R. T. Swelling Properties of Montmorillonite and Beidellite Clay Minerals from Molecular Simulation: Comparison of Temperature, Interlayer Cation, and Charge Location Effects. *J. Phys. Chem. C* **2015**, *119* (36), 20880–20891. https://doi.org/10.1021/acs.jpcc.5b03253.
(20) Schlegel, M. L.; Descostes, M. Uranium Uptake by Hectorite and Montmorillonite: A Solution Chemistry and Polarized EXAFS Study. *Environ. Sci. Technol.* **2009**, *43* (22), 8593–8598. https://doi.org/10.1021/es902001k.
(21) Goldberg, S.; Criscenti, L. J.; Turner, D. R.; Davis, J. A.; Cantrell, K. J. Adsorption–Desorption Processes in Subsurface Reactive Transport Modeling. *Vadose Zone J.* **2007**, *6* (3), 407. https://doi.org/10.2136/vzj2006.0085.
(22) Tournassat, C.; Davis, J. A.; Chiaberge, C.; Grangeon, S.; Bourg, I. C. Modeling the Acid–Base Properties of Montmorillonite Edge Surfaces. *Environ. Sci. Technol.* **2016**, *50* (24), 13436–13445. https://doi.org/10.1021/acs.est.6b04677.
(23) Tournassat, C.; Tinnacher, R. M.; Grangeon, S.; Davis, J. A. Modeling Uranium(VI) Adsorption onto Montmorillonite under Varying Carbonate Concentrations: A Surface Complexation Model Accounting for the Spillover Effect on Surface Potential. *Geochim. Cosmochim. Acta* **2018**, *220*, 291–308. https://doi.org/10.1016/j.gca.2017.09.049.
(24) Alther, G. R. The Qualifications of Bentonite as a Soil Sealant. *Eng. Geol.* **1987**, *23* (3–4), 177–191. https://doi.org/10.1016/0013-7952(87)90089-5.
(25) Birgersson, M.; Karnland, O. Ion Equilibrium between Montmorillonite Interlayer Space and an External Solution—Consequences for Diffusional Transport. *Geochim. Cosmochim. Acta* **2009**, *73* (7), 1908–1923. https://doi.org/10.1016/j.gca.2008.11.027.
(26) Meinrath, G. Uranium(VI) Speciation by Spectroscopy. *J. Radioanal. Nucl. Chem.* **1997**, *224* (1), 119–126. https://doi.org/10.1007/BF02034623.

(27) Mühr-Ebert, E. L.; Wagner, F.; Walther, C. Speciation of Uranium: Compilation of a Thermodynamic Database and Its Experimental Evaluation Using Different Analytical Techniques. *Appl. Geochem.* **2019**, *100*, 213–222. https://doi.org/10.1016/j.apgeochem.2018.10.006.
(28) *Long-Term Performance of Permeable Reactive Barriers*; Roehl, K. E., Ed.; Trace metals and other contaminates in the environment; Elsevier: Amsterdam, 2005.
(29) Yu, Z.; Lin, Y.; Johannesson, K.; Smiecinski, A. J.; Stetzenbach, K. J. Geochemical Modeling of Solubility and Speciation of Uranium, Neptunium, and Plutonium. *UNLV Libr.* **2007**, 55.
(30) McKinley, J. P.; Zachara, J. M.; Smith, S. C.; Turner, G. D. The Influence of Uranyl Hydrolysis and Multiple Site-Binding Reactions on Adsorption of U(VI) to Montmorillonite. *US Dep. Energy Publ.* **1995**, *43* (5), 586–598. https://doi.org/10.1346/CCMN.1995.0430508.
(31) Pabalan, R. T.; Turner, D. R. Uranium(6+) Sorption on Montmorillonite: Experimental and Surface Complexation Modeling Study. *Aquat. Geochem.* **1996**, *2* (3), 203–226. https://doi.org/10.1007/BF01160043.
(32) Pabalan, R. T.; Bertetti, F. P.; Prikryl, J. D.; Turner, D. R. Uranium (VI) Sorption onto Selected Mineral Surfaces: Key Geochemical Parameters. **1996**.
(33) Bachmaf, S.; Planer-Friedrich, B.; Merkel, B. J. Uranium Sorption and Desorption Behavior on Bentonite. In *Uranium, Mining and Hydrogeology*; Merkel, B. J., Hasche-Berger, A., Eds.; Springer Berlin Heidelberg: Berlin, Heidelberg, 2008; pp 515–524. https://doi.org/10.1007/978-3-540-87746-2_63.
(34) Bradbury, M. H.; Baeyens, B. Modelling the Sorption of Mn(II), Co(II), Ni(II), Zn(II), Cd(II), Eu(III), Am(III), Sn(IV), Th(IV), Np(V) and U(VI) on Montmorillonite: Linear Free Energy Relationships and Estimates of Surface Binding Constants for Some Selected Heavy Metals and Actinides. *Geochim. Cosmochim. Acta* **2005**, *69* (4), 875–892. https://doi.org/10.1016/j.gca.2004.07.020.
(35) Marques Fernandes, M.; Baeyens, B.; Dähn, R.; Scheinost, A. C.; Bradbury, M. H. U(VI) Sorption on Montmorillonite in the Absence and Presence of Carbonate: A Macroscopic and Microscopic Study. *Geochim. Cosmochim. Acta* **2012**, *93*, 262–277. https://doi.org/10.1016/j.gca.2012.04.017.
(36) Troyer, L. D.; Maillot, F.; Wang, Z.; Wang, Z.; Mehta, V. S.; Giammar, D. E.; Catalano, J. G. Effect of Phosphate on U(VI) Sorption to Montmorillonite: Ternary Complexation and Precipitation Barriers. *Geochim. Cosmochim. Acta* **2016**, *175*, 86–99. https://doi.org/10.1016/j.gca.2015.11.029.
(37) Davis, J. A.; Meece, D. E.; Kohler, M.; Curtis, G. P. Approaches to Surface Complexation Modeling of Uranium(VI) Adsorption on Aquifer Sediments11Associate Editor: J. Rustad. *Geochim. Cosmochim. Acta* **2004**, *68* (18), 3621–3641. https://doi.org/10.1016/j.gca.2004.03.003.
(38) Curtis, G. P.; Fox, P.; Kohler, M.; Davis, J. A. Comparison of in Situ Uranium KD Values with a Laboratory Determined Surface Complexation Model.

Appl. Geochem. **2004**, *19* (10), 1643–1653. https://doi.org/10.1016/j.apgeochem.2004.03.004.
(39) Fox, P. M.; Davis, J. A.; Zachara, J. M. The Effect of Calcium on Aqueous Uranium(VI) Speciation and Adsorption to Ferrihydrite and Quartz. *Geochim. Cosmochim. Acta* **2006**, *70* (6), 1379–1387. https://doi.org/10.1016/j.gca.2005.11.027.
(40) García-Gutiérrez, M.; Cormenzana, J. L.; Missana, T.; Mingarro, M.; Alonso, U. Analysis of Uranium Diffusion Coefficients in Compacted FEBEX Bentonite. *MRS Proc.* **2003**, *807*. https://doi.org/10.1557/PROC-807-603.
(41) Korichi, S.; Bensmaili, A. Sorption of Uranium (VI) on Homoionic Sodium Smectite Experimental Study and Surface Complexation Modeling. *J. Hazard. Mater. 169* (1–3), 780–793. https://doi.org/10.1016/j.jhazmat.2009.04.014.
(42) Parkhurt, D. L.; Appelo, C. A. J. *Description of Input and Examples for PHREEQC Version 3—A Computer Program for Speciation, Batch-Reaction, One-Dimensional Transport, and Inverse Geochemical Calculations*; U.S. Geological Survey Techniques and Methods; Techniques and Methods; USGS, 2013; p 497.
(43) Kowal-Fouchard, A.; Drot, R.; Simoni, E.; Ehrhardt, J. J. Use of Spectroscopic Techniques for Uranium(VI)/Montmorillonite Interaction Modeling. *Environ. Sci. Technol.* **2004**, *38* (5), 1399–1407. https://doi.org/10.1021/es0348344.
(44) Tinnacher, R. M.; Holmboe, M.; Tournassat, C.; Bourg, I. C.; Davis, J. A. Ion Adsorption and Diffusion in Smectite: Molecular, Pore, and Continuum Scale Views. *Geochim. Cosmochim. Acta* **2016**, *177*, 130–149. https://doi.org/10.1016/j.gca.2015.12.010.

Appendix Table of Contents

Appendix A. PHREEQC, GLE, and BASIC: Modeling Methods – Detailed Information

A.1 PHREEQC

A.1.1 PHREEQC Software and Hardware Specifications

PHREEQC Interactive V. 3.3.11.12535 (Released March 10, 2017) was utilized for all computations in this work. At the beginning of this project the most updated database, ThermoChimie_PHREEQC_eDH_v9b0.dat, was downloaded from https://www.thermochimie-tdb.com/. The computer used to execute these computations was an Intel® Core™ i5 CPU 760 @ 2.80 GHz 1.60 GHz, 16.0 GB RAM running Windows 10 64-bit operating system.

A.1.2 PHREEQC KEYWORD LIST

A.1.2.1 SOLUTION_MASTER_SPECIES

The database provided by Thermochemie includes a plethora of equilibrium reactions and constants that allows a user to perform a wide range of computational experiments. Although the available databases are frequently updated and expanded, it is possible that they may not include a specific constant for a chemical equilibrium of interest or a complexation constant for a specific surface complexation reaction. If this is the case, the keyword SOLUTION_MASTER_SPECIES is used to define element names and associate them with aqueous primary or secondary master species. An example taken from the PHEEQC Version 3 Help:

```
SOLUTION_MASTER_SPECIES
   H      H+       -1.0    1.008    1.008
   H(0)   H2        0.0    1.008
   S      SO4-2     0.0    SO4      32.06
   S(6)   SO4-2     0.0    SO4
   S(-2)  HS-       1.0    S
   Alkalinity    CO3-2     1.0    Ca0.5(CO3)0.5    50.04
   [18O]  H2[18O]  0       [18O]    18
```

Figure 2-1. Sample solution master species showing a variety of input categories.

The first column consists of elements (some with valence states), and the second column lists the master species which they are being defined as for recall associated programming purposes. The PHREEC version 3 manual states “If the *element name* does not contain a valence state in parentheses, the corresponding master species is a primary master species. If the element name does contain a valence state in parentheses, the master species is a secondary master species." The values in the subsequent columns correspond to alkalinity values, gram formula weight, and gram formula weight for the element respectively.

A.1.2.2 SOLUTION_SPECIES

This keyword also functions as an amendment to the database in order to assign equilibrium constants to reactions that are not already listed in the database. In the example below from the PHREEQC help file the reaction or carbonate with a

proton to form bicarbonate is printed along with its associated equilibrium constant. Another important relationship to establish is the association reaction for the identity of a primary master species. This can be seen in the chloride anion relationship with the associated log K value of zero (Figure 2-2).

```
SOLUTION_SPECIES
 CO3-2 + H+ = HCO3-
 log_k  10.329
 delta_h -3.561 kcal
 Cl- =  Cl-
 log_k  0
```

Figure 2-2. Examples of solution species showing a variety of input categories including the log k value of reaction constants.

A.1.2.3 SURFACE_MASTER_SPECIES

This KEYWORD is used to define the names of surface binding sites and the associated master species. Again from the PHREEQC help file:

```
SURFACE_MASTER_SPECIES
  Surf_s  Surf_sOH
  Surf_w  Surf_wOH
```

Figure 2-3. Help file example of surface master species for two different types of sites

In this example, Surf_s and Surf_w are binding site names, and the master species are the associated hydroxyl (OH) forms.

In a similar way, SURFACE_MASTER_SPECIES was used in this work to define the surface of montmorillonite as Mont_s (for strong binding sites) with a Mont_sOH master species and Mont_w (for weak binding sites) with Mont_wOH

as a master species. Based on this definition the software to acknowledges each as hydroxylated initially.

```
SURFACE_MASTER_SPECIES
  Mont_s   Mont_sOH
  Mont_w   Mont_wOH
```

Figure 2-4. Example of Custom Named Surface Master Species For two types of site

A.1.2.4 SURFACE_SPECIES

Species that can exist on the surface of a particle, which is added to the system as defined in this block. Again, referring to an example from this current work (Figure 2-5) when Mont_sOH interacts with uranium(VI) (as $UO2^{+2}$) and CO_2 (as CO_3^{2-}) in solution, the reaction is defined and an equilibrium constant value is assigned from the literature:

```
SURFACE_SPECIES
  Mont_sOH + UO2+2 + CO3-2 = Mont_sOUO2CO3- + H+
    log_k     9.8
```

Figure 2-5. Example of a surface reaction for montmorillonite, uranyl and carbonate with log reaction constant

A.1.2.5 PHASES

In this section phases are defined by specifying the chemical name, an associated chemical reaction, a reaction constant, and potentially temperature dependence or delta H. These components can then be called upon by a name that is not necessarily a chemical or chemical reaction. Many of these relationships are predefined in the chemical database but some relationships must be established by the user for convenience. The most common use of this

is to define Fix_pH or Fix_H+ in order to evaluate systems across a range of fixed pH values. The command to do this is:

```
PHASES
 Fix_pH
 H+ = H+
 log_k 0
```

Figure A-6. Custom phase which can be called upon to specify pH

This relationship is now a phase and can be called upon in EQUILIBRIUM_PHASES by including “Fix_pH.” The desired pH can then be specified as a negative number as this phase’s equilibrium constant is defined in logarithmic notation.

```
DATABASE ThermoChimie_PHREEQC_eDH_v9b0.dat
SURFACE_MASTER_SPECIES
    Mont_s          Mont_sOH #these can be named generally anything the user wishes
    Mont_w          Mont_wOH #markings after the "_" are important to the model
    Clay            Clay-

SURFACE_SPECIES


Clay- = Clay-
    log_k     0
Clay- + Na+ = ClayNa
    log_k     0
2 Clay- + Ca+2 = Clay2Ca
    log_k     0.5

#Mont_s for strong sites and Mont_w for weak sites
#Strong Sites
Mont_sOH = Mont_sOH #this basic realtionship must be defined
    log_k     0
Mont_sOH + H+ = Mont_sOH2+#Aqueous REactions
    log_k     4.5
Mont_sOH = Mont_sO- + H+
    log_k     -7.9

Mont_sOH + UO2+2 = Mont_sOUO2+ + H+ #Strong Surface Uranium Reactions
    log_k     3.1
H2O + Mont_sOH + UO2+2 = Mont_sOUO2OH + 2H+
    log_k     -4.6
2H2O + Mont_sOH + UO2+2 = Mont_sOUO2(OH)2- + 3H+
    log_k     -12.6
3H2O + Mont_sOH + UO2+2 = Mont_sOUO2(OH)3-2 + 4H+
    log_k     -20.9

#Weak Sites
Mont_wOH = Mont_wOH #Aqueous Reactinos
    log_k     0
Mont_wOH + H+ = Mont_wOH2+
    log_k     4.5
Mont_wOH = Mont_wO- + H+
    log_k     -7.9
```

```
Mont_wOH + UO2+2 = Mont_wOUO2+ + H+ #Weak Surface Uranium Reactions
    log_k     0.5
Mont_wOH + UO2+2 + H2O = Mont_wOUO2OH + 2H+
    log_k     -5.7


#Carbonates Strong and Weak
Mont_sOH + UO2+2 + CO3-2 = Mont_sOUO2CO3- + H+
    log_k     9.8
Mont_sOH + UO2+2 + 2CO3-2 = Mont_sOUO2(CO3)2-3 +H+
    log_k     15.5
Mont_wOH + UO2+2 + CO3-2 = Mont_wOUO2CO3- + H+
    log_k     9.3

2ClayNa + UO2+2 = Clay2UO2 + 2Na+
    log_k     0.45


SURFACE 1
    Mont_sOH    1e-06     810       0.5
    #moles of sites, surface=m2/g, surface material (grams)
    Mont_wOH    2e-05
    #moles of sites
END
```

This example show the surface build out in PHREEQC associated with Marques et al. 2012. The surface has been named “Mont” for obvious reasons and two different types of surfaces are differentiated by “s” and “w” identified as strong and weak surfaces in Marques’ paper.

A.1.2.6 SOLUTION

A SOLUTION is defined by default as one liter/kilogram of water. A pH is also specified or has a value of 7 by default. In addition, other specifics can be defined such as pe, redox pairs, and temperature. To this set of initial parameters the user can add any number or amount of ionic species.

In this work all simulations were accomplished with a background electrolyte of 0.1 M NaCl in order to simulate a constant ionic strength. This

technique is often used in laboratory experiments to avoid any ionic strength effects on speciation or reaction over the course of experiments. For this purpose, SOLUTION is defined as containing 100 Na and 100 Cl (default unit is mmol/kg). Of course other components can then be added in a similar fashion at lower concentrations in order to attain the constant ionic strength effect. In the below example from this study, pH is set at a value of 3, pe is set at 10, 0.1 moles of NaCl are added to the system to fix the ionic strength, a small concentration of uranium (10^{-7} through 10^{-5} M) is added to complete the system. Optionally, Ca^{2+} can be added here or through the EQUALIBRIUM_PHASES instruction block depending on the user's intended outcome and desired output. Note that the default units for elements added to the solution is millimoles per kilogram of water (mmol/kgw) by default.

```
SOLUTION 1
 pH 3 #obvious
 pe 10 #conventional negative log of the activity of the electron
  redox          O(-2)/O(0)
 Na 100 #Default is mmol/kgw
 Cl 100 charge
 U(6) 1e-6
 Ca 1
```

Figure A-7. An example of a simple solution definition at a fixed pH of 3

A.1.2.7 EQUILIBRIUM_PHASES

Once a solution has been specified, this solution can then be taken through a range of equilibrium reactions through the use of the keyword EQUILIBRIUM_PHASES. One of the most common uses of this keyword is to

adjust the pH of a solution, in order to evaluate system behavior across the full range of pH scale. For this purpose, the hydronium ion is invoked using “Fix_H+”, which is a phase that was previously defined in the PHASES keyword. Next, a particular pH value is specified and a chemical is listed that is used for the simulated pH adjustment (commonly HCl for acidic conditions or NaOH for basic condition). In order to ensure that enough acid or base is available to reach the desired pH, large concentrations of 10 molar (the default) are typically included.

```
USE SOLUTION 1
EQUILIBRIUM_PHASES 1
Fix_pH -7 NaOH 10 #Final ph is fixed, excess of NaOH or HCl if basic or acidic
```

Figure A-8. The equilibration of a predefined solution 1 with NaOH to reach a pH value of 7.

This keyword is also commonly used to equilibrate solutions with a gas phase containing higher levels of CO_2. In gas phases, the key parameters to include are its partial pressure (e.g. $10^{-3.45}$ in figure 2-9 below) and the total gas concentration. It is common to have a large excess of gas, because of the partitioning between gas an solution phases.

```
USE SOLUTION 1
EQUILIBRIUM_PHASES 1
Fix_pH -7 NaOH 10 #Final ph is fixed, excess of NaOH or HCl if basic or acidic
CO2(g) -3.45 10 #Atmospheric pCO2=10^-3.45, moles present = 10 to ensure an excess
```

Figure A-9. pH and CO_2 both in equilibration with the previously defined solution 1.

Lastly, if

a solid phase is added, then the first value to the right of the solid name is the

saturation index, ($SI = \log_{10} (IAP / K_{sp})$) and the second the ion activation product (IAP). With regards to the SI, and its effect on solutions:

$SI = 0$	$IAP = K_{sp}$	→	saturated (in equilibrium)
$SI < 0$	$IAP < K_{sp}$	→	undersaturated
$SI > 0$	$IAP > K_{sp}$	→	supersaturated

```
USE SOLUTION 1
EQUILIBRIUM_PHASES 1
Fix_pH -7 NaOH 10 #Final ph is fixed, excess of NaOH or HCl if basic or acidic
CO2(g) -3.45 10 #Atmospheric pCO2=10^-3.45, moles present = 10 to ensure an excess
Calcite 0 0.002  #SI, Saturation Index; Moles, default is 10
```

Figure A-10. Equalibration of solution 1 at pH 7, atmospheric CO_2 and 2mmol calcite.

It is important to note that the entire system will be equilibrated with all phases simultaneously when multiple instructions are given over a series of commands.

A.1.2.8 SELECTED_OUTPUT

In the SELECTED_OUTPUT keyword block, the simulation output to a data file is specified starting with the file name. For simulations involving speciation calculations, printing pH is mandatory. Subsequent instructions are given as described below (Figure 2-11) and should, at a minimum, include molalities of relevant species. Other instructions can also be given, such as calculations using the BASIC language and the USER_PUNCH instruction.

```
SELECTED_OUTPUT 1
    -file             UCalSpecATM.prn #name the data file as you want it saved
    -high_precision   true #12 decimal places instead of 3-4.
    -reset            false #sets all output to false so user can subsequently specify
    -pH               true #ensures that pH is printed
    -molalities       CO2  HCO3-  CO3-2  Ca+2 #molalities of these species are printed
    -active           true #turns the printing of data to the output file
    -user_punch       false #allows user_punch instructions to be printed to output file
```

Figure A-11. Selected output specified to format the output file for further external software manipulation

A.1.2.9 PRINT

Print is utilized if the user only wants specific simulation results exported to the PHREEQC specific output file. This is the file that is created after every simulation with the “XYZ.out” file extension, which is different from the data file specified in SELECTED_OUTPUT (Ex. UCalSpecATM.prn)

A.1.2.10 Further KEYWORDS

The previous sections describe the most relevant KEYWORDS that are needed to reproduce the simulations from in this study. Hopefully these brief explanations will help the user to understand how the individual keyword blocks are defined and what the program is doing in response to these inputs. There are dozens of other KEYWORDS available in PHREEQC to accomplish other simulations of reactions and transport mechanisms. These can all be referenced for further work with the PHREEQC help file.

A.1.3 PHREEQC Closing Remarks

PHREEQC can be used methodically to simulate various reactions and conditions for chemical systems at equilibrium. Although in this study it is exclusively used for chemical speciation and sorption modeling, it can also be applied to kinetic and transport modeling. All of the key words discussed in this section can be easily referenced in further detail in the PHREEQC help file that comes standard with all versions of the software. Lastly, if further insight is needed, one of the creators (David Parkhurst) has responded to thousands of questions on online message boards in order to help users with circumstantial or syntax issues.

A.2 BASIC

It is also possible to include BASIC programming instructions in the PHREEQC input file. This allows for generally desirable programming features such as loops to be enabled within PHREEQC. Loops are valuable specifically where the same type of calculations are performed for a series of conditions, such as speciation. This approach simplifies the input file but gives an expanded data output file. It is especially useful for applications where conditions are grouped in small steps over wide ranges, in the case of speciation simulations, the pH on the x-axis as the independent variable.

```
SELECTED_OUTPUT
 -reset false
 -file JCP.loop1
USER_PUNCH
 -start
1150   punch eol$ + 'SOLUTION 1'
1155   punch eol$ + ' pH 7 '
1157   punch eol$ + ' pe 10 '
1160   punch eol$ + ' Na 100'
1170   punch eol$ + ' Cl 100 charge'
1180   punch eol$ + ' U(6) 0.000001'
1181   punch eol$ + 'END'

1300 for k = 3 to 10 step 0.05
1310  punch eol$ + ' USE SOLUTION 1'
1320   punch eol$ + ' EQUILIBRIUM_PHASES 1'
1330   punch eol$ + ' Fix_pH ' + str$(-k) + ' NaOH 10'
1340   punch eol$ + ' CO2(g) -3.45 10'
1350   punch eol$ + 'END'
1360 next k
```

Figure A-12. Example for BASIC instructions within a PHREEQC input file including PUNCH and Looping

It is important to understand that the BASIC functionality is executed in the order of the line numbers included at the beginning of each line of instruction. This allows the user to quickly reorganize the order of instructions in the input file if necessary but also means that the program execution can be nonlinear with respect to the visible lines of text.

As seen in the figure above (Figure 2-12), the SELECTED_OUTPUT key word is used to define the name for the output file that receives the data from the BASIC punch commands. BASIC is then enabled by calling USER_PUNCH.

Subsequently, a start function is called followed by numbers in a series of events which is integral to the function of BASIC and not specific to PHREEQC. Initially in line numbers 1150-1181, we are simply punching a standard SOLUTION to then apply an EQUILIBRIUM_PHASES loop onto. In the section starting with line number 1300, a loop is specified by a string on line 1330 which has a variable “k” that has a range applied to it of numerical values 3-10 with incremental steps ever 0.05 units. This signals the output to punch every increment starting with 3 up to 10 (ex. 3.00, 3.05, 3.10, 3.15, …9.90, 9.95, 10.00).

This is essentially the only area in which BASIC was utilized for this study. However, PHREEQC supports a variety of other BASIC instructions which are described in the standard help file.

A.3 Graphic Output and Calculations

A.3.1 Graphic Layout Engine

Graphic Layout Engine is a graphic scripting language that allows the user to generate high quality images for publications and presentations. The software has no graphic user interface and only produces images as output from text based instructions. In the following sections I will go over some of the guidelines for using the software and finally I will discuss how the software was utilized for complex calculations.

A.3.2. General Instructions for GLE

GLE can accomplish an enormous variety of graphical outputs but in this work it has been used to make relatively simple graphs. I will only be covering the basic instruction to understand or recreate the input files associated with this work

A.3.3 Initial Formatting

In the image below, some basic formatting is programmed in order to let the software know how the graphical output is to appear. The paper size, margins, justification, font, font size and line width are all defined.

```
papersize 10 7
margins 0 0 0 0

set justify cc ! texts are centered (vertical and horizontal
set lwidth 0.04 ! you can change the thickness of the lines. This value gives good results
set font texcmss hei 0.4 ! font for the text and size of the characters
amove 0.5 0.5 ! you can move the graph on your sheet
```

A.2.2 Specifying a Graph and Its Formatting

Next a graph is begun by programming as such. The size of the graph is defined along with formatting such as X and Y axis labels as well as limits for each axis.

```
begin graph
 size 10 7 ! Set the size of the graph
 xtitle "C_{eq} (mol\cdot L^{-1})" ! _ is for subscript. ^ is for superscript. subscripts in {}.
 ytitle "K_D (L\cdot kg^{-1})" !
 xaxis min 1e-10 max 1e-4 log  ! adjust the min and max if needed. Log scale is specified
 yaxis min 1e+1 max 1e+6 log   ! adjust the min and max if needed. Log scale is specified
```

A.3.4 Incorporating Data

Data can then be incorporated by calling upon a data file, in this case this happens to be our PHREEQC output which we will call “test.prn”. It can then be specified which columns from the output file the user wishes to plot be calling the data set, d1, and calling the columns, c1 and c2 (in this case pH and the first species column. Here, the line color and width can also be designated in order to distinguish species from each other in the end result.

```
data "test.prn" d1=c1,c2 ignore 3 ! data are in the file test.prn. C1 and C2 specify column 1 and 2.
d1 line color red ! Specifies that dataset1 produces a red colored line.
```

Appendix B. Diffusion Modeling

B.1 Indirect K_d Model through Reactive Transport Code Model

K_d values for transport cannot be determined directly from reactive transport code that PHREEQC utilizes for its calculations. This is due to the fact that what we are asking the system to evaluate is a fixed total concentration to a virtual infinite number of sites available for sorption. To work through this short coming, it is possible to create a surface complexation model that reproduces the results of a K_d model.

$$K_{D,U} = \frac{c_{surf,U}}{c_U}$$

In the equation above, c_(surf,U) is the concentration of U at the surface in mol·kg-1, and c_U is the total U concentration in solution. In the Appendix XXX, K_0 is taken through a series of transformations in order to relate it to $K_{D,U}$ allowing for a method to set surface complexation reactions as mimics to a K_D model (equations below).

$$K_0 = \frac{K_{D,U} R_{SL}}{[> \mathrm{Bogus}]_{TOT} \gamma_{\mathrm{UO_2^{2+}}}}$$

By choosing an arbitrarily large value for the arbitrary reaction site $[> \mathrm{Bogus}]$ and fixing R_{SL}, the solid concentration, K_0 can be calculated for each species of uranium present in solution.

$$K_1 = \frac{K_{D,U} R_{SL} [\mathrm{Na^+}] \gamma_{\mathrm{Na^+}}}{[\mathrm{Cl^-}] \gamma_{\mathrm{Cl^-}} [> \mathrm{Bogus}]_{TOT} \gamma_{\mathrm{UO_2^{2+}}}}$$

Reactions are then specified and log K values are calculated for each species in solution. As seen previously in the speciation section this must be accomplished for a great many species that arise over the various chemical conditions we have evaluated.

B.3 Understanding of the Parametric Effect

To understand the parametric effect of the system being studied, a few examples were generated to show the user or reader what to expect. In the example below, the GLE calculation file was manipulated by only changing the K_D values used in the calculation. It can be seen that the retention in terms of time in days is heavily affected by this value whereas the flux associated with these calculations remains constant.

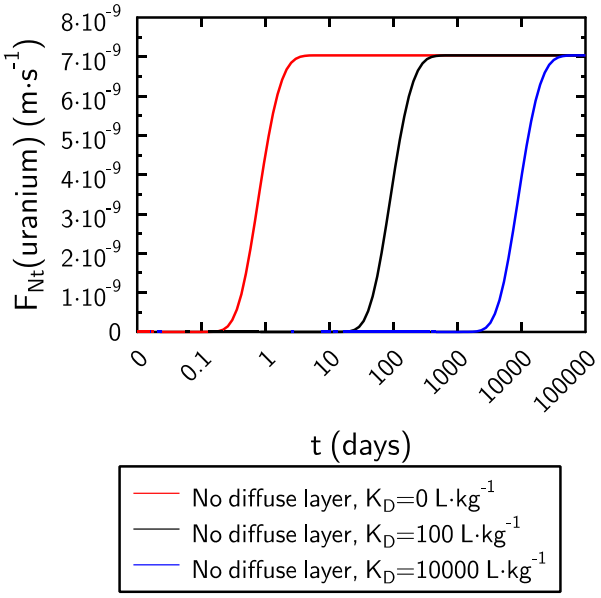

Figure B-1. Diffusion data showing the effect of K_D on the retention of mobility in the system. Flux remains the same but for increasing K_D mobility is attenuated.

To investigate the other parameter, if the diffuse-layer is taken into account and the mobile K_D remains constant, the accumulation factor of U from the 1-D diffusion of equation is what governs the flux of U(VI) through the plug and it can be seen in the figure below (Figure D-2), that both flux and attenuation are reduced with this allowed pathway.

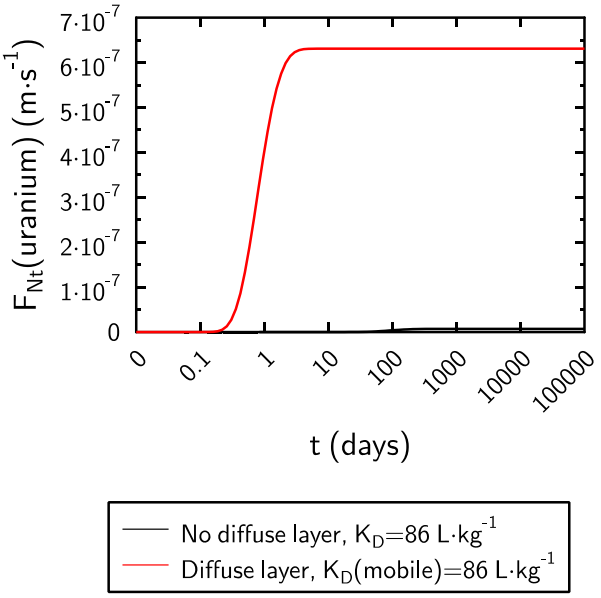

Figure B-2. Diffusion data showing the effect of the diffuse layer affinity of the U(VI) in solution on retardation and flux diffusion.

E. Diffusion Equation Document to Show Derivation of Flux Equation (reproduced with permission from C. Tournassat)

Note on diffusion for Jonathan

Christophe Tournassat

June 29th 2018

Contents

1. Diffusion equation and analytical solution

Diffusion processes are most often treated in terms of Fick's laws. Fick's first law states that the diffusive flux of a species *i* in solution (J_i) is proportional to its concentration (c_i) gradient (here in 1-D along *x*) (Steefel et al. 2014):

$$J_i = -D_{e,i}\frac{\partial c_i}{\partial x} \quad (2)$$

where $D_{e,i}$ is the effective diffusion coefficient that is specific to the chemical species *i*. The diffusion coefficient includes a correction for the tortuosity (τ) and the porosity (ϕ) of the porous media:

$$D_{e,i} = \phi \cdot D_{p,i} = \phi \cdot \tau \cdot D_{0,i} \quad (3)$$

where $D_{0,i}$ is the diffusion coefficient of species *i* in water (or self-diffusion coefficient), and $D_{p,i}$ is the pore diffusion coefficient ($D_{p,i} = \tau \cdot D_{0,i}$). The tortuosity is defined as the square of the ratio of the path length the solute would follow in water alone, *L*, relative to the tortuous path length, it would follow in porous media, *Le* :

$$\tau = (L/Le)^2 \quad (4)$$

Note that the terminology of the diffusion coefficient terms is very diverse . The terminology presented here is the most commonly used in geosciences. In particular, the effective diffusion coefficient is defined here to include the porosity.

Fick's second law is derived from the mass conservation law that includes the divergence of the flux:

$$\frac{\partial C_{tot,i}}{\partial t} = -\frac{\partial J_i}{\partial x} \tag{5}$$

where $C_{tot,i}$ is the concentration of species *i* in the porous media (i.e. the amount of species *i* in the solution and in the solid normalized to the solution and solid volumes). If the species *i* is in the solution only then:

$$\frac{\partial \phi c_i}{\partial t} = \frac{\partial}{\partial x}\left(D_{e,i}\frac{\partial c_i}{\partial x}\right) \tag{6}$$

If the species *i* is also adsorbed on or incorporated into the solid phase, then it is possible to define a rock capacity factor α that relates the concentration in the porous media to the concentration in solution:

$$\alpha_i = \frac{C_{tot,i}}{c_i} \tag{7}$$

The quantification of adsorption processes is commonly translated into distribution ratio values, *Rd* (L·kg^{-1}):

$$Rd_i = \frac{c_{surf,i}}{c_i} \tag{8}$$

where $c_{surf,i}$ is the concentration on the surface of the element of interest (mol·kg^{-1}). If the concentration of species *i* on the solid is only due to adsorption processes, then Equation (7) can be combined with Equation (8), yielding:

$$\alpha_i = \phi + \rho_d Rd_i \tag{9}$$

where ρ_d is bulk dry density of the material. In that case, Equation (5) transforms into:

$$\frac{\partial \alpha_i c_i}{\partial t} = \frac{\partial}{\partial x}\left(D_{e,i}\frac{\partial c_i}{\partial x}\right) \tag{10}$$

When interpreting diffusion data, the distribution ratio is commonly assumed to be constant (the adsorption is linearly dependent on the concentration) and representative of an instantaneous and reversible adsorption process. Under these conditions, the *Rd* value is designated as the distribution coefficient, K_D. If it is further assumed that the media is homogeneous, Equation (10) reduces to:

$$\frac{\partial c_i}{\partial t} = \frac{D_{e,i}}{\phi + \rho K_{D_i}}\frac{\partial^2 c_i}{\partial x^2} \tag{11}$$

The diffusion parameters D_e and α can be evaluated using a "flow-through diffusion" experimental setup (Figure 1), whose results can be compared to an 1D analytical solution equation (1) , if five conditions are met:

- the surface of the sample in contact the high concentration reservoir is the same as that in contact with the low concentration reservoir;

- the reservoir solution composition is homogeneous (infinitely fast mixing of the reservoir, tube, etc., compared to the characteristic time of diffusion) and in direct contact to the clay sample;
- the tracer concentration remains constant in the high concentration reservoir (infinitely large volume of the reservoir, or instantaneous source of tracer to keep its concentration constant);
- the tracer concentration remains constantly at zero in the low concentration reservoir (infinitely large volume of the reservoir, or instantaneous sink of tracer to keep its concentration constant);
- and the tracer concentrations is initially zero in the clay.

$$Q_t = \frac{S \cdot C_0 \cdot D_e}{h} \cdot t - \frac{\alpha \cdot C_0 \cdot S \cdot h}{6} - \frac{2 \cdot \alpha \cdot S \cdot C_0 \cdot h}{\pi^2} \sum_{j=1}^{\infty} \frac{(-1)^j}{j^2} \exp\left(-\frac{D_e \cdot j^2 \cdot \pi^2 \cdot t}{L^2 \cdot \alpha}\right) \qquad (12)$$

In equation (1), C_0 (in mol·m^{-3}) is the concentration of the species of interest in the high and constant concentration reservoir, h (in m) is the thickness of the sample, t is the time (in s), and S (in m^2) is the surface of the sample in contact with each of the reservoir. Q_t (in mol) is the cumulated amount of the tracer that has entered the low concentration reservoir.

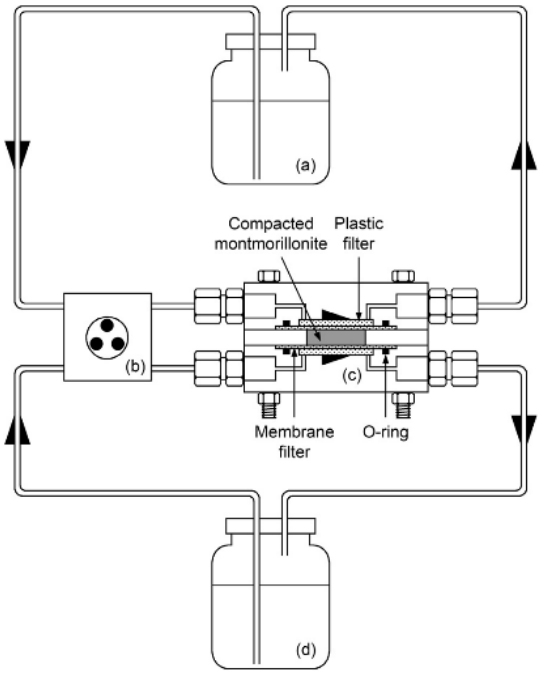

Figure 1. Example of a through diffusion cell setup: (a) inlet reservoir, (b) peristaltic pump, (c) through-diffusion cell, and (d) outlet reservoir. Arrow heads indicates the circulation of water from the reservoir to the filter in order to homogenize the inlet and outlet solutions compositions. Figure from Tachi and Yotsuji .

It is usually preferred to look at the instantaneous flux F_t (in mol·m^{-2}·s^{-1}) of a tracer at the outlet of the clay sample, which can be obtained with the time derivative of Equation (1).

Please calculate F_t.

This flux F_t can be further normalized with regards to C_0:

$$F_{Nt} = \frac{F_t}{C_0} \tag{13}$$

2. Calculations with analytical solution

2.1. First calculations

You can now implement the equation of F_{Nt} in GLE (or another program) to make some calculations and figures.

GLE allows you to define functions and variables. First define the variables and their associated parameters (pay attention to the units):

```
Length=…
C0=…
D0=…
Porosity=…
Tortuosity=…
Drydensity=…
KD=…
De=D0*Tortuosity*Porosity
Alpha=Porosity+Drydensity*KD
```

Then define a “GLE function” to calculate the flux, starting with the keyword sub, and ending with the keyword end sub

```
sub FNt t h C D alph
```

The parameters after the name of the function are the variables you will use below

```
pi=3.14159
```

You need pi in the equation.

You must calculate a sum from 0 to infinity. In practice, use a “FOR…NEXT” loop with a large number (here 500)

First initialize the value of the sum:

```
sumval=0
        for j=1 to 500 step 1
```

```
          sumval=sumval+ the formula inside the sum
        next j
```

The formula must be written as a function of `t h C D alph`

Then write the formula to obtain the desired value as a function of `t h C D alph`

```
result= blablabla
```

`blablabla` must be written as a function of `t h C D alph` and as a function of the `sumval` value.

```
return result
```

The function returns the result you have calculated

```
end sub
```

Then, you can use your function in a graph block.

```
begin graph
 size 10 7
 xtitle "t (days)"
 ytitle "F_{Nt}(Ca^{2+}) (m\cdot s^{-1})"
 xaxis min 0 max 6
 xaxis format "fix 1 nozeroes "
 yaxis format "fix 0 min 0 max 0 sci 2 10 nozeroes" min 0
!2e-3

 let d1= FNt(x*24*3600, Length, C0, De, Alpha)
```

Define the series you want to plot.

In the graph, the time is on x-axis, so `x` is the time. The time is in seconds in the equation but we want to plot the results as a function of days, so we convert it (`x*24*3600`). The other variables were defined at the beginning of the file (`h=Length, C=C0, D=De, alph=Alpha`).

```
d1 line color green key "Analytical solution"
```

Plot the series

```
end graph
```

First, plot one curve, then try to plot several curves on the same graph with different values of `De` and `Alpha`, but with the same `D0`, `Drydensity` and `Porosity` values.

2.2. Second calculations

Let's look at the real world.

In the paper "Tachi, Y. & Yotsuji, K. Diffusion and sorption of Cs+, Na+, I- and HTO in compacted sodium montmorillonite as a function of porewater salinity: Integrated sorption and diffusion model Geochimica et Cosmochimica Acta, 2014, 132, 75-93":

- find the D_e and α value for HTO for the 5 mm sample measured at 0.1 M NaCl;
- calculate ϕ and τ for HTO;
- do the same for Cs^+;
- plot the figures for both elements.

3. K_D in reactive transport codes

K_D values cannot be informed directly in (most of) reactive transport codes because they relate a total concentration of element to an adsorbed amount on a virtually infinite number of sites. It is however possible to create a surface complexation model that reproduces the results of a K_D model.

$$K_{D,U} = \frac{c_{surf,U}}{c_U} \tag{14}$$

where $c_{surf,U}$ is the concentration of U at the surface in mol·kg^{-1}, and c_U is the total U concentration in solution. Let's define a surface complexation reaction with an arbitrary site named ">Bogus":

$$>\text{Bogus} + UO_2^{2+} = >\text{Bogus}UO_2^{2+} \qquad \log K_0 \tag{15}$$

$$K_0 = \frac{(>\text{Bogus}UO_2^{2+})}{(>\text{Bogus})(UO_2^{2+})} \tag{16}$$

$$(>\text{Bogus}UO_2^{2+}) = \frac{[>\text{Bogus}UO_2^{2+}]}{[>\text{Bogus}UO_2^{2+}] + [>\text{Bogus}]} \tag{17}$$

$$(>\text{Bogus}) = \frac{[>\text{Bogus}]}{[>\text{Bogus}UO_2^{2+}] + [>\text{Bogus}]} \tag{18}$$

$$K_0[>\text{Bogus}]\gamma_{UO_2^{2+}} = \frac{[>\text{Bogus}UO_2^{2+}]}{[UO_2^{2+}]} \tag{19}$$

Where values in parentheses are activities, values in square brackets are concentrations (in mol·L^{-1}), and $\gamma_{UO_2^{2+}}$ is the activity coefficient of UO_2^{2+} in solution.

If UO_2^{2+} and $>\text{Bogus}UO_2^{2+}$ are the only U species in solution and on the surface respectively, then:

$$K_{D,U} = \frac{K_0[>\text{Bogus}]\gamma_{UO_2^{2+}}}{R_{SL}} \tag{20}$$

where R_{SL} is the solid concentration (in kg·L^{-1}). It is thus possible to relate the value of K_0 to the K_D value. At constant ionic strength (background electrolyte composition), $\gamma_{UO_2^{2+}}$ has a constant value. Thus we also want that $[>\text{Bogus}]$ takes a constant value. Since $[>\text{Bogus}] = [>\text{Bogus}]_{TOT} - [>\text{BogusUO}_2^{2+}]$, it is sufficient to take an arbitrarily large value for $[>\text{Bogus}]_{TOT}$. In these conditions:

$$K_0 = \frac{K_{D,U} R_{SL}}{[>\text{Bogus}]_{TOT} \gamma_{UO_2^{2+}}} \qquad (21)$$

We have now a method to set a surface complexation reaction that mimics a K_D model:

- calculate with PHREEQC the value of $\gamma_{UO_2^{2+}}$ in the chosen conditions (NaCl concentration is the most important parameter)
- choose an arbitrary very large value of $[>\text{Bogus}]_{TOT}$
- calculate K_0

Please set-up a PHREEQC script with the reaction (15). The conditions are [NaCl]=0.1 M, pH 4, no carbonates and $R_{SL} = \frac{\rho_d}{\phi} = \frac{0.8}{0.72} = 1.11$ kg·L^{-1}. The target K_D is 100 L·kg^{-1}. Calculate with PHREEQC the adsorbed U concentration as function of equilibrium U concentration. Verify that the adsorption is linear and that it does correspond to a K_D of 100 L·kg^{-1}.

The first problem with this approach is that reaction (15) creates the apparition of a net negative charge in solution because UO_2^{2+} is removed from the solution. It is thus better to describe a charge neutral reaction such as:

$$>\text{BogusNa} + UO_2^{2+} + Cl^- = >\text{BogusUO}_2\text{Cl} + Na^+ \qquad \log K_1 \qquad (22)$$

The reaction does not mean that Cl is actually adsorbing: it is merely a numerical trick.

It follows (please verify):

$$K_1 = \frac{K_{D,U} R_{SL} [Na^+] \gamma_{Na^+}}{[Cl^-] \gamma_{Cl^-} [>\text{Bogus}]_{TOT} \gamma_{UO_2^{2+}}} \qquad (23)$$

In our conditions $\frac{[Na^+]\gamma_{Na^+}}{[Cl^-]\gamma_{Cl^-}} \sim \frac{\gamma_{Na^+}}{\gamma_{Cl^-}}$ has a constant value that can be evaluated with PHREEQC.

Please recalculate K_1 and redo the same simulation as above.

The second problem is related to the fact that there are many U species in solution. Here comes the painful part of the model: for each of the different species, we must define one reaction and one associated log K value:

$$>\text{BogusNa} + UO_2^{2+} + Cl^- = >\text{BogusUO}_2\text{Cl} + Na^+ \qquad \log K_1 \qquad (24)$$

$$>\text{BogusNa} + UO_2OH^+ = >\text{Bogus UO}_2\text{OH}^+ + Na^+ \qquad \log K_2 \qquad (25)$$

…

$$>\text{BogusNa} + (UO_2)_2(CO_3)(OH)_3^- + Na^+ = >\text{BogusNa}_2(UO_2)_2(CO_3)(OH)_3 \quad \log K_n \tag{26}$$

…

$$K_2 = \frac{K_{D,U} R_{SL} [\text{Na}^+] \gamma_{\text{Na}^+}}{[> \text{Bogus}]_{TOT} \gamma_{\text{UO2OH+}}} \tag{27}$$

$$K_n = \frac{K_{D,U} R_{SL}}{[\text{Na}^+] \gamma_{\text{Na}^+} [> \text{Bogus}]_{TOT} \gamma_{\text{(UO2)2(CO3)(OH)3}-}} \tag{28}$$

Please enter the equations for all U species, calculate the corresponding log K values and redo the same simulation as above but for different pH: 4, 5, 6, 7, 8, and 9.

D. Modeling Code Zipfile

Attached to the digital version of this thesis is zipfile containing all of the PHREEQC, BASIC, and GLE code used in the production of these modeling results. The file is divided up into three initial folders for speciation, sorption and diffusion. In each of these folders are further divisions for specific solution conditions as discussed in this work. This code is made available for reproduction, variation or to be used as building blocks for individuals interested in accomplishing similar work.